

THESIS FOR THE DEGREE OF DOCTOR OF PHILOSOPHY

## **Kraft pulping of hardwoods**

*Investigating the impact of wood microstructure on impregnation  
and delignification rate*

CAROLINA MARION DE GODOY

Department of Chemistry and Chemical Engineering

CHALMERS UNIVERSITY OF TECHNOLOGY

Gothenburg, Sweden 2026

## **Kraft pulping of hardwoods**

Investigating the impact of wood microstructure on impregnation and delignification rate

CAROLINA MARION DE GODOY

ISBN 978-91-8103-390-8

Acknowledgements, dedications, and similar personal statements in this thesis, reflect the author's own views.

© CAROLINA MARION DE GODOY, 2026.

Doktorsavhandlingar vid Chalmers tekniska högskola, Ny serie nr 5847.

ISSN 0346-718X

<https://doi.org/10.63959/chalmers.dt/5847>

Department of Chemistry and Chemical Engineering

Chalmers University of Technology

SE-412 96 Gothenburg

Sweden

Telephone + 46 (0)31-772 1000

Cover:

Schematic of the three approaches used to study kraft pulping of hardwood chips: chemical analysis, *in-situ* X-ray tomography, and modeling.

Printed by Chalmers Digitaltryck.

Gothenburg, Sweden 2026.

# KRAFT PULPING OF HARDWOODS

## Investigating the impact of wood microstructure on impregnation and delignification rate

CAROLINA MARION DE GODOY

Department of Chemistry and Chemical Engineering  
Chalmers University of Technology

### ABSTRACT

Kraft pulping accounts for most of the global paper pulp production. Nevertheless, the detailed mechanisms that govern delignification during this process are still not fully understood. Hence, this work investigated impregnation and kraft cooking of hardwoods, aiming to strengthen our knowledge regarding the rates and uniformity of lignin removal within wood chips, particularly considering the influence of specific morphological features.

The experiments included wood chips of alder, aspen, beech, and birch, and their behavior was examined from two perspectives: changes in global and local chemical composition, and changes in wood microstructure. The latter was evaluated *in-situ* via synchrotron X-ray tomography. Additionally, a multiscale model describing the delignification of birch chips during kraft cooking was developed.

The results revealed that the concentration and distribution of alkali within the chips after impregnation have major impact on delignification and are strongly affected by wood chip porosity. Furthermore, structural analysis during impregnation showed that vessels provide the main path for liquor penetration and distribution among adjacent cells. No substantial changes in cell wall thickness due to alkaline swelling were observed.

When comparing hardwood species, lignin removal was significantly faster in aspen. Delignification uniformity also increased with chip porosity and was shown to improve when utilizing low cooking temperatures (e.g., 145 °C) or impregnation liquors with high alkali concentrations. Differences in ray cells among the hardwoods had no clear impact on local rates of lignin removal. In terms of microstructural changes, delignification led to increased chip porosity and a minor decrease in cell wall thickness.

Finally, the proposed modeling approach has potential to be used for investigating the defibration point of wood chips. According to it, lignin removal from the cell walls appears to be limited by reaction kinetics and diffusion of lignin fragments, whereas the overall delignification behavior at the chip scale is heavily influenced by the balance between alkali transport and consumption.

**Keywords:** delignification, hardwood, impregnation, *in-situ* tomography, kraft pulping, modeling.



## LIST OF PUBLICATIONS

This thesis is based on the work contained in the following papers, referred to by Roman numerals in the text:

- I **Kraft cooking of birch wood chips: differences between the dissolved organic material in pore and bulk liquor**  
Linus Kron\*, Carolina Marion de Godoy\*, Merima Hasani, and Hans Theliander. *Holzforschung* 2023. 77(8): 598-609.
- II **Kraft pulping of model wood chips: local impact of process conditions on hardwood delignification and xylan retention**  
Carolina Marion de Godoy, Merima Hasani, and Hans Theliander. *Holzforschung* 2024. 78(8): 446-458.
- III **Uniformity of delignification during kraft pulping of hardwood chips: impact of wood structure and the importance of impregnation**  
Carolina Marion de Godoy, Moa Andersson, Merima Hasani, and Hans Theliander.  
*Accepted – Wood Science and Technology.*
- IV **Impregnation and delignification during kraft pulping of hardwood chips: characterization using *in-situ* X-ray tomography**  
Carolina Marion de Godoy, Endri Laçaj, Klara Hackenstrass, Luigi Galluccio, Haiyang Yu, Sara Florisson, Malin Wohlert, Stephen A. Hall, Merima Hasani, and Hans Theliander.  
*Accepted – Wood Science and Technology.*
- V **1D Multiscale modeling of delignification rate in hardwood chips during kraft pulping**  
Carolina Marion de Godoy\*, Linus Kron\*, Merima Hasani, and Hans Theliander.  
*Submitted.*

\* *Shared first authorship.*

## CONTRIBUTION REPORT

- I **Shared first authorship.** LK and CMdG were responsible for planning and executing all experimental work, except for the HSQC NMR measurements. Both first authors performed data analysis. The interpretation of the results was carried out together with co-authors. The first authors were responsible for drafting the manuscript, which was revised together with co-authors.
- II **First author.** CMdG planned and executed all experimental work, except for HSQC NMR and size-exclusion chromatography of holocellulose samples. Preparation of wood sections for microscopy was performed by the Centre for Cellular Imaging. CMdG conducted data analysis. The interpretation of the results was carried out together with co-authors. CMdG drafted the manuscript, which was revised together with co-authors.
- III **First author.** CMdG planned and executed all experimental work related to the samples kraft cooked at 165 °C. CMdG supervised MA, who conducted the experimental work related to the samples cooked at 155 °C (i.e., the samples treated with high alkali concentration). CMdG and MA conducted data analysis. The interpretation of the results was carried out together with co-authors. CMdG drafted the manuscript, which was revised together with co-authors.
- IV **First author.** CMdG planned and executed all experimental work. Synchrotron experiments were supported by co-authors and the beamline staff (ForMAX beamline – MAX IV Laboratory). CMdG and EL conducted data analysis. The interpretation of the results was carried out together with co-authors. CMdG drafted the manuscript, which was revised together with co-authors.
- V **Shared first authorship.** CMdG and LK were responsible for developing the multiscale model and collecting the experimental data used for parameter estimation and model validation. The interpretation of the results was carried out together with co-authors. The first authors were responsible for drafting the manuscript, which was revised together with co-authors.

## LIST OF CONFERENCES

The results achieved in this work have also been presented on the following occasions:

Hardwood Delignification: Influence of Impregnation

Carolina Marion de Godoy, Linus Kron, Merima Hasani, Hans Theliander

**16th European Workshop on Lignocellulosics and Pulp**

Gothenburg, Sweden, June 2022.

*Poster*

Kraft Cooking of Birch: Pore and Bulk Liquor Composition

Linus Kron, Carolina Marion de Godoy, Merima Hasani, Hans Theliander

**21st International Symposium on Wood, Fiber, and Pulping Chemistry**

Venice, Italy, July 2023.

*Poster*

Insights into delignification and xylan removal during kraft cooking of hardwoods

Carolina Marion de Godoy, Merima Hasani, Hans Theliander

**17th European Workshop on Lignocellulosics and Pulp**

Turku, Finland, August 2024.

*Oral presentation*

Kraft cooking of Nordic hardwoods: comparison between delignification profiles and microstructural changes

Carolina Marion de Godoy, Merima Hasani, Hans Theliander

**22nd International Symposium on Wood, Fiber, and Pulping Chemistry**

Raleigh, USA, June 2025.

*Oral Presentation*

Kraft pulping of Nordic hardwoods: delignification profiles and *in-situ* monitoring of microstructural changes

Carolina Marion de Godoy, Merima Hasani, Hans Theliander

**WWSC International Conference**

Stockholm, Sweden, June 2025.

*Poster*



# CONTENTS

<b>1 Introduction.....</b>	<b>1</b>
1.1 Aim.....	3
<b>2 Background.....</b>	<b>5</b>
2.1 Wood.....	5
2.1.1 Macrostructure .....	6
2.1.2 Microstructure.....	7
2.1.3 Wood composition and ultrastructure .....	10
2.1.3.1 Cellulose.....	11
2.1.3.2 Hemicelluloses.....	11
2.1.3.3 Lignin .....	13
2.1.3.4 Ultrastructure .....	14
2.2 Kraft pulping.....	15
2.2.1 Impregnation .....	16
2.2.1.1 Liquor penetration.....	17
2.2.1.2 Diffusion.....	18
2.2.2 Cooking .....	19
2.2.2.1 Delignification .....	20
2.2.2.2 Degradation and dissolution of polysaccharides.....	23
2.2.3 Delignification models for kraft pulping .....	24
<b>3 Material and Methods.....</b>	<b>27</b>
3.1 Materials .....	27
3.1.1 Chemical reagents .....	27
3.1.2 Industrial chips (Paper I) .....	27
3.1.3 Model hardwood chips (Papers II, III) .....	28
3.1.4 Small model chips (Paper IV).....	28
3.2 Determination of wood chip characteristics .....	29
3.2.1 Chip density and porosity (Papers III, IV) .....	29
3.2.2 Microscopy (Papers III, IV).....	29
3.3 Batch kraft cooking ( <i>ex-situ</i> experiments) .....	29

3.3.1	Cooking conditions – industrial chips (Paper I) .....	30
3.3.2	Cooking conditions – model hardwood chips (Papers II, III) .....	31
3.4	Chip sectioning (Papers II, III).....	33
3.5	Lignin isolation from black liquor (Paper I).....	34
3.6	Xylan isolation from wood/pulp (Paper II) .....	34
3.7	Determination of lignin and carbohydrates (Papers I-IV).....	35
3.7.1	Klason lignin .....	35
3.7.2	Acid-soluble lignin.....	36
3.7.3	Carbohydrates .....	36
3.7.4	Local composition – estimate of local yield .....	36
3.8	Determination of molar mass distribution (Papers I, II).....	37
3.9	Assessment of residual alkali and degree of penetration in wood chips (Paper III) .....	37
3.10	<i>In-situ</i> X-ray tomography (Paper IV) .....	38
3.10.1	Batch kraft cooking in small reactor .....	38
3.10.2	Image acquisition.....	40
3.10.3	Image reconstruction and processing .....	40
3.11	Modeling (Paper V) .....	41
3.11.1	General assumptions.....	42
3.11.2	Macroscale modeling.....	42
3.11.3	Microscale modeling.....	43
<b>4</b>	<b>Results and Discussion .....</b>	<b>45</b>
4.1	Hardwood chips: composition and structural characteristics .....	45
4.2	Kraft pulping of hardwood chips: impregnation .....	48
4.2.1	Liquor penetration and the impact of microstructural features during impregnation.....	48
4.2.2	Impregnation of model chips .....	50
4.2.3	Impregnation of chips prepared in an industrial chipper .....	54
4.3	Kraft pulping of hardwood chips: cooking .....	56
4.3.1	Delignification – cell wall separation and structural changes .....	56
4.3.2	Batch kraft cooking of model chips.....	59

4.3.2.1 Lignin removal .....	59
4.3.2.2 Xylan removal .....	63
4.3.3 Batch kraft cooking of chips prepared in industrial chipper .....	65
4.4 Multiscale model .....	67
<b>5 Conclusion .....</b>	<b>71</b>
5.1 Concluding remarks .....	71
5.2 Future work .....	73
<b>Acknowledgements .....</b>	<b>75</b>
<b>References .....</b>	<b>77</b>
<b>List of symbols .....</b>	<b>87</b>
<b>Appendix .....</b>	<b>89</b>
Determination of extractives .....	89



*To my mom, for everything.*



# 1 Introduction

The kraft process is the dominant technology used in pulp production. However, despite its well-established position, kraft pulping still faces many challenges, including low resource efficiency (Mboowa, 2024; Rajan *et al.*, 2024). This issue is linked directly to the decreased profitability of mills, as pulpwood prices continue to rise while pulping yields remain as low as 45-55% (Bajpai, 2015; Skogsstyrelsen, 2026). In addition, the shift toward more sustainable and circular manufacturing practices also pressures the pulp industry into updating or adapting existing processes. For instance, there is a trend to increase the number of times fibers can be recycled (i.e., the number of recycling cycles) and expand the share of new feedstocks used for pulp production, including new woody sources and residues of annual crops (Hujala *et al.*, 2013; Rajan *et al.*, 2024). On a related note, forestry strategies driven by climate change or aiming to reduce wood prices may increase the supply of hardwoods (Hart and Nutter, 2012; Forest Europe, 2020), compelling mills to re-evaluate their capacity for hardwood processing.

In this context, a thorough understanding of kraft delignification of different feedstocks is imperative to fine-tune the operation and thus achieve higher pulping yields and more uniform lignin removal. Still, studies on kraft pulping of hardwoods often tend to focus on assessing their fiber quality and overall pulpability, e.g., Patt *et al.* (2006), rather than investigating the governing mechanisms affecting their behavior during pulping. Moreover, most of these studies are centered around fast-growing species, with emphasis on

eucalyptus (Santiago *et al.*, 2008; Hart and Nutter, 2012; Neiva *et al.*, 2015; Favaro *et al.*, 2021). Hence, there is a need for more in-depth research on hardwood delignification, especially considering their great diversity and complexity in both chemical composition and morphology.

The few existing studies exploring the factors affecting hardwood delignification highlight differences in reaction kinetics and lignin structure, suggesting that higher syringyl/guaiacyl (S/G) ratios and a greater proportion of non-condensed lignin units are associated with easier and faster delignification (Pinto *et al.*, 2005b; Santos *et al.*, 2011). Mass transport limitations have also been suggested to impact kraft pulping of hardwoods (Egas *et al.*, 2002; Simão *et al.*, 2008), although studies directly comparing species and examining the role of wood microstructure remain scarce. Some contributions that provide insight into the influence of wood morphology during pulping include works on impregnation and liquor penetration in wood (Wardrop and Davies, 1961; Ahmed *et al.*, 2011), as well as research on delignification of specific wood tissues (Whiting and Goring, 1981; Koch *et al.*, 2003; Rehbein *et al.*, 2010; Aguayo *et al.*, 2014; Takada *et al.*, 2016; Takada *et al.*, 2021). However, few of these studies focus on kraft pulping, and they often rely on *ex-situ* analyses that require extensive sample preparation, such as microscopy and scanning UV microspectrophotometry. Therefore, further research on the topic can be of great value, particularly for achieving a detailed description of the microstructural changes in wood throughout kraft delignification.

Kraft pulping models describing the delignification of hardwood chips could also benefit from further development. There is still a limited number of models that incorporate both kinetic mechanisms and transport phenomena (Wisniewski *et al.*, 1997; Gilbert *et al.*, 2021), and the vast majority neglects mass transport resistance across the fiber walls. Furthermore, the estimation of model parameters and validation of model predictions can be quite challenging due to the lack of delignification data generated under pulping conditions that minimize external influences, especially data describing the internal gradients of wood components and cooking chemicals in hardwood chips.

In light of the issues discussed above, the current knowledge regarding the different mechanisms taking place during hardwood delignification remains deficient – especially concerning the impact and evolution of wood structure. Moreover, expanding the scope of investigated wood species seems warranted in order to get a more complete picture of the progression of kraft pulping.

## 1.1 Aim

This thesis aimed to investigate the behavior of hardwood chips during batch kraft pulping, with focus on the impact of wood microstructure on impregnation and lignin removal. The experiments were conducted under controlled pulping conditions utilizing economically relevant species, including alder (*Alnus glutinosa*), aspen (*Populus tremula*), beech (*Fagus sylvatica*), and birch (*Betula pendula* and *Betula pubescens*). The study combined average and local compositional analyses, imaging techniques, and modeling efforts to achieve the following goals:

- 1) Evaluate how process conditions influence the rate and uniformity of lignin and xylan removal in hardwood chips, examining cooking parameters (namely, temperature and alkali concentration) and liquor composition during impregnation.
- 2) Compare how delignification and xylan removal progress within wood chips of different hardwood species during kraft cooking.
- 3) Investigate liquor penetration and the evolution of wood microstructure in different hardwoods during kraft pulping using *in-situ* X-ray tomography – a technique that has shown promising results in the analysis of soda pulping (Wagih *et al.*, 2022).
- 4) Expand upon the delignification model developed by Kron *et al.* (2025) using a multiscale approach to describe the lignin removal in birch chips during kraft pulping, accounting for mass transport limitations at both the cell wall and chip levels. Additionally, utilize the experimental data generated in this work for model validation.



## 2 Background

This chapter introduces general concepts related to wood chemistry, hardwood morphology and kraft pulping. Additionally, the main phenomena taking place during wood impregnation and kraft delignification are highlighted. Finally, a short review of the modeling efforts carried out to describe these processes is presented.

### 2.1 Wood

Wood is the biological material that makes up the xylem of trees (Figure 2.1). Its morphology is highly intricate and specialized in fulfilling several essential functions, including mechanical support; conduction of water, photosynthetic products, and other nutrients between roots and leaves; and the production and storage of biochemical compounds (Wiedenhoef, 2005).

Through evolutionary and adaptive processes, the chemistry and structure of wood have come to vary substantially among species (Esteban *et al.*, 2024). These differences are particularly evident when comparing hardwoods (i.e., broad-leaved, deciduous angiosperms) with softwoods (i.e., needle-leaved evergreen gymnosperms). In general, hardwoods are considered more anatomically complex than softwoods due to their greater diversity of cell types and arrangements (Wiedenhoef, 2005; Esteban *et al.*, 2024).

The following sections focus on explaining the spatial organization of wood across its different structural levels.

### 2.1.1 Macrostructure

As shown in Figure 2.1, wood is one of the concentric tissues that form the trunk of trees. From the outermost region inwards, these tissues are the outer bark, inner bark, vascular cambium, xylem (wood), and pith.

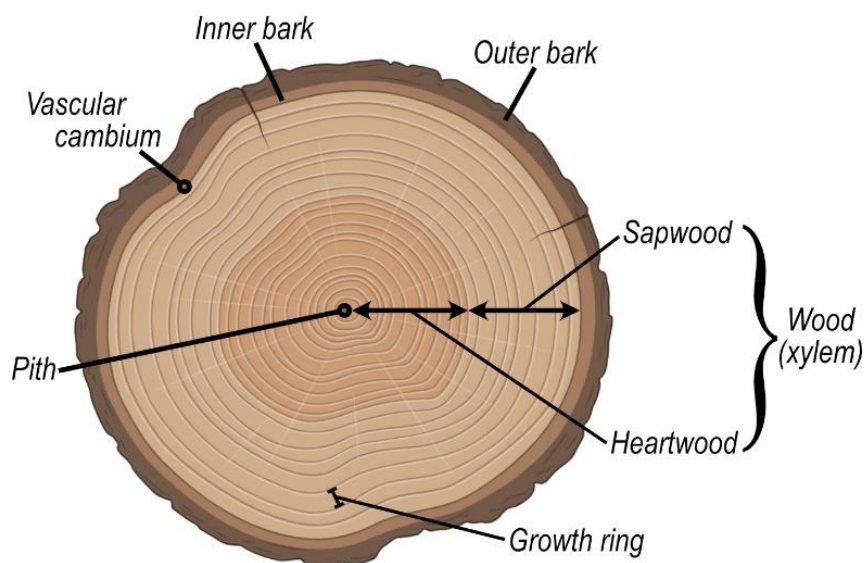


**Figure 2.1** Schematic of the transverse section of a tree trunk showing the different tissues that make up the stem. Image created in [BioRender.com](https://www.biorender.com).

The outer bark is composed of dead cells whose main purpose is to protect the trunk and minimize the loss of water. The next layer (inner bark) consists of living cells called phloem, which transport sugars through the tree. Between the inner bark and the xylem lies the vascular cambium, a thin layer responsible for producing cells for both surrounding tissues (Biermann, 1996a; Wiedenhoef, 2005).

The following layer is the wood tissue (xylem), which can be further divided into sapwood and heartwood. Sapwood is the portion responsible for transporting water and nutrients. It is also characterized by containing both dead and metabolically active cells. Over time, these cells die, gradually converting the sapwood in the inner parts of the xylem into heartwood. The latter consists exclusively of dead cells that provide mechanical support and storage space for chemicals (e.g., extractives). The accumulation of these chemicals gives heartwood a distinct dark color in some wood species, as illustrated in Figure 2.1 (Sjöström, 1993a; Wiedenhoef, 2005).

The wood tissue can also display clearly defined growth rings. These are concentric rings made of xylem cells produced during the same period, often representing seasonal growth over a year. Within each individual ring, earlywood (i.e., cells formed at the beginning of the growth season) transitions into latewood (formed at the end of the season). This transition is often accompanied by changes in cell patterns across the ring, which may be associated with gradual or abrupt changes in the diameter of conducting elements and in cell wall thickness from earlywood to latewood (Sjöström, 1993a; Wiedenhoef, 2005; Daniel, 2009).

The innermost feature in Figure 2.1 is the pith. This tissue is the remnant of the early stages of plant development, before the xylem was formed (Wiedenhoef, 2005). In mature plants, it has been associated with the formation of heartwood and storage of starch (Shunn and Gee, 2023).

### **2.1.2 Microstructure**

The microstructure of wood refers to the different cell types and anatomical features that make up the three-dimensional structure of the xylem, as well as the way these components are organized.

In softwoods, the microstructure is relatively simple, consisting primarily of tracheids, which account for about 90-95% of the xylem (in volume), and parenchyma cells, which make up the remaining 5-10% (Koch, 2006). The tracheids serve both support and conductive functions. They are oriented mainly in the longitudinal direction, although they can also be arranged radially in heterocellular rays. The parenchyma cells are responsible for storage and are typically arranged radially in homocellular and/or heterocellular rays. In some species, a small percentage of the parenchyma cells also occurs in the longitudinal direction. Furthermore, certain softwoods contain epithelial parenchyma cells that secrete resins, which are then stored in adjacent intercellular spaces known as resin canals (Sjöström, 1993a; Koch, 2006; Daniel, 2009).

In hardwoods, however, the microstructure is considerably more complex, comprising not only tracheids and parenchyma cells, but also vessel elements and fibers. Hardwood cells also exhibit a wider range of sizes and shapes than those found in softwoods. Moreover, the contribution of each cell type to the total volume of the xylem varies substantially; however, most hardwood species contain significant amounts of fibers (including libriform fibers and fiber tracheids), vessel elements, and both radial and longitudinal parenchyma (Daniel, 2009).

Fibers primarily provide structural support to the wood tissue. Compared with the longitudinal tracheids of softwoods, hardwood fibers are significantly shorter, usually ranging from 0.5 to 1.8 mm in length, while softwood

tracheids often exceed 3 mm. In addition, hardwood fibers have thicker cell walls and smaller lumens (i.e., the cavities in the center of the cells). Variations in fiber cross-sectional dimensions across growth rings are also less pronounced than those observed in softwood tracheids. For example, from earlywood to latewood, fiber diameter decreases by about 1-3  $\mu\text{m}$  in hardwoods (*Alnus glutinosa*, *Fagus sylvatica*, *Fraxinus excelsior*, *Populus* sp., among others), whereas tracheid lumen diameter in softwoods (such as *Pinus sylvestris*, and *Taxus baccata*) may decrease by 10-24  $\mu\text{m}$  (Koddenberg, 2025).

The vessel elements are thin-walled cells that function as the main water-conducting components of the hardwood xylem. They form stacked longitudinal structures, called vessels or pores, which can stretch for centimeters or even meters (Daniel, 2009). Within these structures, the vessel elements connect end-to-end via their perforation plates – which vary among different species. Some examples of perforation plates include simple plates with a single opening and scalariform plates with parallel openings separated by bars (Koddenberg, 2025).

Vessels also differ substantially in size, frequency and distribution across growth rings. The latter is often used to classify hardwood species into two main groups: diffuse-porous and ring-porous. In diffuse-porous species, the vessels are distributed fairly uniformly throughout the growth ring, with similar diameters in both earlywood and latewood. In contrast, ring-porous species exhibit an abrupt increase in vessel diameter at the transition from latewood to earlywood (Ruffinatto and Crivellaro, 2019; Koddenberg, 2025). A third group, semi-ring-porous species, is also recognized by some authors. In this case, the vessels can either decrease gradually in diameter from earlywood to latewood, or they may be more closely packed in earlywood than in latewood (Koch, 2006; Ruffinatto and Crivellaro, 2019).

Parenchyma cells are significantly more abundant in hardwoods than in softwoods (Daniel, 2009). In general, longitudinal parenchyma (also called axial parenchyma) accounts for 1-25% of the hardwood xylem, although values at the upper end of this range are found only in tropical species (Esteban *et al.*, 2024). Radial parenchyma, on the other hand, usually represents 8-25% of the wood and constitutes the sole component of hardwood rays. These rays can be uniseriate (one cell wide in the tangential plane) or multiseriate (more than one cell wide). In addition, rays can display special arrangements in the xylem, such as aggregate rays, which consist of closely packed rays separated by axial elements (Esteban *et al.*, 2024; Koddenberg, 2025).

Table 2.1 presents some of the main microstructural characteristics of the hardwoods investigated in this work.

**Table 2.1** Microstructure of selected hardwoods.

Microstructural feature	Alder <i>A. glutinosa</i>	Birch <i>Betula</i> sp.	Beech <i>F. sylvatica</i>	Aspen <i>Populus</i> sp.
<b>Fibers</b>				
% of xylem	-	64.8 <sup>a</sup> 63.0 <sup>c</sup>	37.4 <sup>b</sup> 40.0 <sup>c</sup>	61.8 <sup>b</sup> 61.0 <sup>c</sup>
Length (mm)	> 1.0 <sup>d</sup> 1.3 <sup>e</sup>	0.8-1.8 <sup>a</sup> 1.3 <sup>c</sup>	0.6-1.3 <sup>b</sup> 1.3 <sup>c</sup> 0.7 <sup>d</sup>	0.7-1.6 <sup>b</sup> 1.3 <sup>c</sup> 0.7-0.9 <sup>d</sup>
Diameter (µm)	33 <sup>e</sup>	18-36 <sup>a</sup> 19 <sup>c</sup>	15-20 <sup>b</sup> 18 <sup>c</sup>	20-40 <sup>b</sup> 21 <sup>c</sup>
Lumen diameter (µm)	12-14 <sup>d</sup> 20 <sup>e</sup>	-	6-9 <sup>d</sup>	12-14 <sup>d</sup>
<b>Vessels</b>				
Distribution <sup>d,f</sup>	Diffuse-porous	Diffuse-porous	Diffuse-porous / Semi-ring-porous	Diffuse-porous / Semi-ring-porous
% of xylem	-	24.7 <sup>a</sup> 25.0 <sup>c</sup>	31.0 <sup>b</sup> 40.0 <sup>c</sup>	26.9 <sup>b</sup> 26.0 <sup>c</sup>
Diameter (µm)	< 80 <sup>f</sup>	< 80 <sup>f</sup>	5-100 <sup>b</sup> 40-55 <sup>d</sup> < 80 <sup>f</sup>	20-150 <sup>b</sup> 62-83 <sup>d</sup> < 130 <sup>f</sup>
<b>Rays</b>				
% of xylem	-	8.5 <sup>a</sup> 12.0 <sup>c</sup>	27.0 <sup>b</sup> 20.0 <sup>c</sup>	11.3 <sup>b</sup> 13.0 <sup>c</sup>
Arrangement <sup>d</sup>	Uniseriate, aggregate	Multiseriate (1-3 cells)	Multiseriate (> 30 cells)	Uniseriate
<b>Axial parenchyma</b>				
% of xylem	-	-	4.6 <sup>b</sup>	-

<sup>a</sup> Daniel (2009); <sup>b</sup> Koch (2006); <sup>c</sup> Patt *et al.* (2006); <sup>d</sup> Koddenberg (2025); <sup>e</sup> Kiaei and Moya (2015); <sup>f</sup> Ruffinatto and Crivellaro (2019).

Other anatomical features of particular relevance in the context of pulping include pits and tyloses. Pits are openings in the cell wall that connect different cells and allow the transport of liquid between them (Sjöström, 1993a). They vary significantly in size, shape, and arrangement, depending on the wood species and cell type. For example, pits connecting vessel elements laterally (i.e., intervessel pits) are bordered and have apertures that can range from small ( $\leq 4 \mu\text{m}$ ) to large ( $\geq 10 \mu\text{m}$ ). Bordered pits are also

observed between vessels and fibers, but specialized simple pits connect vessel elements and rays (Esteban *et al.*, 2024). Additionally, pits between parenchyma cells are usually simple or slightly bordered, while pits between parenchyma and fibers are half-bordered (Daniel, 2009; Esteban *et al.*, 2024). Tyloses are organic deposits of cell wall components (e.g., cellulose, hemicellulose, lignin, pectin), mainly found inside heartwood vessels. They may also appear in other cells, such as hardwood fibers, although this is less common (Esteban *et al.*, 2024). Their formation takes place under two main circumstances: during the conversion of sapwood into heartwood and following sapwood damage. In both cases, parenchyma cells invade the lumens of adjacent cells via pits, partially or completely filling them. This obstruction compromises liquid penetration, significantly hindering wood impregnation (Daniel, 2009; Esteban *et al.*, 2024).

### **2.1.3 Wood composition and ultrastructure**

The main structural components of wood are cellulose, hemicelluloses, and lignin, which combined constitute about 90% of the dry weight of both hardwoods and softwoods. Nevertheless, their individual concentrations vary substantially among species, or even between individual trees, as wood composition is affected by growth conditions, mechanical stress (i.e., the formation of reaction wood), growth stage, and the position across the xylem (e.g., sapwood or heartwood) (Pettersen, 1984; Sjöström, 1993a).

The same variation can also be observed among minor non-structural wood components. For instance, inorganics can be quite sensitive to environmental conditions (Koch, 2006). In fact, the level of calcium in wood has been shown to vary substantially depending on the growth site (Vegunta *et al.*, 2022). Still, the content of inorganics in wood from temperate zones is usually lower than 1% (Pettersen, 1984).

The content of extractives can also be affected by environmental factors and development stage, although the types of extractives found in wood are often species-specific (Koch, 2006; Gao *et al.*, 2024). Notably, differences in the content of extractives between species can be massive. In larch, for example, extractives represent up to 30% of wood, whereas in spruce they can be as low as 0.9% (Gao *et al.*, 2024). Nonetheless, in most temperate species extractives account for 4-10% of wood (Pettersen, 1984).

The following sections describe the chemical structures of cellulose, hemicelluloses, and lignin, as well as their organization in the cell wall.

### 2.1.3.1 Cellulose

Cellulose is the main component of wood, forming the backbone of the cell wall. It consists of  $\beta$ -D-glucopyranose units linked by (1 $\rightarrow$ 4) glycosidic bonds (Klemm *et al.*, 2005), resulting in a linear homopolymer, as depicted in Figure 2.2. In its native form, wood cellulose exhibits an average degree of polymerization (DP) of about 9000-10000, at times reaching 15000. However, the cellulose found in bleached pulps has a much lower DP, usually about 1000 (Biermann, 1996a; Rowell *et al.*, 2005; Henriksson and Lennholm, 2009).

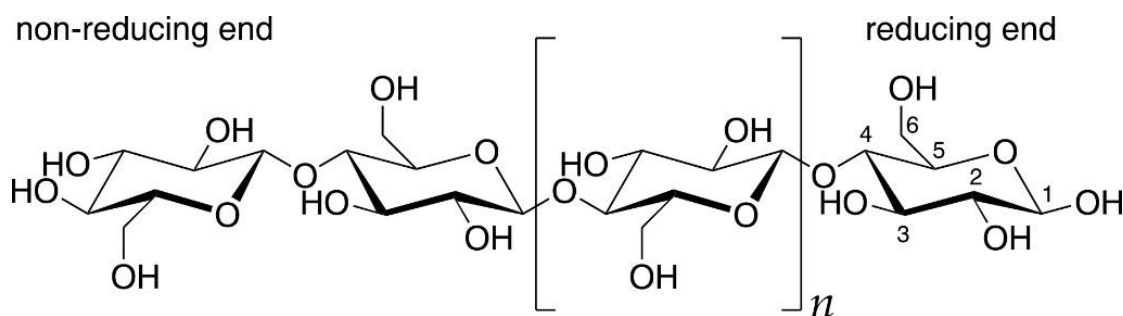


**Figure 2.2** Molecular structure of cellulose based on its biosynthesis,  $n = \text{DP}-3$ .

In wood cell walls, cellulose primarily provides structural support and mechanical strength (Biermann, 1996a), being organized in fibrils that, in turn, are formed by cellulose microfibrils. These microfibrils are bundles of cellulose chains containing both highly crystalline regions and less ordered regions (Sjöström, 1993b; Henriksson and Lennholm, 2009).

This complex spatial organization is a consequence of different intra- and intermolecular interactions among cellulose chains. For instance, intramolecular hydrogen bonds stabilize glycosidic linkages and provide stiffness to the cellulose chains, whereas intermolecular hydrogen bonds lead to the formation of cellulose sheets. Then, these sheets can further interact – for instance, via van der Waals interactions – creating cellulose crystallites (Henriksson and Lennholm, 2009).

### 2.1.3.2 Hemicelluloses

Hemicelluloses are heteropolysaccharides that contribute to the mechanical properties of wood through different levels of association with cellulose fibrils (Rowell *et al.*, 2005; Dammström *et al.*, 2009; Teleman, 2009). In addition, they are potentially involved in the interactions between cellulose and lignin within the cell walls (Teleman, 2009).

In terms of chemical composition, hemicelluloses encompass a whole class of polysaccharides with average DP in the range of 100-200 and varying

degrees of branching. Their primary components are hexoses – namely D-glucose, D-mannose, and D-galactose – and/or pentoses, such as D-xylose and L-arabinose. Nevertheless, their side groups may also include L-rhamnose, uronic acids, acetyl groups, and other minor components (Sjöström, 1993b; Biermann, 1996a; Teleman, 2009).

Usually, hemicelluloses represent 20 to 30% of the wood tissue, but their composition and structure in softwoods are very different from those in hardwoods. In general, softwood is rich in glucomannan (10-15%), followed by arabinoglucuronoxylan (5-10%) and galactoglucomannan (~6%), whereas hardwood contains mainly glucuronoxylan (15-30%) and small quantities of glucomannan (2-5%) (Sjöström, 1993b; Biermann, 1996a). As glucuronoxylan makes up a substantial percentage of the hardwood xylem, it is described in detail in the following paragraphs.

Glucuronoxylan (GX) comprises a backbone of  $\beta$ -D-xylopyranose units linked by (1 $\rightarrow$ 4) bonds and decorated with different substituents, including acetyl (Ac), glucuronic acid (GlcA), and 4-O-methylglucuronic acid (4-O-MeGlcA). The acetylation takes place in O-2 and/or O-3 (i.e., positions C-2 and C-3 in the backbone), whereas the substitution with uronic acids occurs via (1 $\rightarrow$ 2) bonds (Sjöström, 1993b; Teleman, 2009; Qaseem *et al.*, 2025). A scheme highlighting the structure of glucuronoxylan and its decorations is shown in Figure 2.3.

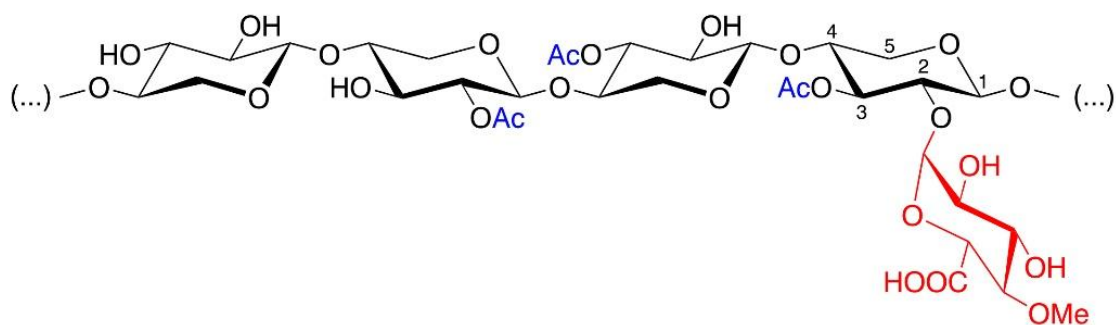


**Figure 2.3** Schematic of glucuronoxylan illustrating the linear backbone and examples of acetylation and substitution with 4-O-MeGlcA. The depicted frequency and proportion of the side groups do not reflect their actual occurrence. Adapted from Marion de Godoy (2024).

The distribution of decorations along the backbone divides glucuronoxylan into different domains: one with a regular pattern of substitution and one with arbitrary arrangements. The former corresponds to the majority of the GX chains and consists in acetylation occurring every second xylopyranose residue and glucuronidation every eighth. Glucuronoxylan also exhibits a special pattern at the reducing ends, in which an  $\alpha$ -L-rhamnose residue and

an  $\alpha$ -D-galacturonic acid residue are interposed between the GX backbone and the terminal D-xylose unit (Qaseem *et al.*, 2025). Moreover, some hardwood species present specific arrangements. For example, Pinto *et al.* (2005a) noted that most residues substituted with 4-O-MeGlcA in birch GX were also acetylated at the O-3 position (as shown in Figure 2.3). Additionally, GX in *Eucalyptus* sp. is known for the presence of galactopyranosyl (or even glucopyranosyl) linked to part of the 4-O-MeGlcA side groups (Pinto *et al.*, 2005a; Heinonen *et al.*, 2025).

These different patterns of substitution have a major influence on the interactions of GX in the cell wall assembly. For instance, the association with cellulose microfibrils was found to occur primarily via helical structures that arise from hydrogen bonding and amphiphilic associations – which depend on the distribution and frequency of the side groups in GX (Qaseem *et al.*, 2025). In this sense, even acetylation has been identified as a main enabler of the association with cellulose (Busse-Wicher *et al.*, 2014; Grantham *et al.*, 2017), although other factors, such as the DP and the degree of glucuronidation, are also relevant (Qaseem *et al.*, 2025). Still, the exact organization of GX in the cell wall is elusive. This is particularly true with respect to its potential association with lignin. It has been speculated that minor domains in GX containing high degree of substitution could favor interactions with lignin (Dammström *et al.*, 2009; Sivan *et al.*, 2024). At the same time, covalent bonds between GX and lignin through  $\gamma$ -ether, phenylglycoside and benzylether bonds have been suggested, although the last two seem to be less frequent in highly acetylated xylan (Giummarella and Lawoko, 2016).

### **2.1.3.3 Lignin**

Lignin is the second main component of wood. In hardwoods, for example, it usually accounts for 18 to 25% of the xylem (Koch, 2006). In the cell wall, lignin functions as the embedding material, surrounding the cellulose fibrils and hemicelluloses and acting as a glue between neighboring cells. Besides these structural roles, lignin imparts hydrophobicity to the cell wall, creating a barrier that protects wood polysaccharides against water, enzymatic degradation and microbial attack (Henriksson, 2009).

Still, the definition of lignin itself remains an active area of research (Ralph *et al.*, 2019). In general, it can be understood as a complex phenolic macromolecule formed primarily by monolignols linked through ether (e.g.,  $\beta$ -O-4, 4-O-5 and 1-O-4) or carbon-carbon (e.g., 5-5,  $\beta$ -5,  $\beta$ - $\beta$  and  $\beta$ -1) bonds. A wide range of monolignols – and even other phenolic molecules – has been identified within this network. Among these, *p*-coumaryl alcohol, coniferyl

alcohol, and sinapyl alcohol are regarded as the main precursors of lignin (Henriksson, 2009). Their chemical structures are presented in Figure 2.4.

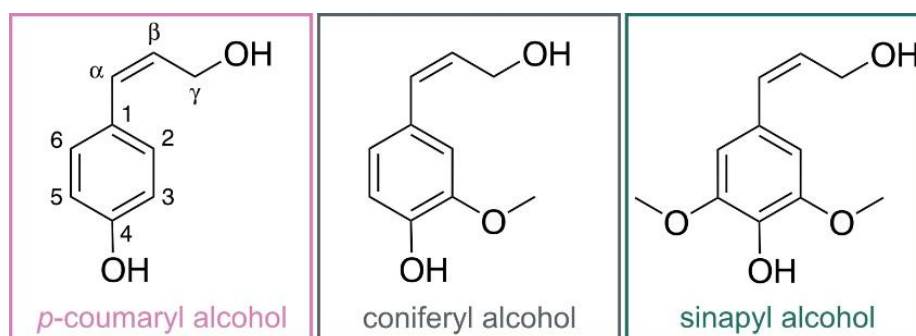


**Figure 2.4** Main monolignols found in lignin. Adapted from Marion de Godoy (2024).

Nevertheless, the ratio between these monolignols in lignin changes significantly depending on wood species, cell type and cell wall layer. In softwoods, coniferyl alcohol is the main precursor and the lignin is often referred to as guaiacyl lignin (Sjöström, 1993c; Koch, 2006). In hardwoods, however, there is a higher variability in the composition of lignin. Parenchyma cells and the secondary wall of fibers are remarkably rich in sinapyl alcohol units (syringyl lignin), with increasing amounts of coniferyl alcohol (guaiacyl lignin) occurring in the middle lamella. Vessels, on the other hand, exhibit guaiacyl lignin (Sjöström, 1993c; Koch, 2006; Yamashita *et al.*, 2016). In addition, there is a large variation between the overall S/G ratio in different hardwoods (Sjöström, 1993c; Santos *et al.*, 2012a).

Beyond the intricate chemical structure, lignin also displays complex interactions with other components of the cell wall. For instance, as mentioned in Section 2.1.3.2, lignin can interact with hemicelluloses via covalent bonds, forming lignin carbohydrate complexes (LCCs) (Lawoko *et al.*, 2005; You *et al.*, 2015; Giummarella and Lawoko, 2016; Zhao *et al.*, 2020).

#### **2.1.3.4 Ultrastructure**

The ultrastructure of wood describes the organization of the cell walls into distinct regions that differ according to the content and arrangement of cellulose, hemicelluloses, and embedding material (mostly lignin and pectin) (Sjöström, 1993a; Koch, 2006). Overall, the ultrastructure can be represented by the model illustrated in Figure 2.5. In this model, the lumen – the central cavity of the cell – is enclosed by a wall comprising two main regions: the primary wall, located in the outer portion of the cell, and the secondary wall, which is further divided into three layers (S1, S2 and S3).

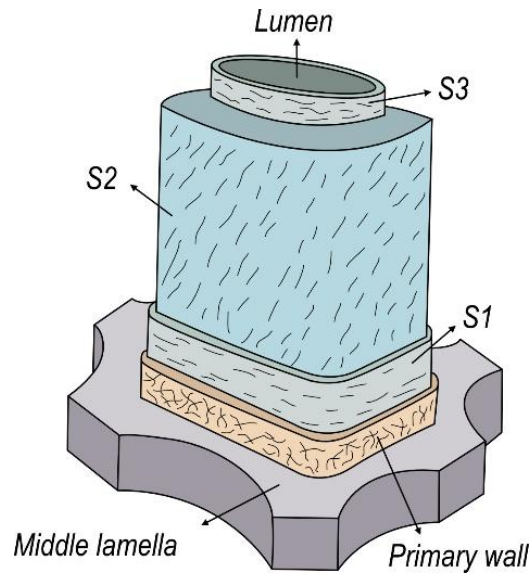


**Figure 2.5** Schematic illustration of the middle lamella and cell wall layers. Adapted from Sjöström (1993a).

The primary wall is quite thin, typically 0.1-0.2  $\mu\text{m}$  thick, and exhibits randomly oriented cellulose fibrils. Conversely, all three layers of the secondary wall feature cellulose fibrils aligned in specific angles. Both the S1 and S3 layers are thin (0.1-0.3  $\mu\text{m}$ ) and have high microfibril angles (i.e., the angle between the microfibrils and the cell axis): 50-70° for S1, and above 70° for S3. In contrast, the S2 layer is the thickest portion of the cell wall (2-5  $\mu\text{m}$ ) and exhibits low microfibril angles (5-30°) (Sjöström, 1993a; Wiedenhoef, 2005; Koch, 2006).

The outermost region shown in Figure 2.5 is the middle lamella, the extracellular layer providing adhesion between neighboring cells. Its main components are lignin (~60%) and pectin, with lignin concentrations being especially high at the cell corners. Unsurprisingly, removing the lignin from the middle lamella is one of the main goals of kraft pulping, as it allows the separation of the wood fibers. Nevertheless, the delignification of the cell wall is also significant. The behavior of the S2 layer is of particular interest during pulping, as it contains most of the xylem's lignin (63-74%), cellulose (90%), and hemicelluloses (70-80%) and largely dictates the properties of the cell wall (Wiedenhoef, 2005; Koch, 2006).

## 2.2 Kraft pulping

The kraft process, also known as sulfate process, is a well-established pulping method that accounts for about 82% of all virgin wood pulp produced globally (FAO, 2023). As a chemical pulping technique, it separates wood

fibers by lignin removal through chemical reactions that break down the lignin network. More specifically, kraft pulping accomplishes delignification by treating wood chips with white liquor – an aqueous solution containing hydroxide and hydrosulfide ions – at temperatures above 140 °C (Sixta *et al.*, 2006).

The main steps of the kraft process can be divided into woodyard operations, fiberline, and chemical recovery. The woodyard operations convert logs into wood chips of acceptable sizes and include steps such as debarking, chipping, and screening. The fiberline is the section of the process responsible for liberating cellulose fibers from wood chips. It involves treating the chips with white liquor, which leads to the degradation and/or dissolution of part of the hemicelluloses and lignin. As a result, two main streams are generated: washed kraft pulp and black liquor (i.e., spent white liquor containing dissolved wood components). In terms of its main operations, the fiberline comprises impregnation (including steaming), cooking, washing, and screening/cleaning. In the production of bleached pulp grades, bleaching operations are also included in the fiberline. Lastly, the chemical recovery system aims to regenerate the spent cooking chemicals as new cooking liquors. Additionally, it encompasses the combustion of dissolved wood components from black liquor, generating steam and electricity used in the pulp mill (Biermann, 1996b; Sixta *et al.*, 2006; Mboowa, 2024).

The impregnation and cooking operations are discussed in more detail in Sections 2.2.1 and 2.2.2.

### **2.2.1 Impregnation**

The purpose of impregnation is to transport cooking chemicals into wood chips prior to the cooking stage, ensuring they are distributed as evenly as possible both within each chip and among different chips. Hence, an efficient impregnation step is essential to increase the uniformity of delignification and minimize downstream issues, as poorly impregnated chips have been shown to result in high amounts of rejects/shives, low pulp yields, and pronounced lignin gradients in the cooked material (Gullichsen *et al.*, 1992; Malkov *et al.*, 2002; Malkov *et al.*, 2003; Brännvall, 2009). Additionally, these non-uniform effects may lead to reduced pulp strength, and even increased consumption of bleaching agents (Gullichsen *et al.*, 1992; Bacarin *et al.*, 2017).

Current best practices for impregnation involve steaming the wood chips and then treating them with white liquor and recirculated black liquor at 100-110°C for 30-40 min (Brännvall, 2009; Foelkel, 2009; Bajpai, 2015). The steaming step is often carried out with saturated steam (100-120°C) and has two main purposes: to preheat the wood chips and to remove the air entrapped in the lumens of the wood cells. The latter is of particular importance to the

impregnation efficiency, as entrapped air slows down impregnation by creating backpressure inside the chips, opposing the movement of the cooking liquors introduced in the subsequent steps (Malkov *et al.*, 2002; Sixta *et al.*, 2006). Other effects caused by steaming include changes in wood structure and composition, e.g., removal of extractives and disruption of ray parenchyma cells (Matsumura *et al.*, 1999).

The use of both white liquor and black liquor during impregnation aims to reduce heat demand, increase the content of HS<sup>-</sup> at the beginning of cooking and decrease the initial effective alkali to minimize carbohydrate losses – although the exact alkali profiling depends on process configuration (Bajpai, 2015). Still, different impregnation strategies have been suggested, such as employing high alkali concentrations (Brännvall and Bäckström, 2016) or prolonging the operation (Tavast and Brännvall, 2017). Regardless of the approach, the transport of cooking chemicals during impregnation relies on two governing phenomena: liquor penetration and diffusion. Their respective mechanisms are explained in the following sections.

### **2.2.1.1 Liquor penetration**

Liquor penetration is the movement of liquor through the lumens of wood cells due to a pressure gradient. During impregnation, this phenomenon is influenced by many different parameters. For example, the rate of penetration is affected by process conditions, in particular temperature and pressure. In addition, the amount of entrapped air inside the chips (which is related to the efficiency of the steaming process) and the properties of the liquor, including viscosity and surface tension, play a significant role (Malkov *et al.*, 2001a; Malkov *et al.*, 2001b; Sixta *et al.*, 2006).

Wood structure is also a major factor dictating the rate and uniformity of penetration. In softwoods, liquor penetration was shown to occur primarily via tracheids and resin canals, whereas in hardwoods, vessels were found to offer the preferred penetration path (Wardrop and Davies, 1961). Consequently, the arrangement of these cells causes liquor penetration to be substantially faster in the longitudinal direction of the wood chips than in the radial or tangential directions, making chip length the limiting dimension of penetration (Malkov *et al.*, 2001a).

From tracheids and vessels, liquor penetration spreads to neighboring cells via pits, besides extending laterally through rays (Wardrop and Davies, 1961). Hence, as one could expect, lumen diameter and pit structure have been found to strongly influence penetration (Singh *et al.*, 1999; Ahmed *et al.*, 2011). Additionally, factors altering the permeability of wood have been shown to affect liquor penetration. For instance, the presence of tyloses in hardwoods is known to slow down or even halt penetration (Stone and Green,

1959; Daniel, 2009; Esteban *et al.*, 2024). Furthermore, high concentrations of extractives and entrapped air make liquor penetration in heartwood slower than in sapwood (Brännvall, 2009; Malkov *et al.*, 2001b).

### **2.2.1.2 Diffusion**

Diffusion is the transport of chemicals driven solely by differences in concentration and not aided by fluid flow. It is also the only mass transport mechanism acting within the wood chips after liquor penetration is complete. Therefore, it has a direct impact on the distribution of cooking chemicals inside the chips, particularly since a significant portion of the alkali introduced during penetration is readily consumed in reactions with carbohydrates and minor wood components (e.g., in neutralization of acid groups and deacetylation) (Brännvall, 2009; Foelkel, 2009).

Like the penetration process, diffusion is also influenced by several parameters. Overall, they comprise the concentrations of the dissolved species, both in the bulk liquor and within the chips, and their effective diffusivities. These effective diffusivities depend on the chemical species and are significantly affected by process conditions (especially temperature), and wood structure.

There are several different ways to estimate the effective diffusivity of cooking chemicals (namely,  $\text{HO}^-$ ,  $\text{HS}^-$ ,  $\text{Na}^+$ , among other ionic species) in fully penetrated wood chips (Sixta *et al.*, 2006). For instance, McKibbins (1960) used experimental data to fit correlations for the diffusion coefficient of sodium across the longitudinal and transverse sections of kraft cooked chips. In these expressions, the diffusion coefficients were calculated as a function of temperature and two parameters were adjusted: the activation energy and the frequency factor. Another common approach entails correcting the diffusion coefficient of the ionic species in aqueous media by the effective capillary cross-sectional area (ECCSA), which represents the area of the paths available for diffusion (Sjöström, 1993d; Sixta *et al.*, 2006; Inalbon *et al.*, 2013). Given the anisotropic nature of wood, the ECCSA value varies in the chips, with the highest one occurring in the longitudinal direction and the lowest in the tangential direction. Nevertheless, this difference has been shown to decrease as the ECCSA values increase in elevated pH (12.5-13.5), which is likely related to the swelling of the cell walls (Stone, 1957). Similarly, increased extents of deacetylation and degradation of galactoglucomannan seem to increase ECCSA and reduce the gap between the longitudinal, tangential and radial values (Inalbon *et al.*, 2013; Montagna *et al.*, 2013). Therefore, although the effective diffusivity of an ionic species varies with direction within the wood chips, it remains of the same order of magnitude.

The small variations in effective diffusivity suggest that the characteristic diffusion time of cooking chemicals within the wood chips is largely determined by the chip dimensions. In particular, the chip thickness acts as the limiting dimension for diffusion and a key factor in ensuring uniform pulping (Brännvall, 2017; Tripathi *et al.*, 2018). On an industrial scale, the preferred chip thickness lies between 2 and 5 mm, as thinner chips are prone to greater fiber damage and thicker chips are more difficult to impregnate (Foelkel, 2009). Still, delignification experiments conducted with softwood chips indicate that a virtually uniform lignin removal could only be achieved using thin chips, i.e., thickness below 2 mm (Gullichsen *et al.*, 1992).

A factor that may influence how cooking chemicals diffuse – at least locally – is the concentration and type of ionic species present in the liquor. The hypothesis is that changes in the liquor's ionic strength could modify the Donnan equilibrium established due to the negatively charged cell walls. This, in turn, could either increase or decrease the local concentration of cooking chemicals surrounding the cell walls (Bygrave and Englezos, 2000; Bogren *et al.*, 2009b; Nieminen *et al.*, 2014).

### **2.2.2 Cooking**

The cooking step refers to the operation in which lignin is dissolved and transported out from the impregnated wood chips. In modern kraft cooking systems, the operation often relies on specific temperature and alkali profiles. Current target cooking temperatures are often in the range of 145 to 155 °C, as opposed to historically harsher conditions (e.g., 160-170 °C previously used for softwoods) (Bajpai, 2015). White liquor is usually charged at specific points during cooking, which, combined with the recirculation of black liquor, strategically controls the concentration of hydroxide and hydrosulfide ions throughout delignification. In general, the concentrations of these cooking chemicals in fresh white liquor are about 1.0-1.4 mol HO<sup>-</sup>/L and 0.20-0.28 mol HS<sup>-</sup>/L, and the liquor-to-wood ratio inside the digesters is on average 3-5 L/kg (Brännvall, 2017). Additionally, many pulping additives (e.g., surfactants) can be incorporated either during cooking or impregnation to stabilize carbohydrates, control pitch, among other functions (Bajpai, 2015).

The cooking operation is terminated when the lignin content in the chips is sufficiently low. For unbleached grades (e.g., kraftliner and sack paper), this lignin concentration can be relatively high, generally ranging from Kappa number 55 to 100, depending on the product (Brännvall and Annergren, 2009). For bleached softwood grades, the final lignin content after cooking is about Kappa number 26-35, whereas for bleached hardwood grades the content is lower. For instance, birch is typically cooked until Kappa number 17-22 (Bajpai, 2015; Brännvall, 2017). Afterwards, the cooked material is

transferred to a blow tank, where it is discharged at low pressure. Then the liberated fibers are screened and washed to remove the black liquor (Sixta *et al.*, 2006).

The next sections discuss the main mechanisms involved in lignin and carbohydrates removal during kraft cooking.

### 2.2.2.1 Delignification

Delignification is a process that involves both chemical reactions and the transport of dissolved lignin fragments out of the middle lamella and cell walls. During kraft cooking, the lignin reactions that contribute to delignification are responsible for breaking down the lignin network while introducing hydrophilic groups, generating lignin fragments that can dissolve in the cooking liquor (Potthast, 2006; Gellerstedt, 2009). Among these reactions, the cleavage of ether linkages is remarkably significant, as they constitute a large percentage of the chemical bonds in the lignin structure.

In particular, the cleavage of  $\beta$ -O-4 bonds in phenolic structures has been considered one of the most significant reactions taking place in the beginning of kraft cooking (Potthast, 2006). The main reaction pathway starts with the formation of quinone methide, as illustrated in the first step of Figure 2.6. This step involves the ionization of the phenolic residue in the  $\beta$ -aryl ether structure followed by the elimination of the substituent in the  $\alpha$ -position (Gierer, 1980).

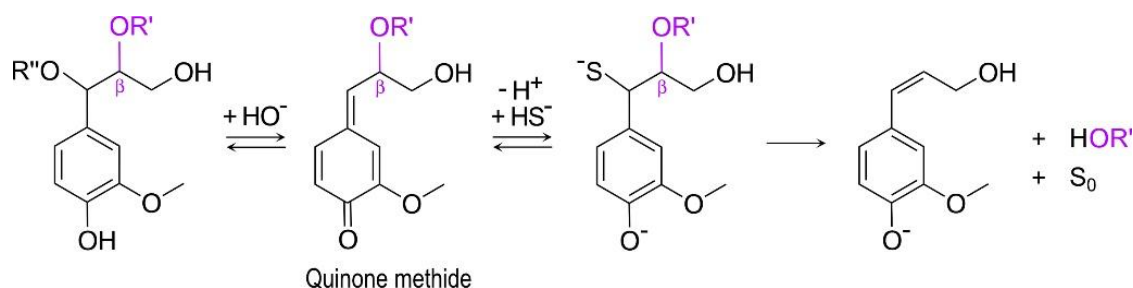


**Figure 2.6** Simplified scheme showing the formation of quinone methide intermediate and the preferred reaction pathway for cleaving  $\beta$ -O-4 bonds in phenolic lignin structures during kraft cooking.  $OR'$  is an aryl structure.  $OR''$  represents a generic substituent (e.g., aryl group, hydroxyl group, etc.). Intermediate steps are omitted.

The quinone methide intermediates then react further, which, in the case of kraft cooking, happens predominantly via addition of hydrosulfide ions in the C- $\alpha$  position (Figure 2.6). The nucleophilic attack results in the formation of benzyl mercaptide structures, which, in turn, go through an intramolecular attack at position C- $\beta$ , effectively cleaving the  $\beta$ -O-4 bonds and resulting in the formation of elemental sulfur and lignin fragments containing phenolic groups. This reaction pathway is one of the main reasons for the faster delignification rates observed in kraft pulping compared with soda pulping

(conducted with aqueous NaOH), as it proceeds relatively quickly and generates new phenolic groups that can undergo further reactions (Gierer, 1980).

Another mechanism that can lead to cleavage of  $\beta$ -O-4 bonds in phenolic structures involves the reduction of quinone methide intermediates in the presence of reducing agents, such as pulping additives, or carbohydrates-related structures. Nevertheless, this only plays a minor role during delignification (Potthast, 2006). On the other hand, competing reactions involving quinone methide intermediates include the elimination of a  $\beta$ -hydrogen or a  $\gamma$ -hydroxymethyl group. These pathways, while not as significant in kraft pulping as in soda pulping, contribute to reducing the rate of delignification and generating alkali-resistant structures (Gierer, 1980; Potthast, 2006).

The other main reaction pathway to cleave  $\beta$ -O-4 linkages occurs in non-phenolic lignin units, as shown in Figure 2.7. This reaction is considerably slower than that in phenolic structures and depends on the formation of alkoxide anions, which subsequently perform a nucleophilic attack on the  $\beta$ -carbon. The attack results in the cleavage of the ether linkage and the formation of an oxirane intermediate, which can further react through different pathways, such as the nucleophilic opening of the oxirane ring by hydroxide ions (as depicted in Figure 2.7), by hydrosulfide ions, or even by hydroxyl groups from carbohydrates (Gierer, 1980; Potthast, 2006).

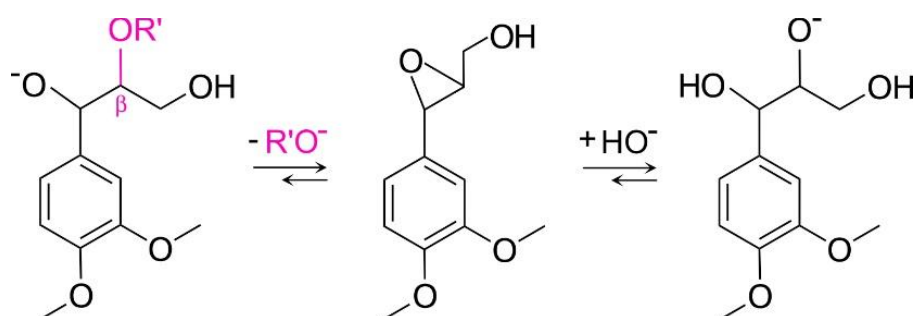


**Figure 2.7** Simplified scheme showing the main reaction pathway for  $\beta$ -O-4 bond cleavage in non-phenolic lignin structures during kraft cooking. OR' is an aryl structure.

Besides depolymerization, other relevant lignin reactions during kraft cooking include demethylation and condensation reactions. Demethylation occurs due to strong nucleophiles (e.g.,  $\text{HS}^-$ ) and removes about 5% of the methoxy groups in lignin. The reaction results in the formation of mercaptans and the introduction of new hydroxy groups on the lignin structure. Condensation reactions comprise the formation of stable carbon-carbon bonds between

lignin units, hindering delignification; however, the exact mechanisms behind these reactions and their degree of incidence during pulping are still the subject of debate (Sjöström, 1993d; Potthast, 2006; Gellerstedt, 2009).

As dissolved lignin fragments are produced across the cell wall and middle lamella, they are transported towards the bulk liquor outside the wood chip via diffusion, while continuing to undergo further chemical reactions. This transport can be quite slow, as indicated in studies reporting high concentrations – or even accumulation – of dissolved material within the pore system of wood compared to the bulk liquor (Simão *et al.*, 2011; Pakkanen and Alén, 2012; Brännvall and Rönnols, 2021). In addition, the transport of lignin seems to be significantly affected by process conditions. For example, local variations in the pH or ionic strength can alter the solubility of lignin fragments and how they interact, potentially leading to lignin aggregation or deposition onto cellulose fibers (Dang *et al.*, 2016; Kishani *et al.*, 2020; Ghaffari, 2023). Moreover, the diffusion rate depends on the size of the lignin fragments. Hence, given the heterogeneity of the lignin fragments and the series of parameters affecting their transport, estimated values for the diffusion coefficient of lignin during cooking vary substantially, with results differing by several orders of magnitude (Sixta *et al.*, 2006). These large differences can partially explain experimental data showing that the molar mass of lignin released during kraft cooking increases throughout the process (Dang *et al.*, 2016; Kron *et al.*, 2024)

Other potential aspects influencing the rate of delignification during kraft cooking are associated with the cell wall organization and the chemical structure of lignin. For instance, Whiting and Goring (1981; 1982) found that delignification occurred faster in secondary layer tissue than in middle lamella tissue of black spruce, which they suggested could be related to the higher swelling of the secondary wall (caused by the dissolution/degradation of hemicelluloses). They also proposed that the lignin present in the middle lamella could be less reactive due to its lower content of methoxy groups and potentially higher contents of condensed structures (Whiting and Goring, 1982). The degree of lignin condensation was also mentioned by Pinto *et al.* (2005b) as a potential determining factor leading to differences in the delignification rate among hardwoods, together with the average proportion between syringyl and guaiacyl lignin. The latter was examined in more detail by Santos *et al.* (2011), who compared the delignification of 10 hardwoods revealing a linear correlation between the rate of lignin removal and the S/G ratio, although birch was a noteworthy exception to this pattern.

### **2.2.2.2 Degradation and dissolution of polysaccharides**

Reactions involving carbohydrates begin quite early during pulping. Still under relatively low temperatures, reactions with hemicelluloses consume significant percentages of the total alkali typically added to the system (e.g., about 20-25% in the case of hardwoods). These reactions involve hydrolysis of acetyl groups – for instance, in glucuronoxylan – and neutralization of carboxyl groups, such as those in uronic acids and in the acetic acid released during deacetylation (Potthast, 2006; Foelkel, 2009). At higher temperatures, the alkali consumption in neutralization remains significant, as degradation products include different types of acids.

Above 80 °C, the peeling of carbohydrates is a main reaction that takes place and is one of the primary reasons for the low yields in kraft pulping. This reaction involves the consecutive removal of terminal monosaccharide units from polysaccharides. In short, it comprises the rearrangement of a reducing end into a 2-keto intermediate, followed by a  $\beta$ -alkoxy elimination, which creates a new reducing end and releases the former terminal unit. In turn, this unit is particularly unstable under alkaline conditions and is prone, among other things, to the formation of isosaccharinic acids via benzilic acid rearrangements. The peeling process is terminated when competing reactions, known as stopping reactions, stabilize the reducing end groups, for example, via conversion to metasaccharinic acid (Sjöström, 1993d; Potthast, 2006).

Peeling affects both cellulose and hemicelluloses, however, at different extents. Xylan is particularly resistant to peeling due to its arabinopyranose and 4-O-methylglucuronic acid substituents. Additionally, other minor side groups, such as rhamnose groups in C2, can also contribute to hinder xylan depolymerization. Other hemicelluloses, however, are susceptible to substantial decrease in their degrees of polymerization during peeling, which can even lead to the solubilization of the remaining chains. In the case of cellulose, the impact is less pronounced, given its high DP and crystallinity (Sjöström, 1993d; Potthast, 2006; Gellerstedt, 2009).

At high temperatures (~150 °C), alkaline hydrolysis becomes an important reaction pathway. This reaction is the main responsible for the decrease in pulp viscosity, as it leads to cleavages along the polysaccharide chain, substantially decreasing the DP. In addition, alkaline hydrolysis results in the formation of new reducing ends, which causes further peeling to take place (i.e., secondary peeling) (Gierer, 1980; Gellerstedt, 2009).

Another relevant reaction involving carbohydrates during cooking is the elimination of the methoxy group from 4-O-methylglucuronic acid. The elimination generates methanol and converts the 4-O-MeGlcA groups in xylan into hexenuronic acid (HexA) groups, which are considerably stable

under alkaline conditions. Hence, the formation of HexA has been linked to further stabilization of xylan against degradation. Moreover, the presence of hexenuronic acid also affects eventual bleaching steps, as HexA reacts with bleaching agents, such as chlorine dioxide and ozone (Jiang *et al.*, 2000; Gellerstedt, 2009).

Other mechanisms influencing the behavior of xylan throughout kraft pulping include dissolution and re-adsorption processes. During impregnation, a significant fraction of xylan is readily dissolved in the alkaline liquor. Then, with the progression of delignification, lower alkali concentrations and increasingly exposed cellulose fibers cause part of this dissolved xylan to re-adsorb (Danielsson and Lindström, 2005; Pinto *et al.*, 2005a). The degree of dissolution and re-adsorption is, of course, dependent on liquor composition and cooking conditions, but also on the characteristics of xylan. For instance, Pinto *et al.* (2005b) suggested that the higher average molar mass and the presence of specific substituents cause eucalyptus xylan to be retained to a greater extent than birch xylan during kraft pulping.

### 2.2.3 Delignification models for kraft pulping

Modeling lignin removal during kraft cooking can serve many purposes, such as process control, optimization of cooking conditions, and equipment design. Accordingly, there are several attempts to describe delignification, with approaches ranging from highly simplified concepts, like the H-factor (Vroom, 1957), to complex semi-mechanistic models (Grénman *et al.*, 2010; Gilbert *et al.*, 2021; Bijork *et al.*, 2022). Overall, in order to capture the non-uniformity of lignin removal inside wood chips, modeling efforts need to describe reaction kinetics and transport phenomena taking place in the system.

The kinetics of lignin reactions is often portrayed according to either a parallel reaction model (Smith, 1974; Andersson *et al.*, 2003; Bogren *et al.*, 2008; Bogren *et al.*, 2009a) or a consecutive reaction model (Gustafson *et al.*, 1983). The first approach is characterized by dividing lignin and other wood components into fractions with distinct reactivities or, in the case of Bogren's model, a continuous distribution of reactivity. Each fraction is described by its own reaction rate equation, which remains unchanged throughout the entire cooking process. The second approach, however, assigns different equations to describe the reaction rate of each component, depending on the extent of cooking (Nieminen and Sixta, 2012). For instance, Gustafson *et al.* (1983) considered three stages of delignification – initial, bulk, and residual – each governed by its own rate equations.

Regardless of the approach, the reaction rate equations of lignin removal are usually proportional to the lignin content, temperature ( $T$ ), and the concentrations of hydroxide and hydrosulfide ions (i.e.,  $[HO^-]$  and  $[HS^-]$ ). For

example, in the traditional Purdue (Smith, 1974) and Gustafson (Gustafson *et al.*, 1983) models this dependency can be expressed as in Equation 2.1:

$$\frac{dL}{dt} = (k_1\sqrt{T} + k_2[HO^-]^a + k_3[HO^-]^b[HS^-]^c)(L - d) \quad (2.1)$$

Where  $L$  stands for lignin,  $k_{1-3}$  can be interpreted as rate constants following Arrhenius-like equations, and  $a, b, c, d$  are constants. Other modeling efforts may consider more complex expressions and include the concentration of other ionic species (e.g., sodium or calcium) and correction factors based on lignin properties (e.g., S/G ratio) (Bogren *et al.*, 2008; Correa *et al.*, 2023).

The degradation of carbohydrates during kraft cooking also needs to be accounted for in delignification models, as it is responsible for a substantial consumption of alkali. This can be accomplished by linking the rate of carbohydrate reactions to lignin removal (Gustafson *et al.*, 1983), which requires previous knowledge about the proportionality between them (often acquired experimentally). Another strategy involves modeling the degradation of carbohydrates explicitly, using rate equations based on their concentrations, temperature, and the hydroxide content (Andersson *et al.*, 2003).

In terms of alkali consumption, the reaction rates of hydroxide and hydrosulfide ions during cooking are dependent on the rates of lignin depolymerization and carbohydrates degradation. The specific consumption factors are usually attained experimentally. Correa *et al.* (2023), for example, considered 0.05 kg HS<sup>-</sup>/kg reacted lignin, 0.21 kg HO<sup>-</sup>/kg reacted lignin, and 0.49 kg HO<sup>-</sup>/kg reacted carbohydrates.

Despite the widespread use of these kinetic models, it is worth noting that they neglect any mass transport limitations across the cell walls, which is an assumption liable to scrutiny – specially for the lignin fragments and dissolved polysaccharides (Mattsson *et al.*, 2017; Brännvall and Rönnols, 2021; Kron *et al.*, 2024). A recent approach to overcome this limitation was proposed by Kron *et al.* (2025). In their model, the reaction rates are combined with the transport of alkali and lignin fragments through the cell wall, and the diffusion coefficient of lignin is described as a function of molar mass, hydroxide content and temperature, following the Arrhenius-like equation proposed by McKibbins (1960).

On a wood chip level, recent modeling strategies combine reaction kinetics with mass transport along the chip. One simple approach based on nuclei growth in heterogeneous media was suggested by Dang and Nguyen (2008). In this case, a power law factor based on wood chip thickness was used to

correct the rate of delignification and account for the heterogeneity of the reaction. A more complex approach was suggested by Wisniewski *et al.* (1997) and Gilbert *et al.* (2021). Besides reaction kinetics, these authors modeled the diffusion of chemical species and wood components to and from different phases within the system, namely the solid wood phase, the entrapped liquor, and the bulk liquor. Another strategy was proposed by Grénman *et al.* (2010). They described delignification and carbohydrates degradation while also incorporating wood anisotropy in their model. Different rates of diffusion were considered along the length, width and thickness of the chips, which were also affected by changes in wood porosity and composition during pulping, similar to the effective diffusivity approach discussed in Section 2.2.1.2. More recently, Bijok *et al.* (2022; 2023) combined these last strategies, describing a three-phase system in which chemical species and wood components were transported according to diffusion coefficients that varied depending on the chip direction.

Although these modeling efforts improve upon the purely kinetic delignification models, some issues still need to be addressed. Validation of multidimensional and/or multiscale models can be considerably challenging, given the lack of experimental data about local conditions inside digesters and wood chips. Moreover, the data used to fit kinetic parameters is often subjected to external influences: for instance, Gilbert *et al.* (2021) used data based on kraft cooking experiments conducted with low liquor-to-wood ratios (4 to 6), which leads to significant changes in the bulk concentration of cooking chemicals throughout the process and may result in non-uniform conditions inside the digester. Additionally, the experimental data used in model development and validation may come from systems with long heating-up periods, such as 60 min (Gilbert *et al.*, 2021) or even 120 min (Gustafson *et al.*, 1983; Grénman *et al.*, 2010), during which extensive carbohydrate degradation may occur before the high temperatures required for delignification are reached. Another issue related to multiscale or multidimensional approaches is the high computational cost that is often demanded to solve these models, which can limit their applicability (Liu *et al.*, 2014). Hence, these aspects should be considered in future modeling attempts.

## 3 Material and Methods

This chapter describes the materials utilized in the project, as well as the methodology adopted to conduct the experiments discussed in Chapter 4. More detailed descriptions can be found in the appended papers (Papers I-IV). This chapter also introduces the framework used to develop the 1D multiscale model of delignification proposed in Paper V, including the key equations and their main assumptions.

### 3.1 Materials

#### 3.1.1 Chemical reagents

All chemicals were analytical grade. The molar mass distributions of lignin and xylan samples were analyzed using pullulan standards (PL2090-0100 Varian Inc., 0.180 to 708 kDa) for calibration.

#### 3.1.2 Industrial chips (Paper I)

Birch chips prepared in an industrial chipper were supplied by Södra Skogsägarna. The samples originated from southern Sweden and comprised a mix of *Betula pendula* and *Betula pubescens*. Before use, the chips were air dried and manually screened to attain a uniform fraction. These samples (Figure 3.1 a) were free of bark and knots and had thickness between 2 and

6 mm. Their final dry content was  $93.2 \pm 0.5\%$  (w/w), measured by oven-drying ( $105\text{ }^{\circ}\text{C}$ , overnight).

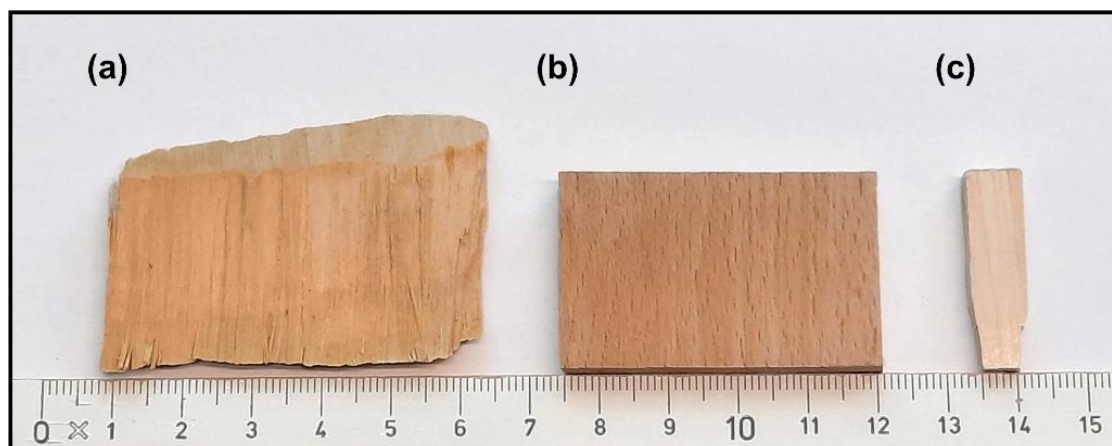


**Figure 3.1** Examples of wood samples utilized in the project. (a) Industrial chip (birch). (b) Model chip of beech. (c) Small model chip of aspen. Scale in cm.

### 3.1.3 Model hardwood chips (Papers II, III)

Logs of four different hardwoods were provided by Södra Skogsägarna, including *Alnus glutinosa* (alder,  $43 \pm 2$  years old), *Betula pubescens* (birch,  $27 \pm 1$  years old), *Fagus sylvatica* (beech,  $44 \pm 5$  years old) and *Populus tremula* (aspen,  $28 \pm 1$  years old). All logs were cut at breast height from trees grown in southern Sweden and were approximately 1 m long.

To prepare the model chips, each log was sawn to remove the bark and heartwood fractions. Then the remaining sapwood portions were cut into blocks with specific dimensions, namely  $30 \pm 1$  mm in length,  $45 \pm 1$  mm in width and  $8 \pm 1$  mm in thickness, as shown in Figure 3.1 (b). These dimensions were selected based on the upper limits used to classify industrial chips (large accepts) and to ensure repeatability when sectioning the samples after cooking (as described in Section 3.4).

Before use, the model chips were air-dried, and their final water content was determined via oven-drying ( $105\text{ }^{\circ}\text{C}$ , overnight).

### 3.1.4 Small model chips (Paper IV)

The same samples of alder, aspen and birch described in Section 3.1.3 were used to prepare the small model chips. In this case, after sawing the logs and isolating the sapwood fractions, the wood was cut into small blocks with length of  $30 \pm 1$  mm, width of  $5 \pm 1$  mm, and thickness of  $8 \pm 1$  mm at the top and  $5 \pm 1$  mm at the bottom, as indicated in Figure 3.1 (c). These specific dimensions were defined to ensure that the chips would fit the sample holder used in the *in-situ* X-ray tomography experiments (Section 3.10).

After preparation, the small model chips were air-dried to a final dry content above 89.0%, measured by oven-drying (105 °C, overnight).

## 3.2 Determination of wood chip characteristics

### 3.2.1 Chip density and porosity (Papers III, IV)

Density measurements were conducted in replicates (at least three) using air-dried model chips. First, the volume of each model chip was calculated based on their dimensions (accuracy:  $\pm 1 \text{ mm}^3$ ). Then, the chips were oven-dried at 105 °C overnight and weighed to determine their dry mass. The chip density of each wood species ( $\rho$ ) was calculated by dividing the dry mass by the chip volume.

Next, chip porosity ( $\varepsilon$ ) was calculated according to Equation 3.1:

$$\varepsilon_s = 1 - \frac{\rho_s}{\rho_w} \quad (3.1)$$

In this Equation,  $\varepsilon_s$  is the chip porosity of species  $s$ ,  $\rho_s$  is the chip density of species  $s$ , and  $\rho_w$  denotes the density of the wood substance, approximated as  $1500 \text{ kg/m}^3$ , as described by Malkov *et al.* (2001a).

### 3.2.2 Microscopy (Papers III, IV)

Microscope slides were prepared using air-dried sapwood samples of each hardwood studied in the project. First, the samples were cut into small pieces (approx.  $1.5 \text{ cm} \times 8 \text{ mm} \times 8 \text{ mm}$ ). Then, they were softened in deionized water by soaking the pieces for 10 min inside a vacuum chamber, followed by heating at 80 °C for 1-2 h. Afterwards, transverse sections ( $100\text{-}150 \text{ }\mu\text{m}$ ) of the sapwood pieces were produced with the aid of a microtome.

The sections were placed in microscope slides and covered with coverslips after one drop of deionized water was added. Optical micrographs were acquired with a light microscope (Axio Imager Z2m, Zeiss) in bright-field mode with a maximal magnification of 100x.

## 3.3 Batch kraft cooking (*ex-situ* experiments)

The kraft cooking experiments conducted in Papers I-III employed 1.5 L vessels equipped with valves to allow pressurization and evacuation during impregnation. The impregnation step was carried out at room temperature,

followed by cooking in a heating bath: the vessels, mounted on a rotating axis, were immersed in a polyethylene glycol bath regulated by a temperature controller. Previous studies (Bogren *et al.*, 2007) showed that the vessels required approximately 25 min to reach the target temperature. To halt delignification, the vessels were transferred to a cooling bath and disassembled after 10 min.

The specific steps and conditions used in the experiments are outlined in the following sections, while the rationale behind the choice of impregnation and cooking conditions is addressed in Marion de Godoy (2024).

### 3.3.1 Cooking conditions – industrial chips (Paper I)

The cooking experiments conducted with industrial chips had two main goals: to investigate how mass transport limitations within the chips can impact the process, and to assess how the composition of the impregnation liquor can affect delignification. Thus, the samples were treated with different liquors during impregnation (Table 3.1), including liquors with different concentrations of cooking chemicals (hydroxide and hydrosulfide ions) and different ionic strengths – achieved by the addition of NaCl.

**Table 3.1** Composition of the liquors used to impregnate industrial chips.

Impregnation liquor <sup>a</sup>	HO <sup>-</sup> (mol/kg liquor)	HS <sup>-</sup> (mol/kg liquor)	Na <sup>+</sup> (mol/kg liquor)
WL	0.60	0.15	0.75
WL+Na <sup>b</sup>	0.60	0.15	2.00
W	-	-	-
W+Na <sup>c</sup>	-	-	2.00

<sup>a</sup> WL = white liquor, WL+Na = white liquor with increased Na<sup>+</sup> content, W = deionized water, W+Na = deionized water with increased Na<sup>+</sup> content.

<sup>b</sup> Additional 1.25 mol NaCl/kg liquor.

<sup>c</sup> Additional 2.00 mol NaCl/kg liquor.

To perform impregnation, the chips were loaded in the cooking vessels with one of the four impregnation liquors listed in Table 3.1, using a liquor-to-wood ratio of 10:1 (w:w). The vessels were evacuated for 5 min and then pressurized with N<sub>2</sub> (5 bar) for 15 min. Afterwards, the impregnation liquor was filtered out, and fresh cooking liquor was added to the vessels. The composition of this liquor and the cooking conditions are summarized in Table 3.2.

**Table 3.2** Cooking parameters during the analysis of industrial chips.

Parameter	Value
<b>Cooking liquor, <sup>a</sup></b>	
HO <sup>-</sup> (mol/kg liquor)	0.60
HS <sup>-</sup> (mol/kg liquor)	0.15
<b>Liquor-to-wood ratio (w:w) <sup>b</sup></b>	20:1
<b>Target temperature (°C)</b>	160
<b>Cooking time (min) <sup>c</sup></b>	10, 20, 30, 60, 90, 120

<sup>a</sup> Composition in terms of effective alkali (expressed as NaOH) and sulfidity: 48% and 40%, respectively.

<sup>b</sup> Calculated based on the original mass of wood (i.e., the mass before impregnation).

<sup>c</sup> In the first time points (10 and 20 min), the cooking step was terminated before reaching the target temperature.

After the cooking step was completed, three samples were collected from each vessel. First, the bulk fraction of the black liquor (BL) was isolated via filtration. Then, part of the black liquor remaining within the cooked chips was isolated by centrifuging the wet pulps at 3500 rpm for 10 min, following the procedure reported by Brännvall and Rönnols (2021). This centrifuged fraction (CL) represented the liquor inside the pores of the wood chips during cooking. Lastly, the pulp was collected after leaching in distilled water for about 5 days, with the water replaced every other day until no further changes in pH or color were observed.

### 3.3.2 Cooking conditions – model hardwood chips (Papers II, III)

The experiments conducted with model chips aimed to assess local changes in composition inside the samples during kraft cooking and how they were affected by wood microstructure and process conditions. Notably, two sets of experiments were carried out: one set using the same liquor during the impregnation and cooking steps, and the other using different liquors to evaluate the impact of employing high alkali concentrations during impregnation. Table 3.3 describes the cooking conditions investigated in the first set of experiments.

**Table 3.3** Cooking parameters in the first set of experiments with model chips.

Parameter <sup>a</sup>	Level (-1)	Level (0)	Level (+1)
Target temperature (°C)	145	155	165
HO <sup>-</sup> (mol/kg liquor) <sup>b</sup>	0.25	0.40	0.55
HS <sup>-</sup> (mol/kg liquor) <sup>c</sup>		0.25	
Na <sub>2</sub> CO <sub>3</sub> (mol/kg liquor)		0.10	
Liquor-to-wood ratio (w:w)		22:1	
Cooking time (min) <sup>d</sup>	15, 30, 45, 60, 90, 120		

<sup>a</sup> Except for temperature and hydroxide concentration, the parameters were the same in all levels. <sup>b</sup> Composition in terms of effective alkali (as NaOH): level (-1) = 22%, level (0) = 35%, level (+1) = 48%. <sup>c</sup> Composition in terms of sulfidity: level (-1) = 100%, level (0) = 77%, level (+1) = 63%. <sup>d</sup> In the first point (15 min), the cooking step was terminated before reaching the target temperature.

All conditions in Table 3.3 were used to study the behavior of birch model chips; however, only the cooking conditions of level (+1) were applied when comparing different hardwoods.

When evaluating the use of high alkali concentrations during impregnation, the experiments followed the conditions in Table 3.4.

**Table 3.4** Cooking parameters in the experiments investigating the use of high alkali concentrations.

Parameter <sup>a</sup>	Strategy 1	Strategy 2	Strategy 3
HO <sup>-</sup> (mol/kg liquor)			
Impregnation <sup>b</sup>	0.55	2.00	2.00
Cooking <sup>c</sup>	0.55	0.55	2.00
HS <sup>-</sup> (mol/kg liquor) <sup>d</sup>		0.25	
Na <sub>2</sub> CO <sub>3</sub> (mol/kg liquor)		0.10	
Liquor-to-wood ratio (w:w)		22:1	
Target temperature (°C)		155	
Cooking time (min)		45	

<sup>a</sup> The difference between strategies 1-3 was the concentration of hydroxide ions used in the impregnation and cooking liquors. The other parameters were the same. <sup>b</sup> Composition in terms of effective alkali (as NaOH): strategy 1 = 48%, strategy 2 = 176%, strategy 3 = 176%. <sup>c</sup> Composition in terms of effective alkali (as NaOH): strategy 1 = 48%, strategy 2 = 48%, strategy 3 = 176%. <sup>d</sup> Composition in terms of sulfidity: strategy 1 = 63%, strategy 2 (impregnation) = 22%, strategy 2 (cooking) = 63%, strategy 3 = 22%.

In all experiments with model chips, four chips were loaded in each cooking vessel. In addition, the impregnation step was longer than the one described in Section 3.3.1: the evacuation and pressurization times were extended to 10 and 20 min, respectively. Similarly, the leaching time of the samples after cooking was prolonged to two weeks to ensure the removal of any traces of black liquor. No black liquor samples (BL or CL) were collected during these experiments.

### 3.4 Chip sectioning (Papers II, III)

To measure local changes in composition inside model chips, the leached cooked samples were divided into different sections, following a methodology inspired by Wojtasz-Mucha *et al.* (2017). Initially, the samples were sawn into pieces with approximate dimensions of 1 cm x 1.5 cm x 0.8 cm (length x width x thickness), as shown in Figure 3.2 (a). The pieces were classified as corners, sides (tangential or transverse) or center. Then, thin sections were sliced from each piece using a microtome (Jung AG, Heidelberg), dividing the samples into three layers (Figure 3.2 b): surface (combined thickness ~3 mm), intermediate (combined thickness ~3 mm) and center (~2 mm thick).

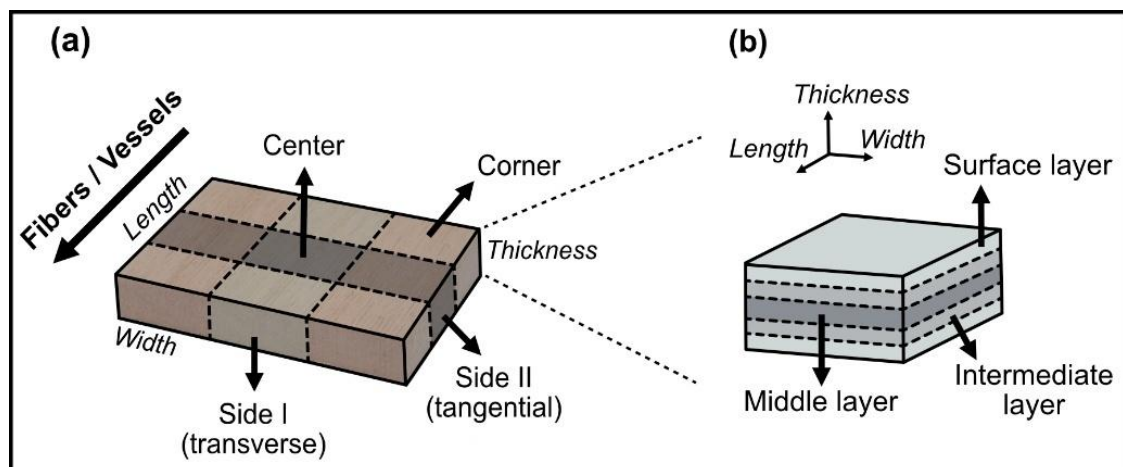


**Figure 3.2** Sectioning of model wood chips. (a) Division into different pieces/regions: corners, sides (transverse and tangential), and center. (b) Division of pieces into different layers: surface, intermediate and middle. Adapted from Papers II and III.

### 3.5 Lignin isolation from black liquor (Paper I)

Lignin was precipitated from black liquor fractions following a procedure adapted from Dang *et al.* (2016). First, concentrated sulfuric acid was added to 50 mL black liquor samples until the pH dropped to 3.0. Next, the acidified samples were left at room temperature for 2 h before being placed in a freezer overnight. Afterwards, the samples were thawed and vacuum-filtered using sintered glass filters (grade 4). The residue was washed with acidic deionized water (pH 2.5, adjusted with sulfuric acid) and then dried in an oven at 40°C for three days.

### 3.6 Xylan isolation from wood/pulp (Paper II)

To isolate xylan from sapwood and various pulps, it was first necessary to remove all lignin from the samples. This procedure was based on peracetic acid delignification, combining the methods reported by Chang and Holtzapfle (2000) and Kumar *et al.* (2013).

Initially, samples of sapwood or cooked chips (from the middle, intermediate, or surface layers, as defined in Section 3.4) were milled to a particle size of less than 1 mm and dried overnight at 105 °C. Then, the solid material was placed in a beaker and mixed with peracetic acid (5.5 g of acid: 1 g of solids). The system was diluted with deionized water to a final solids concentration of 5% (w/w) and covered with parafilm. Delignification was carried out at 25 °C for 48 h under constant stirring (300 rpm). Afterwards, the resulting holocellulose samples were collected by vacuum filtration using glass microfiber filters (Whatman GF/A 55 mm, Cytiva) and washed first with distilled water, then with a 50:50 (v/v) ethanol:acetone mixture. Lastly, the holocellulose samples were dried at 40°C for four days.

After delignification, xylan was isolated from the holocellulose samples using a procedure based on the methods described by Evtuguin *et al.* (2003), Pinto *et al.* (2005a), and Corradini *et al.* (2018). First, xylan was extracted from holocellulose using dimethyl sulfoxide (1 g of holocellulose: 60 g of DMSO). The extraction was carried out at 50 °C for 20 h under nitrogen atmosphere and constant stirring (300 rpm). Then, the solid residue was separated from the xylan-rich extract using vacuum filtration and glass microfiber filters (Whatman GF/A 55 mm, Cytiva). Next, the extract was diluted with ethanol (1:2, v/v), and concentrated acetic acid was added until a xylan suspension was formed. The suspension was left at 4 °C overnight, then centrifuged at 4500 rpm and 4 °C for 30 min (Heraeus Megafuge 40R, Thermo Scientific).

The solid fraction was collected and freeze-dried (FreeZone Triad benchtop freeze dryer, Labconco). The final xylan recovery was  $\geq 33\%$ .

## **3.7 Determination of lignin and carbohydrates (Papers I-IV)**

### **3.7.1 Klason lignin**

The Klason lignin content in wood, pulp and black liquor samples was measured after acidic hydrolysis, using adapted versions of the NREL's procedure for lignin determination (Sluiter *et al.*, 2012). The analysis was conducted in replicates (at least two).

Solid samples were initially milled to a particle size of less than 1 mm and dried overnight at 105 °C. Next, 200 mg of the dried material was transferred to a beaker, and 3 mL of sulfuric acid (72%, w/w) was added. The system was stirred with a glass rod and transferred to a vacuum chamber for 15 min. After that, the beaker was placed in a water bath (Isotemp, Fisher Scientific) at 30 °C for 1 h, and stirred with a glass rod every 20 min. Then, the beaker was removed from the bath, diluted with 84 g of distilled water, and covered with aluminum foil. The system was placed inside an autoclave (CV-EL 125/140°C, CertoClav) and left at 125 °C for 1 h. Afterwards, the autoclave was turned off and the system cooled down. When the temperature reached 80 °C, the content of the beaker was vacuum-filtered using glass microfiber filters (Whatman GF/A, diameter: 24 mm). The filtrate was diluted with distilled water up to 100 mL and used in the analysis of acid-soluble lignin and carbohydrates. The filters containing the solid residue were dried overnight in an oven at 105 °C and weighed. The Klason lignin was calculated as the difference between the mass of the filters with and without the solid residue.

Due to the small quantities of pulp available, the mass of solids was reduced from 200 mg to 75 mg when these samples were analyzed, and the amounts of acid and water were adjusted accordingly. Furthermore, pulp and wood samples were not extracted prior to hydrolysis, leading to an overestimation of the Klason lignin content. Nevertheless, as shown in the Appendix, the difference between results from extractives-containing and extractives-free samples is less than 10%; moreover, comparisons of local results within cooked chips do not seem to be compromised.

When analyzing black liquor, 10 mL of sample was transferred to a beaker and mixed with 1 mL of sulfuric acid (72%, w/w). The system was left at room temperature for 30 min and then placed in a water bath (30 °C/ 1 h), with

stirring every 20 min. Afterwards, the content of the beaker was diluted up to 20 mL with distilled water, and the system was covered with aluminum foil. The remaining steps were the same ones described for solid samples.

### **3.7.2 Acid-soluble lignin**

The filtrate solutions attained after acidic hydrolysis (Section 3.7.1) were diluted with distilled water (1:10) and then used to determine the acid-soluble lignin content in wood, pulp, and black liquor samples. The analysis was based on spectrophotometry, as described by Dence (1992). The samples were transferred to 1 cm quartz cuvettes, and their absorption at 205 nm was measured in a UV spectrophotometer (Specord 205, Analytik Jena). Absorption readings outside the 0.2-0.7 range were discarded, and the measurements were repeated after adjusting the dilution of the samples. The absorptivity constant was  $110 \text{ Lg}^{-1}\text{cm}^{-1}$  and distilled water was used as blank.

### **3.7.3 Carbohydrates**

High-performance anion exchange chromatography with pulsed amperometric detection was used to measure the concentration of carbohydrates in the filtrate samples attained in Section 3.7.1. First, the filtrate solutions were diluted with distilled water (1:10). Then, the samples were filtered in 0.2  $\mu\text{m}$  PTFE filters and transferred to 2 mL vials. The vials were analyzed in a Dionex ICS-5000 Ion Chromatography System (Thermo Fisher Scientific) equipped with a gold reference electrode and Dionex CarboPac PA1 columns: one guard column (2 x 50 mm) and one analytical column (2 x 250 mm). Detailed elution conditions are described elsewhere (Marion de Godoy, 2024).

The content of carbohydrates was expressed as anhydro sugars by correcting monosaccharide concentrations for the loss of water, as described by Jedvert *et al.* (2012), and by accounting for the yields of hydrolysis measured by Wojtasz-Mucha *et al.* (2017).

### **3.7.4 Local composition – estimate of local yield**

To determine the local concentrations of lignin and hemicelluloses inside cooked wood chips relative to the original mass of wood (i.e., g/g odw), local pulping yields had to be estimated. This was achieved by assuming that glucan was not degraded significantly during the cooking experiments – an assumption based on the low glucomannan content of the wood samples (which means the glucan came mainly from cellulose) and on the short cooking times and/or mild conditions employed. Equations 3.2 and 3.3

introduce, respectively, the expressions used to estimate pulping yields ( $\eta$ ) and to calculate local concentrations of wood components in g/g odw ( $x$ ):

$$\eta_i = \frac{G_0}{G_i} \quad (3.2)$$

$$x_i = X_i \eta_i = X_i \left( \frac{G_0}{G_i} \right) \quad (3.3)$$

In these equations,  $\eta_i$  is the pulping yield of chip section  $i$ ;  $G_0$  is the glucan concentration in the untreated wood;  $G_i$  is the glucan concentration of chip section  $i$ ;  $x_i$  is the content of a given wood component (Klason lignin, acid-soluble lignin, or anhydro sugars) in chip section  $i$ , expressed as g/g odw; and  $X_i$  is the corresponding concentration of that component in section  $i$ , expressed as g/g cooked material.

### 3.8 Determination of molar mass distribution (Papers I, II)

Gel permeation chromatography was used to determine the molar mass distributions of precipitated lignin and isolated xylan. The analysis was carried out with a PL-GPC 50 Plus Integrated Gel Permeation Chromatography system (Polymer Laboratories, Varian Inc.) equipped with three PolarGel-M columns: one guard column (50 x 7.5 mm) and two analytical columns (300 x 7.5 mm). Lignin samples were measured at 280 nm using a UV detector, while xylan samples were measured with a refractive index (RI) detector. In both cases the system was calibrated based on Pullulan standards (0.180 to 708 kDa).

The analysis was carried out in duplicates. Each sample was dissolved in mobile phase (DMSO + LiBr 10mM) overnight, followed by further dilution. The final lignin and xylan concentrations were, respectively, ~0.25 mg/mL and ~2 mg/mL. Details about the elution conditions are described elsewhere (Marion de Godoy, 2024).

### 3.9 Assessment of residual alkali and degree of penetration in wood chips (Paper III)

To assess the extent of impregnation in model wood chips, two parameters were evaluated: the degree of liquor penetration and the local residual alkali

concentration. This analysis was carried out in duplicates of model chips collected immediately after impregnation and at different points during cooking (e.g., after 30 min). The procedure was inspired by the work of Zanuttini *et al.* (2000) and began by weighing the samples before and after impregnation/cooking. Next the samples were placed in liquid nitrogen for 5 minutes and sawn into different pieces, as indicated in Figure 3.2 (a). Each piece was then leached overnight in approximately 70 mL of distilled water with continuous agitation.

The degree of penetration ( $p$ ) was calculated with Equation 3.4:

$$p(\%) = \frac{(m_t - m_0) + (m_0 w_{H2O})}{\left[ \varepsilon_s \rho_{H2O} \frac{m_0}{\rho_s} (1 - w_{H2O}) \right]} \times 100 \quad (3.4)$$

Where  $(m_t - m_0)$  is the liquor uptake, i.e., the difference between the mass of the chip after impregnation/cooking ( $m_t$ ) and its initial mass ( $m_0$ );  $w_{H2O}$  denotes the mass fraction of water in the chip before pulping;  $\varepsilon_s$  is the chip porosity from wood species  $s$ , as estimated by Equation 3.1;  $\rho_s$  is the density of chips from species  $s$ ; and  $\rho_{H2O}$  is the density of water at 20 °C.

The local residual alkali concentration inside the model chips was determined by neutralizing the leaching water obtained from each wood piece. Average local concentrations were calculated from titrations of 2-4 wood pieces using either 0.02 M or 0.2 M HCl solutions as titrants.

## 3.10 *In-situ* X-ray tomography (Paper IV)

### 3.10.1 Batch kraft cooking in small reactor

To perform *in-situ* tomography, kraft cooking experiments were conducted at a synchrotron facility using a small reactor designed by Wagih *et al.* (2022) to withstand the harsh pulping conditions and, at the same time, allow high transmission of X-rays and easy assembly. The main components of the reactor are illustrated in Figure 3.3 (a).

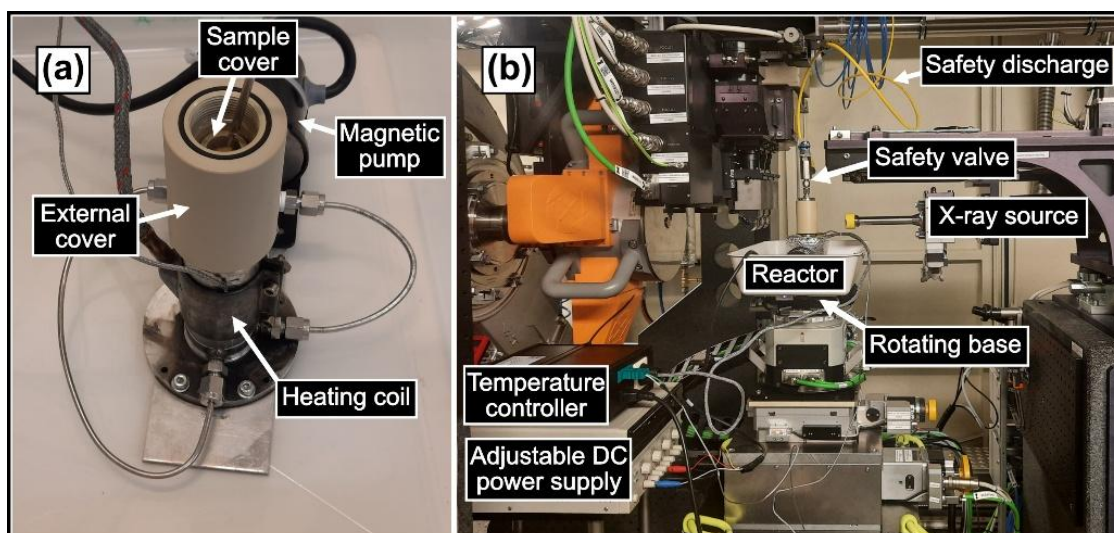


**Figure 3.3** Small reactor for *in-situ* tomography. (a) Open cell highlighting the main components. (b) Reactor mounted at the ForMAX beamline. Adapted from Paper IV.

The experiments were carried out in duplicates at the MAX IV Laboratory (Lund, Sweden). Initially, the reactor was assembled by placing one small model chip (Figure 3.1 c) in the sample holder, which was then enclosed by the sample cover and the external cover. Cooking liquor was added until the sample cover was fully submerged. Next, the system was purged to remove large air bubbles, and the safety valve was attached. The reactor was then moved to the ForMAX beamline, where it was mounted (Figure 3.3 b).

To start the cooking experiment, the pump and the temperature controller were switched on. Each sample was cooked for 4 hours, during which fifteen tomography measurements were conducted, as described in Section 3.10.2. The composition of the liquor and the cooking conditions are summarized in Table 3.5. However, it must be noted that the temperature of the system varied between 135 and 150 °C, as liquor circulation was interrupted whenever the reactor was exposed to the X-ray beam. Also, no pre-steaming or separate impregnation steps were performed.

**Table 3.5** Cooking conditions and white liquor composition.

Parameter	Value
<b>Cooking liquor, <sup>a</sup></b>	
HO <sup>-</sup> (mol/kg liquor)	0.55
HS <sup>-</sup> (mol/kg liquor)	0.25
Na <sub>2</sub> CO <sub>3</sub> (mol/kg liquor)	0.10
Liquor-to-wood ratio (w:w)	~90:1
Target temperature (°C) <sup>b</sup>	141

<sup>a</sup> Composition in terms of effective alkali (expressed as NaOH) and sulfidity: 198% and 63%, respectively. <sup>b</sup> Achieved in 10 min.

### 3.10.2 Image acquisition

Each small model chip was measured fifteen times during the kraft cooking experiment. The local tomography measurements covered a nominal field-of-view of 1.1 mm x 0.7 mm<sup>2</sup> in the middle of the chip. The first seven measurements occurred every 10 min to capture liquor penetration and the beginning of delignification. The last eight acquisitions took place every 15 min to minimize radiation damage.

While the samples were scanned, the pump connected to the reactor was switched off to prevent motion-induced artifacts. During acquisition, the rotation stage was rotated through 180°, with scans recorded at 0.1° increments, resulting in 1800 projections. An exposure time of 10 ms was used and the beam energy was 22.5 keV. The detection system provided an effective pixel size of 0.65 x 0.65 μm<sup>2</sup>.

### 3.10.3 Image reconstruction and processing

To apply phase contrast, phase retrieval was conducted prior to image reconstruction using  $\alpha_{\text{regularization}} = 0.001$  and a sample-to-detector distance of 1 cm. The subsequent reconstruction was implemented in *TomoPy* (Gürsoy *et al.* 2014) employing the Gridrec algorithm (Dowd *et al.* 1999; Rivers 2012). The resulting 3D images were realigned using zero-normalized correlation routines and then Gaussian-filtered to reduce noise.

Additional image processing was carried out to measure sample properties (e.g., porosity and cell wall thickness) and to follow the spatial evolution of cell wall separation. These analyses were carried out using *ImageJ-Fiji* (Schindelin *et al.* 2012), as outlined below:

Porosity and cell wall measurements: First, each 3D image was segmented (binarized) into two categories, namely cell walls and pores, using the *Trainable Weka Segmentation* plugin (Arganda-Carreras *et al.* 2017). Next, the binary images were corrected to remove unconnected regions and outliers. Then, the porosity of the sample was estimated by computing the percentage of dark voxels within the binary volume, with an estimated error of 5%. To measure cell wall thickness, the binary images were analyzed using the *Local Thickness* plugin (Dougherty and Kunzelmann 2007), with no distinction between the different types of cells. The results were reported as either double wall thickness – distance between two lumens measured before cell wall separation – or single wall thickness – distance between lumen and extracellular space measured after cell wall separation.

Evolution of cell wall separation: Initially, all reconstructed images under investigation were realigned locally to allow reliable comparisons. Next, the

analysis was performed examining changes in grayscale levels between the reconstructed volumes and a reference (the first volume acquired after complete liquor penetration). The changes were calculated by subtracting the reference from each volume and then applying a mask (the segmented reference). Additionally, the evolution of grayscale levels was also measured along the cell wall thickness. In this case, the *MorphoLibJ* plugin (Legland *et al.* 2016) was used to generate a distance field based on the segmented reference, which was then used to calculate local grayscale averages in each reconstructed volume.

### 3.11 Modeling (Paper V)

A multiscale one-dimensional model was developed to describe the delignification of the least accessible fibers in wood chips during kraft cooking. The approach coupled radial diffusion of alkali across the chip thickness (macroscale) with the delignification model proposed by Kron *et al.* (2025), which considers diffusion and reactions at the cell wall level (microscale).

The model was solved by linking the two scales (Figure 3.4): the relative lignin removal for each element at the macroscale was set equal to the lignin loss calculated for a single fiber at the microscale. The predicted results were then validated against delignification data from kraft cooking experiments on birch model chips.

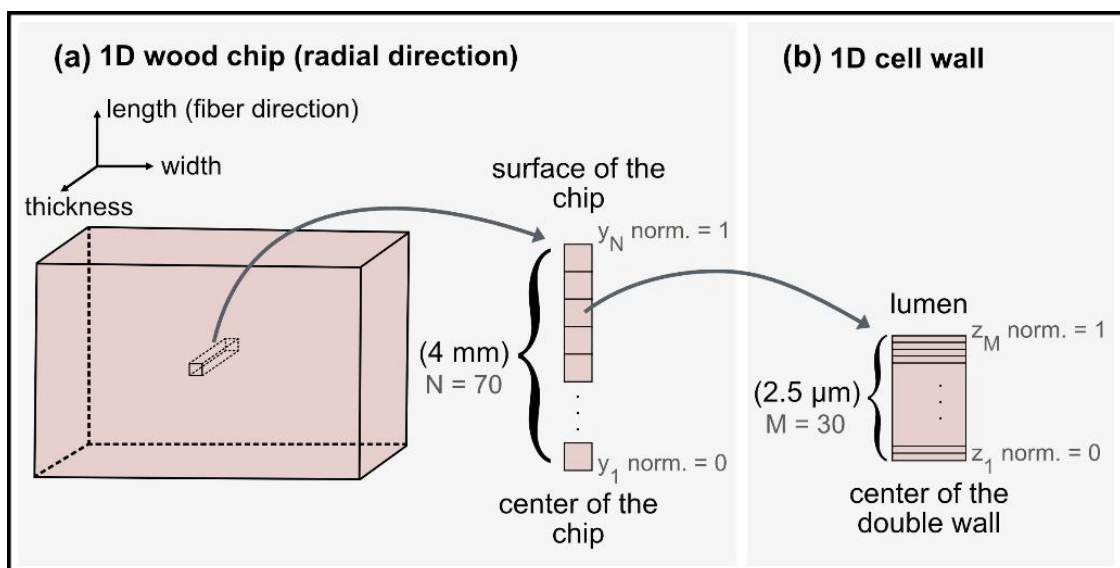


**Figure 3.4** Different scales considered in the model. (a) Radial direction in the center of the model wood chip. (b) Fiber wall. Discretization: wood chip = 70 elements; fiber wall = 30 elements. Adapted from Paper V.

### 3.11.1 General assumptions

Building on the work of Kron *et al.* (2025), most of the assumptions utilized in their cell wall model were also considered in the multiscale approach. Additional assumptions included:

- (a) The lignin content at the wood chip ( $L_C$ ) was the sum of the two lignin fractions at the fiber wall, i.e., the “bound” lignin ( $L_S$ ) and the dissolved lignin ( $L_D$ ).
- (b) As the impact of  $\text{HS}^-$  was not considered explicitly in the cell wall delignification rate, the diffusion of cooking chemicals at the wood chip level considered hydroxide ions only.
- (c) The diffusion of dissolved lignin at the macroscale was not included in the model, as the dissolved lignin outside the cell wall is assumed to be removed from the samples when leaching/washing the pulp.
- (d) The temperature across the model geometries was assumed to be spatially uniform and equal to that of the bulk cooking liquor.

### 3.11.2 Macroscale modeling

At the macroscale level, two equations were used to describe the behavior of the system. The first one (Equation 3.5) defined the lignin content at a given position of the wood chip ( $L_C$ ) as the average lignin content at the corresponding fiber wall:

$$\frac{\partial L_C}{\partial t} = \frac{\partial \overline{L_S}}{\partial t} + \frac{\partial \overline{L_D}}{\partial t} \quad (3.5)$$

In which  $\overline{L_S}$  and  $\overline{L_D}$  denote the average values of bound and dissolved lignin across the fiber wall (respectively), and  $t$  is the time.

The second equation (Equation 3.6) described the behavior of hydroxide ions at the wood chip level ( $OH_C$ ):

$$\frac{\partial OH_C}{\partial t} = D_{OH_C} \frac{\partial^2 OH_C}{\partial y^2} - \left( \frac{\partial \overline{OH_w}}{\partial t} - \beta \frac{\partial \overline{L_S}}{\partial t} \right) \left( \frac{1}{\varepsilon} - 1 \right) \quad (3.6)$$

In this expression,  $\overline{OH_w}$  denotes the average hydroxide concentration across the fiber wall,  $y$  is the position along the thickness of the chip,  $\varepsilon$  is the wood chip porosity,  $\beta$  is the alkali consumption factor, and  $D_{OH_C}$  is the effective hydroxide diffusivity.

The alkali consumption factor ( $\beta$ ) was calculated based on Equation 3.7, which accounts for the hydroxide lost during delignification (in reactions with both  $L_S$  and  $L_D$ ) and during carbohydrate reactions:

$$\beta = \frac{(0.21 + 0.49\alpha)\rho_w L_0}{M_{NaOH}} \quad (3.7)$$

Here, 0.21 and 0.49 are empirical coefficients corresponding to 0.21 g of NaOH consumed per gram of lignin reacted and 0.49 g of NaOH consumed per gram of carbohydrates reacted, respectively. Additionally,  $\rho_w$  is the density of the wood substance,  $M_{NaOH}$  is the molar mass of sodium hydroxide and  $L_0$  is the initial concentration of lignin in the chip. The variable  $\alpha$  denotes the ratio of carbohydrates to lignin in the pulp. This ratio changed during cooking and was determined experimentally.

The effective diffusivity of hydroxide in the radial direction of the wood chip ( $D_{OH_C}$ ) was calculated using Equation 3.8:

$$D_{OH_C} = ECCSA \times D_{OH,free} \quad (3.8)$$

Where the local effective capillary cross sectional area ( $ECCSA$ ) was a function of  $OH_C$  and was estimated based on the data reported by Stone (1957).  $D_{OH,free}$  is the corrected diffusivity of sodium hydroxide in water at infinite dilution, which was calculated according to Poling *et al.* (2001).

To solve Equations 3.5 and 3.6, the initial value of  $L_C$  was 0.94, calculated based on the lignin content remaining in the chips after removal of the easily dissolved fraction. In addition, different initial hydroxide concentrations ( $OH_0$ ), ranging from 0.06 M to 0.55 M, were used as the initial value of  $OH_C$ . Regarding the boundary conditions of Equation 3.6, they included symmetry at the middle of the chip and outward diffusion of alkali at the chip surface.

### 3.11.3 Microscale modeling

At the microscale, the model describes the bound lignin ( $L_S$ ), the dissolved lignin ( $L_D$ ), and the hydroxide concentration in the fiber wall ( $OH_W$ ), as defined by Equations 3.9-3.11:

$$\frac{\partial L_S}{\partial t} = -r_L \quad (3.9)$$

$$\frac{\partial L_{D,i}}{\partial t} = D_{L_{D,i}} \frac{\partial^2 L_{D,i}}{\partial z^2} + r_L w_i, \quad i = [1, 2, \dots, 7] \quad (3.10)$$

$$\frac{\partial OH_w}{\partial t} = D_{OH_w} \frac{\partial^2 OH_w}{\partial z^2} - r_L \beta \quad (3.11)$$

In which  $r_L$  is the intrinsic reaction rate accounting for all reactions leading to lignin solubilization, the subscript  $i$  denotes one among seven dissolved lignin fractions with specific sizes,  $D_{L_D,i}$  is the effective diffusivity of dissolved lignin fraction  $i$ , and  $w_i$  is the mass fraction of said dissolved lignin fraction. The detailed definition of these parameters is provided by Kron *et al.* (2025).

Still in Equations 3.10 and 3.11,  $z$  is the position along the cell wall thickness, and  $D_{OH_w}$  is the diffusivity of hydroxide in the cell wall, which was calculated considering the temperature dependence suggested by McKibbins (1960).

To solve the microscale equations, the same logic used at the macroscale was applied to define the initial conditions:  $L_S$  was set to 0.94,  $L_D$  to 0, and  $OH_w$  to  $OH_0$ . The boundary conditions assumed symmetry at  $z = 0$  and outward diffusion of alkali and dissolved lignin at the interface between cell wall and lumen.

## 4 Results and Discussion

This chapter summarizes the key findings of the project, covering results reported in the appended papers/manuscripts (Papers I-V). Initially, a brief characterization of the hardwood chips studied in the project is presented, including chemical composition, as well as structural properties. Then, the behavior of the chips during kraft pulping is compared. First, the focus is on the impregnation step. A detailed description of liquor penetration in hardwoods is provided, followed by a discussion of how impregnation affects the subsequent delignification, considering the influence of liquor composition and wood morphology. Next, the kraft cooking step is examined. Microstructural changes happening during cooking are analyzed, and the uniformity of lignin removal in different hardwoods is compared. The behavior of xylan throughout the process is also discussed. Additionally, the effect of cooking conditions, namely temperature and alkali content, is assessed. Finally, the potential to describe the delignification of wood chips using the simplified multiscale model developed in this work is evaluated.

### 4.1 Hardwood chips: composition and structural characteristics

Table 4.1 presents the composition of the wood samples used as model chips in the project, expressed as Klason lignin, acid-soluble lignin (ASL) and carbohydrates. The results agree with data found in literature (Pettersen,

1984; Gabrieli *et al.*, 2000; Patt *et al.*, 2006; Santos *et al.*, 2011; Kron *et al.*, 2024), although the reported values can vary depending on quantification methods and on intrinsic characteristics of the samples (e.g., place of origin, growth conditions, age, etc.).

In the context of this work, understanding the differences in the contents of Klason lignin, xylan, mannan, and glucan among the samples is particularly important. Beech and alder showed higher Klason lignin concentrations than aspen and birch, which, while not necessarily affecting the delignification rate, indicates these hardwoods probably require longer cooking times to reach the defibration point, as more lignin needs to be removed. The relatively high content of mannan in aspen compared to the other samples is also noteworthy, as it hints at a higher concentration of glucomannan, a component that is more readily degraded during cooking than xylan and cellulose. Lastly, the glucan-to-xylan ratio in the samples is of interest, as it reflects, to some extent, the ratio between cellulose and hemicelluloses. Among the hardwoods under study, birch had the highest concentration of xylan, whereas aspen had the highest amount of glucan.

**Table 4.1** Composition of the hardwoods investigated in this project (sapwood, dry basis).

<b>Composition <sup>a</sup></b> <b>(%, w/w)</b>	<b>Alder</b> <b><i>A. glutinosa</i></b>	<b>Aspen</b> <b><i>P. tremula</i></b>	<b>Beech</b> <b><i>F. sylvatica</i></b>	<b>Birch</b> <b><i>B. pubescens</i></b>
Klason lignin	24.9 ± 0.4	19.6 ± 0.6	21.3 ± 0.1	19.3 ± 0.4
ASL	3.5 ± 0.0	5.1 ± 0.1	5.2 ± 0.1	5.3 ± 0.1
Carbohydrates				
Glucan	40.0 ± 0.6	43.0 ± 0.8	36.4 ± 0.4	37.0 ± 0.2
Xylan	17.6 ± 0.2	16.5 ± 0.3	20.6 ± 0.4	23.2 ± 0.2
Arabinan	0.4 ± 0.0	0.3 ± 0.0	0.4 ± 0.0	0.3 ± 0.0
Galactan	1.0 ± 0.0	0.5 ± 0.0	0.6 ± 0.0	0.8 ± 0.0
Mannan	1.6 ± 0.1	3.0 ± 0.2	2.0 ± 0.1	2.3 ± 0.1
<b>TOTAL</b>	<b>89.0 ± 0.8</b>	<b>88.0 ± 1.1</b>	<b>86.5 ± 0.6</b>	<b>88.2 ± 0.5</b>

<sup>a</sup> Minor components, such as extractives and ash, were not analyzed.

Other relevant characteristics of the model chips are given in Table 4.2, such as the water content. The results show similar moisture levels in all hardwood samples, although slightly higher averages were measured in beech. The range of measurements also indicates that the water content in the samples was fairly stable throughout the project, ensuring consistent conditions for the pulping experiments.

**Table 4.2** Water content and structural characteristics in the air-dried model chips.

<b>Characteristic</b>	<b>Alder <i>A. glutinosa</i></b>	<b>Aspen <i>P. tremula</i></b>	<b>Beech <i>F. sylvatica</i></b>	<b>Birch <i>B. pubescens</i></b>
Water content (% w/w)	5.9-9.7	5.9-8.8	9.7-10.9	5.3-10.1
Density (kg/m <sup>3</sup> )	500 ± 15	428 ± 27	603 ± 18	575 ± 01
Porosity (%)				
density-based <sup>a</sup>	66.7 ± 1.0	71.5 ± 1.8	59.8 ± 1.2	61.7 ± 0.0
Image-based <sup>b</sup>	65.4 ± 3.3	68.5 ± 3.4	-	56.6 ± 2.8
Fiber <sup>c</sup>				
double wall (µm)	7.1 ± 1.8	7.2 ± 1.9	-	7.4 ± 1.7
lumen (µm)	12.7 ± 4.0	11.4 ± 3.4	-	11.5 ± 2.7

<sup>a</sup> Estimated considering the density of the wood substance = 1500 kg/m<sup>3</sup>.

<sup>b</sup> Estimated based on tomography measurements. Standard deviations calculated based on the estimated error of segmentation (5%).

<sup>c</sup> Double wall and lumen diameter were determined via tomography. Standard deviations calculated based on the distribution of values measured in segmented volumes.

Regarding structural characteristics, Table 4.2 highlights significant differences in density and porosity among the hardwood chips. These measurements concur with literature data (Patt *et al.*, 2006; Kiaei and Moya, 2015; Ruffinatto and Crivellaro, 2019) and reflect the distinct microstructural features in each wood species. For example, the low porosity observed in beech likely results from its thicker fiber walls and reduced vessel and lumen sizes compared to those of the other hardwoods, as shown in Figure 4.1. At the opposite end, the high porosity of aspen probably originated from slightly larger vessels than those in alder and from a higher frequency of vessels than in birch. In this case, lumen diameter and cell wall thickness appear to have had only a minor impact, as Table 4.2 indicates no significant differences among these hardwoods. Closer inspection of Figure 4.1 also reveals specific features in alder and beech that further distinguish them from aspen and birch: alder exhibits aggregate rays, while beech has rays that are wider than its vessels, as usually found in this species (Ruffinatto and Crivellaro, 2019).

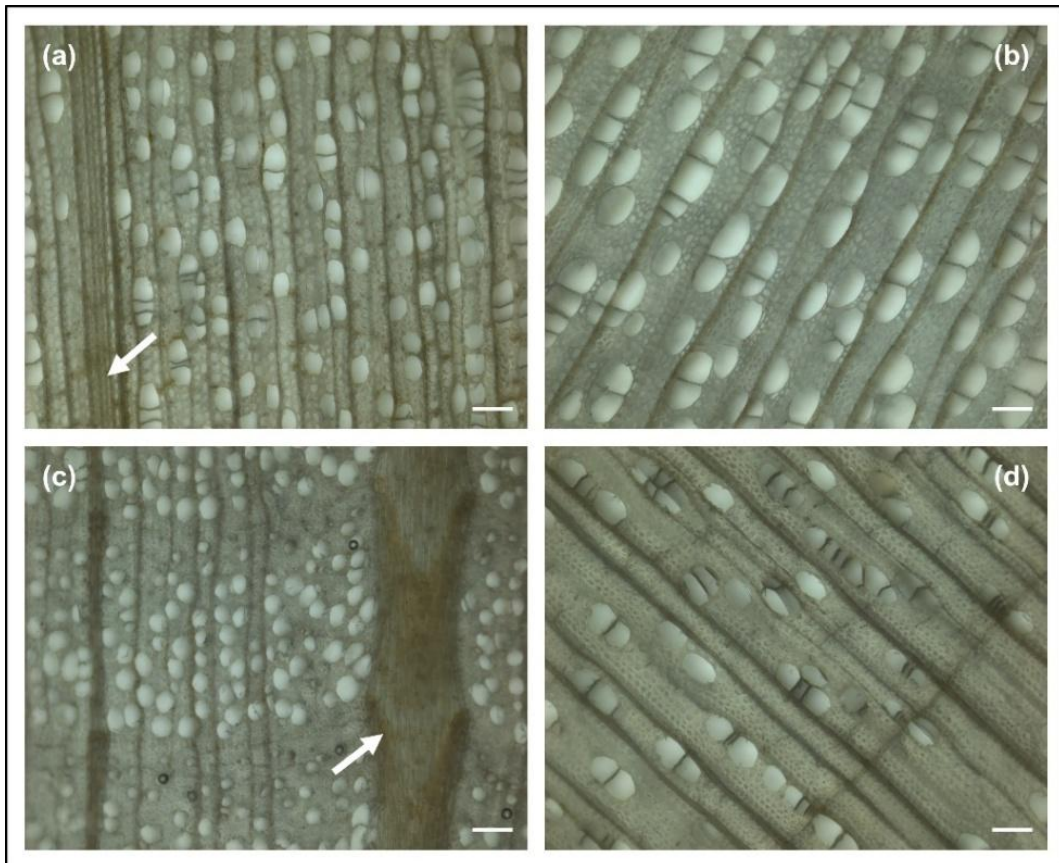


**Figure 4.1** Transverse sapwood sections of the four hardwoods under study. Scale bar = 100  $\mu\text{m}$ . (a) Alder with arrow indicating aggregate rays; (b) aspen; (c) beech with arrow indicating large ray; (d) birch. Adapted from Supplementary Material – Paper III.

## 4.2 Kraft pulping of hardwood chips: impregnation

### 4.2.1 Liquor penetration and the impact of microstructural features during impregnation

As mentioned in Chapter 2, liquor penetration is one of the main mass transport mechanisms taking place during the impregnation of wood chips. A high degree of penetration is essential to avoid undercooked chips during kraft pulping, reduce the amount of rejects, and increase the uniformity of lignin removal (Stone and Green, 1959; Gustafson *et al.*, 1989; Brännvall, 2018). Hence, this project revisited the penetration of kraft liquor in hardwoods, comparing how the penetration occurs in small model chips of different species (as the ones described in Section 3.1.4). Moreover, the experiments applied *in-situ* imaging to follow the process on a single sample from beginning to end, and to minimize artifacts from sample preparation. The comparison of liquor penetration in hardwoods with distinct porosities is illustrated in Figure 4.2, which shows the progression of penetration in the

center of birch chips (Figure 4.2 a-c, representing low porosity) and aspen chips (Figure 4.2 d-f, representing high porosity). At the start of the process, the same behavior was observed in both species. The rays were the first cells to be filled with liquor, together with a few vessels, as indicated by the arrows in Figure 4.2 (a,d). As time went by, penetration spread to adjacent cells. Interestingly, Figure 4.2 (b,e) suggests that rays provide a poor pathway for cross penetration, since fibers closer to vessels were filled with liquor faster. This trend can be seen by comparing the areas highlighted in green and pink in Figure 4.2 (b,e): fibers close to rays (green rectangles) have empty lumens, whereas fibers close to vessels (pink circles) are filled with liquor. These observations agree with the findings of Wardrop and Davies (1961), who identified vessels as the primary pathway for penetration in hardwoods during kraft pulping. In addition, the hindered passage of liquor from rays to fibers seems to reinforce the importance of pits in liquor distribution, as their number, size and structure may explain the more efficient penetration via vessels (Singh *et al.*, 1999; Carlquist, 2007; Ahmed and Chun, 2011).

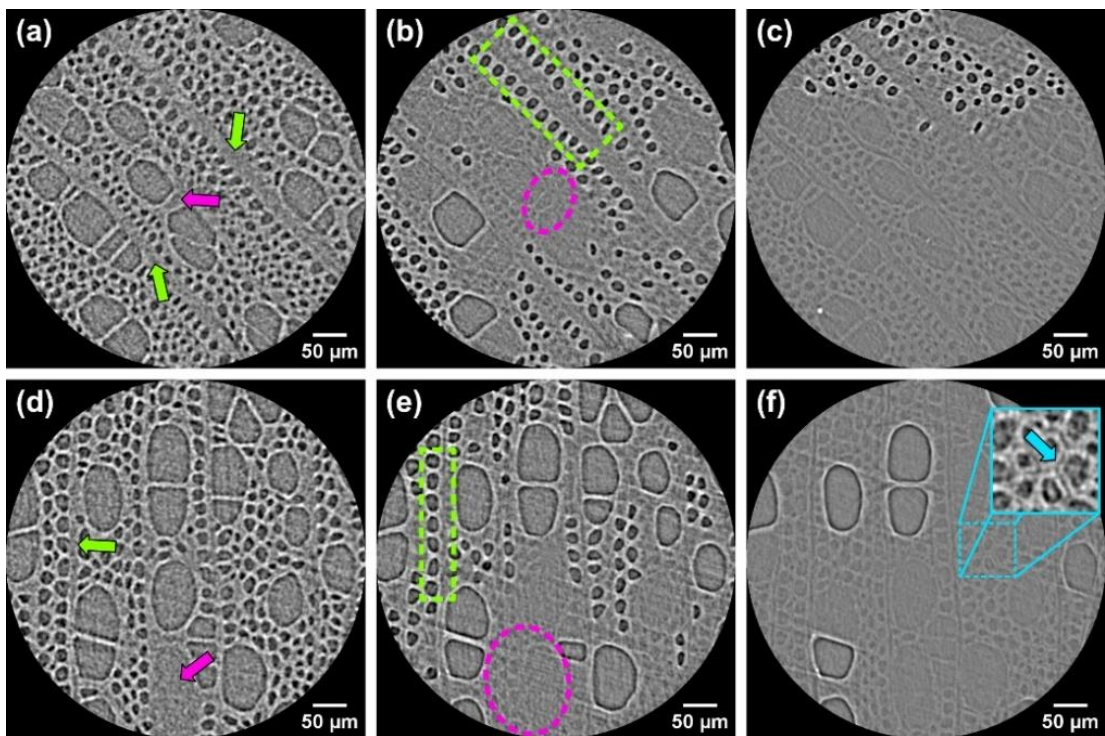


**Figure 4.2** Penetration of kraft liquor in the center of hardwood chips observed via 2D slices of reconstructed CT images. (a)-(c) Birch chip after 15, 29, and 43 min of pulping (141 °C). (d)-(f) Aspen chip after 24, 39, and 67 min of pulping (141 °C). The regions filled with liquor appear with lower contrast. In images (a) and (d), the green and pink arrows indicate, respectively, some of the first rays and vessels to be filled. In images (b) and (e) the highlighted areas in green and pink indicate fibers adjacent to a ray (rectangles) and a vessel (circles). In (f), the magnified area shows the beginning of cell wall separation. Adapted from Paper IV.

At the end of the penetration process (Figure 4.2 c,f) the last cells to be filled with liquor differed between the hardwoods: in birch they were fibers, whereas in aspen they were vessels. Furthermore, the aspen chip required more time to be completely penetrated: approx. 1.4 h against 1 h for birch. These differences suggest that hardwoods with high porosity demand extended impregnation times, as they require larger intake of liquor and the removal of more entrapped air (if steaming is not conducted effectively). However, the higher porosity can also mean more contact points between fibers and vessels, which, combined with differences in capillarity between these cells, might explain why the fibers were filled before all vessels in aspen. Additionally, the longer time for complete penetration does not appear to delay delignification, since aspen experienced the beginning of cell wall separation even before all vessels were filled, as seen in the zoomed-in area in Figure 4.2 (f).

The overall behavior outlined in this experiment – specifically the influence of wood microstructure on liquor penetration – should also apply to the impregnation step in the fiberline, albeit with a different penetration rate. In the case of chips prepared in an industrial chipper, the presence of cracks is expected to speed up liquor penetration (Gustafson *et al.*, 1989). Similarly, steaming should aid liquor penetration by removing entrapped air, thereby lowering the back pressure during impregnation (Malkov *et al.*, 2001b).

#### **4.2.2 Impregnation of model chips**

After investigating the impact of morphological features in the progression of liquor penetration, the following experiments analyze the performance of impregnation in hardwoods with low and high porosity. Once more, model chips of birch and aspen are used as examples. Figure 4.3 presents a comparison between their degree of penetration, liquor uptake and concentration of hydroxide ions at two points of the process: right after impregnation, and after impregnation followed by 30 minutes of kraft cooking.

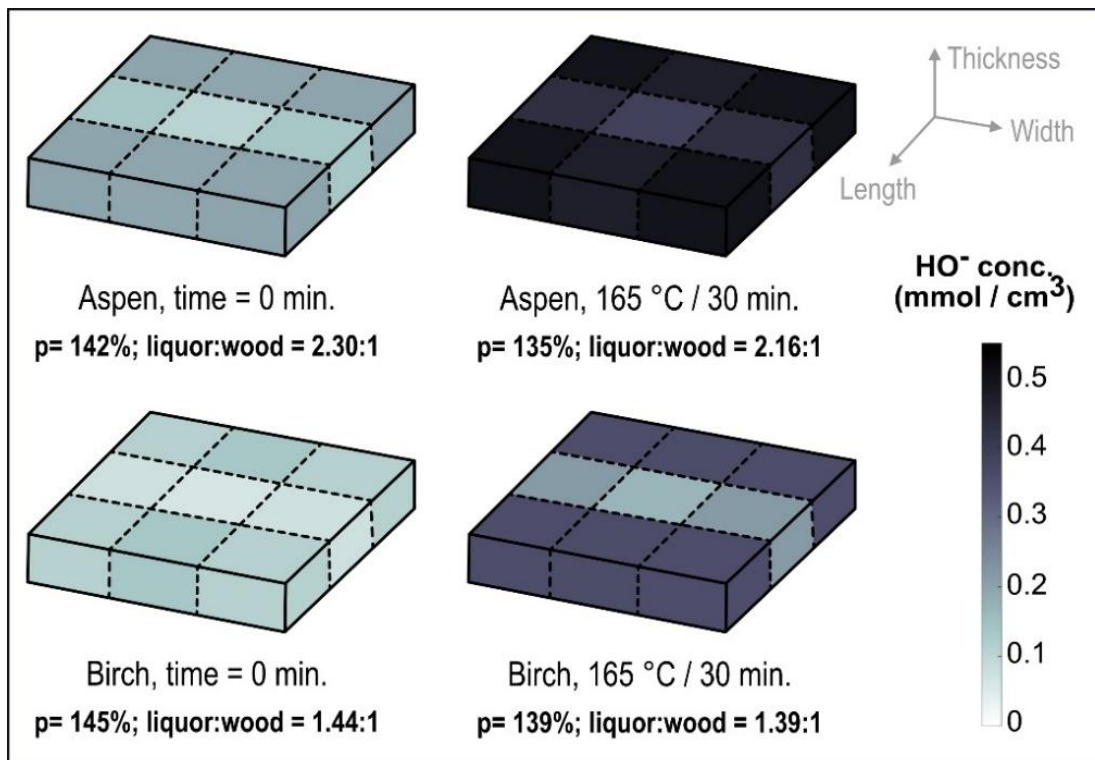


**Figure 4.3** Degree of liquor penetration ( $\rho$ ), liquor uptake and distribution of hydroxide ions in model wood chips of aspen and birch. The measurements were conducted after impregnation (20 °C, time = 0 min.) and after impregnation followed by kraft cooking (165 °C / 30 min). The results are in mmol of hydroxide ions per volume of impregnated wood. Max. RSD = 18%. Adapted from Paper III.

In these experiments, impregnation was conducted at room temperature (20 °C) and included a partial vacuum stage (10 min) followed by an overpressure stage (5 bar N<sub>2</sub> / 20 min), thus aiding liquor penetration by minimizing and offsetting the back pressure caused by entrapped air. Accordingly, the results regarding the degree of penetration showed high efficiency of liquor penetration inside the samples; moreover, the chips were filled to similar extents, regardless of their porosity. This observation reinforces the importance of overcoming the back pressure raised by the air inside the chips, and it shows that the time for complete penetration of highly porous hardwoods (like aspen) can be reduced when applying steaming or other strategies to remove the entrapped air.

The impact of wood porosity, however, is clear when comparing the proportion between the mass of liquor and the mass of solid wood inside the chips. On average, this proportion was 57% higher in aspen than in birch, which partially explains the differences in alkali distribution inside these samples. After impregnation, the average concentration of hydroxide ions in the aspen chip was almost twice the one in birch: about 0.17 mmol/cm<sup>3</sup>

against  $0.10 \text{ mmol/cm}^3$ . More importantly, these concentrations were remarkably low compared to the content of alkali in the liquor (approx.  $0.57 \text{ mmol/cm}^3$ ), which suggests a fast intake of  $\text{HO}^-$  during impregnation, even at room temperature. This initial consumption was most likely associated with the neutralization of acidic groups in hemicelluloses and extractives (e.g., the 4-O-methylglucuronic acid in xylan). Also, these results indicate that, at this stage, the diffusion of hydroxide between the surface and the center of the chips was insufficient to counterbalance the alkali consumption.

After 30 minutes of kraft cooking, the average hydroxide concentration inside the chips increased. This was a result of more alkali being transported inwards with time, combined with increasingly higher rates of diffusion due to further swelling of fibers and extensive removal of wood components. Furthermore, the rate of alkali consumption at the cell wall level changed during the process. At first, the rise in temperature likely accelerated alkali-consuming reactions; however, as cooking progressed, many of these reactions – such as neutralization of acidic groups formed during peeling of hemicelluloses – ceased or slowed down, thus decreasing the rate of  $\text{HO}^-$  consumption (Sjöström, 1993d).

Still, the differences in alkali distribution between the hardwoods were even more pronounced than after impregnation. In aspen, the hydroxide concentration not only increased but also became more uniform across different parts of the chip. In birch, on the other hand, the alkali content increased more in the corners and transverse sides than in the center and tangential sides of the chip. This uneven behavior in the birch sample hints that the initially low hydroxide concentrations in the least accessible parts of the chip might have led to a near depletion of alkali in these regions, which was probably avoided in aspen due to the higher initial availability of ions after impregnation. In addition, this difference between the alkali distribution in aspen and birch could be related to distinct radial effective diffusivities of  $\text{HO}^-$  in the two species.

Given the results in Figure 4.3, it is evident that ensuring the same degree of liquor penetration in hardwoods with different porosities is not enough to guarantee a similar distribution of alkali within their chips during pulping. Hence, when dealing with low porous species, different impregnation conditions should be considered to avoid depleting most of the hydroxide in the liquor during penetration and to allow sufficient diffusion of alkali before the cooking step (when the delignification rate becomes significant). For example, one can consider extending the impregnation time or increasing the hydroxide concentration in the impregnation liquor.

The impact of the impregnation conditions in birch and aspen was further explored by comparing three pulping strategies: 1) impregnation and cooking steps utilizing kraft liquor with 0.55 mol HO<sup>-</sup>/kg; 2) impregnation with kraft liquor containing 2.00 mol HO<sup>-</sup>/kg, followed by cooking using liquor containing 0.55 mol HO<sup>-</sup>/kg; 3) impregnation and cooking steps utilizing kraft liquor with 2.00 mol HO<sup>-</sup>/kg. The strategies were evaluated based on their effect on the uniformity of lignin removal, as shown in Figure 4.4.

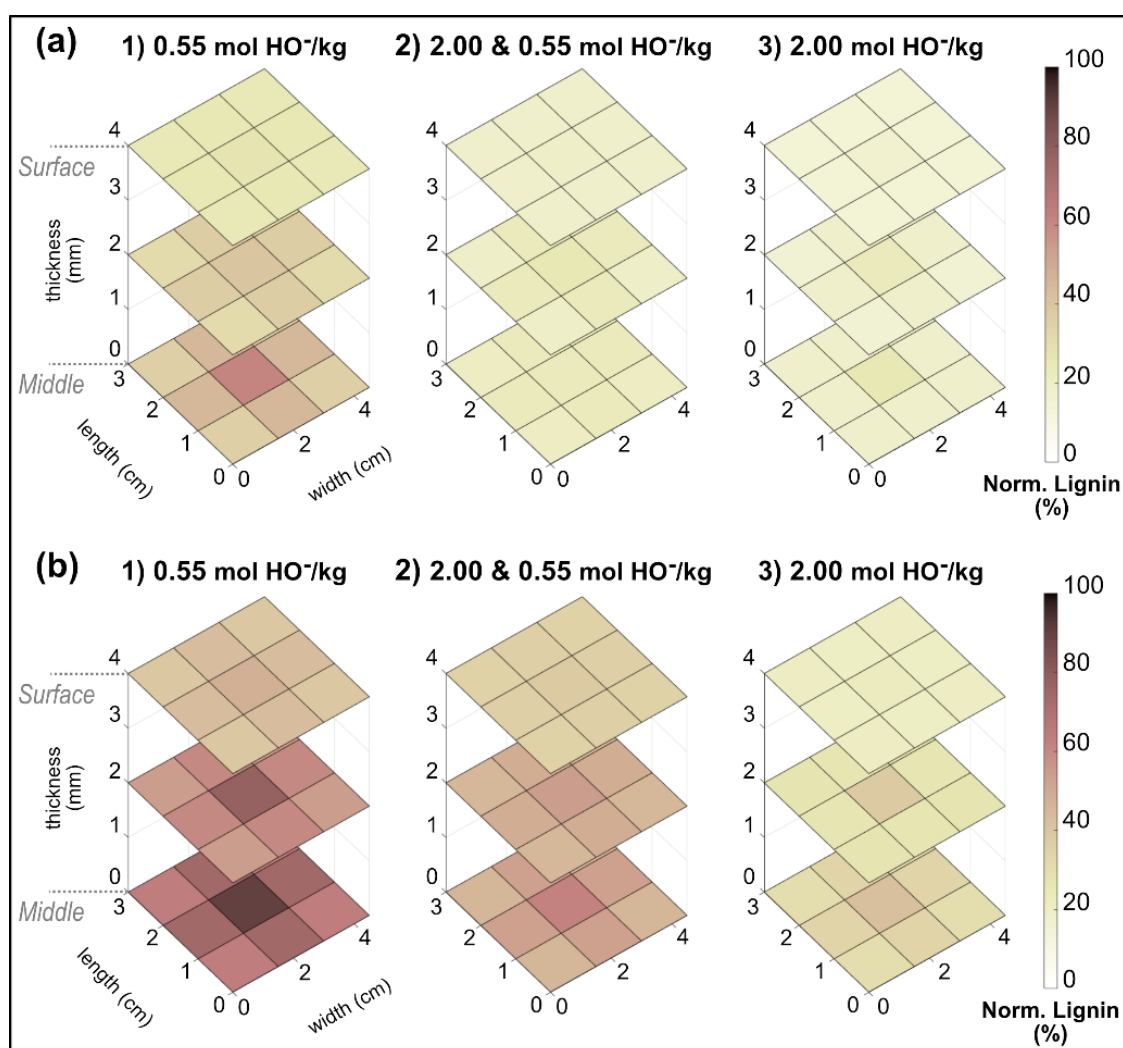


**Figure 4.4** Distribution of Klason lignin (%) in model wood chips of (a) aspen and (b) birch. Pulping strategies: 1) impregnation and cooking liquors containing 0.55 mol HO<sup>-</sup>/kg; 2) impregnation using liquor with 2.00 mol HO<sup>-</sup>/kg and cooking with 0.55 mol HO<sup>-</sup>/kg; 3) impregnation and cooking liquors containing 2.00 mol HO<sup>-</sup>/kg. In all cases the chips were cooked for 45 min at 155 °C. Lignin results were normalized according to the initial lignin content in each untreated wood. No distinction was made between transverse and tangential sides. Max. RSD = 13%. Adapted from Paper III.

The results in Figure 4.4 confirm that the initial hydroxide concentration inside the chips after impregnation has lasting effects on the progression of delignification. For example, when comparing strategies 1 and 2, the use of higher alkali content during impregnation improved the uniformity of lignin removal in both hardwoods significantly. In this case, the use of high alkali likely increased the initial hydroxide content within the chips before cooking and, at the same time, led to slightly faster diffusion of cooking chemicals, as the samples were probably more swollen than the ones treated with low alkali. Furthermore, the results from strategies 2 and 3 show that adjusting the concentration of hydroxide in the impregnation liquor alone can be sufficient to increase the extent and uniformity of delignification. Moreover, for highly porous hardwoods, this adjustment can be as effective as altering both the impregnation and cooking liquors (Figure 4.4 a), as the alkali distribution within these samples is less sensitive to small differences in the rates of hydroxide diffusion during cooking. These observations agree with experiments conducted in softwoods (Brännvall and Bäckström, 2016), which suggest that using high hydroxide concentrations during impregnation, followed by cooking with lower alkali content, is a potential approach for achieving more uniform pulps.

### **4.2.3 Impregnation of chips prepared in an industrial chipper**

While the analyses presented in Sections 4.2.1 and 4.2.2 were designed to provide controlled conditions for the reliable local comparison between the impregnation of different hardwood chips, they cannot capture the behavior taking place in samples produced in industrial chippers. These samples exhibit cracks and angled surfaces and are, on average, thinner, which aids liquor penetration and accelerates the diffusion of cooking chemicals (Gustafson *et al.*, 1989). Hence, these chips are the focus of this Section.

The following experiments examined how the composition of the impregnation liquor can impact the delignification of industrial hardwood chips, namely, a mix of *Betula pubescens* and *Betula pendula*. As described in Section 3.3.1, four impregnation liquors were tested: white liquor (WL), water (W), white liquor with increased ionic strength through the addition of NaCl (WL+Na), and aqueous solution of NaCl (W+Na). After impregnation, the spent impregnation liquors were discarded, and all samples were cooked under the same conditions using white liquor as the cooking medium. The influence of the impregnation liquors on delignification can be seen in Figure 4.5, which presents the profiles of Klason lignin content over time in pulp samples and in the black liquor fractions isolated from pulp (“pore liquor”).

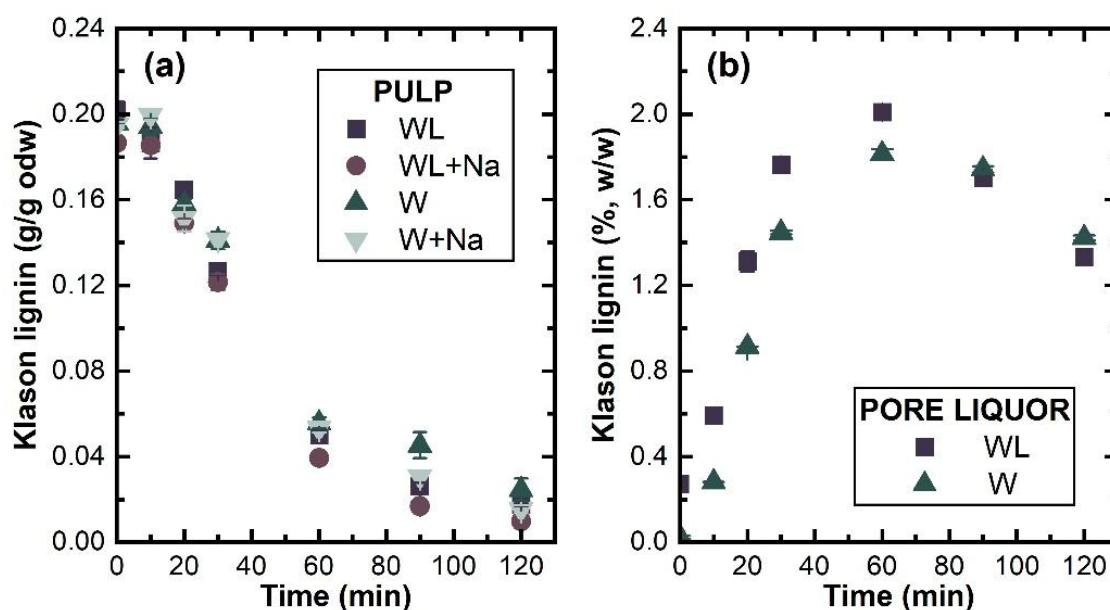


**Figure 4.5** Impact of impregnation liquor on delignification (160 °C) of samples prepared in an industrial chipper. (a) Average Klason lignin content over cooking time in pulp samples; impregnation used one of the following: WL – white liquor (0.60 mol HO<sup>-</sup>/kg liq. + 0.15 mol HS<sup>-</sup>/kg liq.), WL+Na – white liquor with NaCl (WL + 1.25 mol NaCl/kg liq.), W – water or W+Na – NaCl solution (2.00 mol NaCl/kg liq.). (b) Average Klason lignin concentration over cooking time in the black liquor samples isolated from pulps impregnated with white liquor (WL) or water (W). Values at 0 min refer to the composition of the impregnated chips or the composition of the spent impregnation liquor isolated from the chips. Error bars represent the standard deviation of measurements. Adapted from Paper I.

As expected, the impact of the liquor composition inside the samples after impregnation is not as substantial in industrial chips as it was in the model chips used in Section 4.2.2, likely due to the lower characteristic time for diffusion. Nevertheless, Figure 4.5 (a) shows a modest increase in the extent of lignin removal in the samples impregnated with liquors containing HO<sup>-</sup> and HS<sup>-</sup> (i.e., WL and WL+Na). This influence is clearer in Figure 4.5 (b), where it can be observed that, in the sample impregnated with white liquor, the accumulation of dissolved lignin in the pore liquor occurs earlier than in the sample impregnated with water. This behavior suggests that delignification was slightly delayed in the samples impregnated without cooking chemicals (W and W+Na), indicating that, while the diffusion of alkali is less limiting than in model samples, it still influences the progression of lignin removal in industrial chips.

Furthermore, an interesting effect shown in Figure 4.5 (a) is the consistently higher delignification extent in samples impregnated with supplemented liquor (WL+Na) compared to samples treated with regular liquor (WL). As proposed by Nieminen *et al.* (2014), this increase in the rate of lignin removal could be explained by a shift in Donnan equilibrium: the extra cationic species

in the supplemented liquor likely balanced part of the negative charges in the fiber walls (originated from phenols and acidic groups), thereby causing an increase in the local concentration of HO<sup>-</sup> and HS<sup>-</sup>. Nonetheless, the effect of adding extra charged species in the impregnation liquor appears to be highly dependent on the proportion between the different ions. For instance, the differences between the delignification in samples treated with water (W) and samples treated with a solution of NaCl (W+Na) were not as apparent (Figure 4.5 a). In addition, higher concentrations of salt have been shown to decrease lignin removal (Dang *et al.*, 2013; Brännvall and Rönnols, 2021), although the reasoning in these cases was associated with a decrease in lignin solubility. Therefore, predicting whether increased ionic strength has a positive or negative effect on delignification rate is rather complicated, as it involves the concentration of different ions, and the properties of lignin.

### 4.3 Kraft pulping of hardwood chips: cooking

#### 4.3.1 Delignification – cell wall separation and structural changes

Before comparing the evolution of delignification in different wood species on a macroscale, this Section focuses on explaining the progression of cell wall separation in hardwoods and the associated microstructural changes taking place during kraft cooking.

Figure 4.6 (a) tracks the process of cell wall separation by following the average variations in grayscale level across the cell wall and middle lamella of birch. The grayscale profile of the reference (1.0 h of pulping) indicates the initial state of the sample, right after complete liquor penetration. As cooking develops, a continuous decrease in gray-level is observed close to the boundaries between adjacent cells, i.e., at radial positions close to or beyond half the average double wall thickness. This behavior agrees with the growing dissolution of the middle lamella. After 1.4 h of pulping, the first signs of material loss are visible in the reconstructed images – especially in the middle lamella corners. Then, after 2.0 h of pulping, new interfaces between cell wall and liquor are formed, as fiber separation appears to be almost complete. Accordingly, at this stage, the average grayscale results shown in the boundaries between cells become similar to the results observed close to the lumen. The increase in grayscale across the secondary wall (~ from 0 to 2.0 μm), however, cannot be associated directly with a specific phenomenon. The phase-contrast in this area is affected by the new wall-liquor interfaces. Additionally, small movements of the wall and intrinsic changes, such as the loss of hemicelluloses and lignin, or the aggregation of cellulose fibrils (Hult *et al.*, 2001; Bardage *et al.*, 2004), could affect the results.

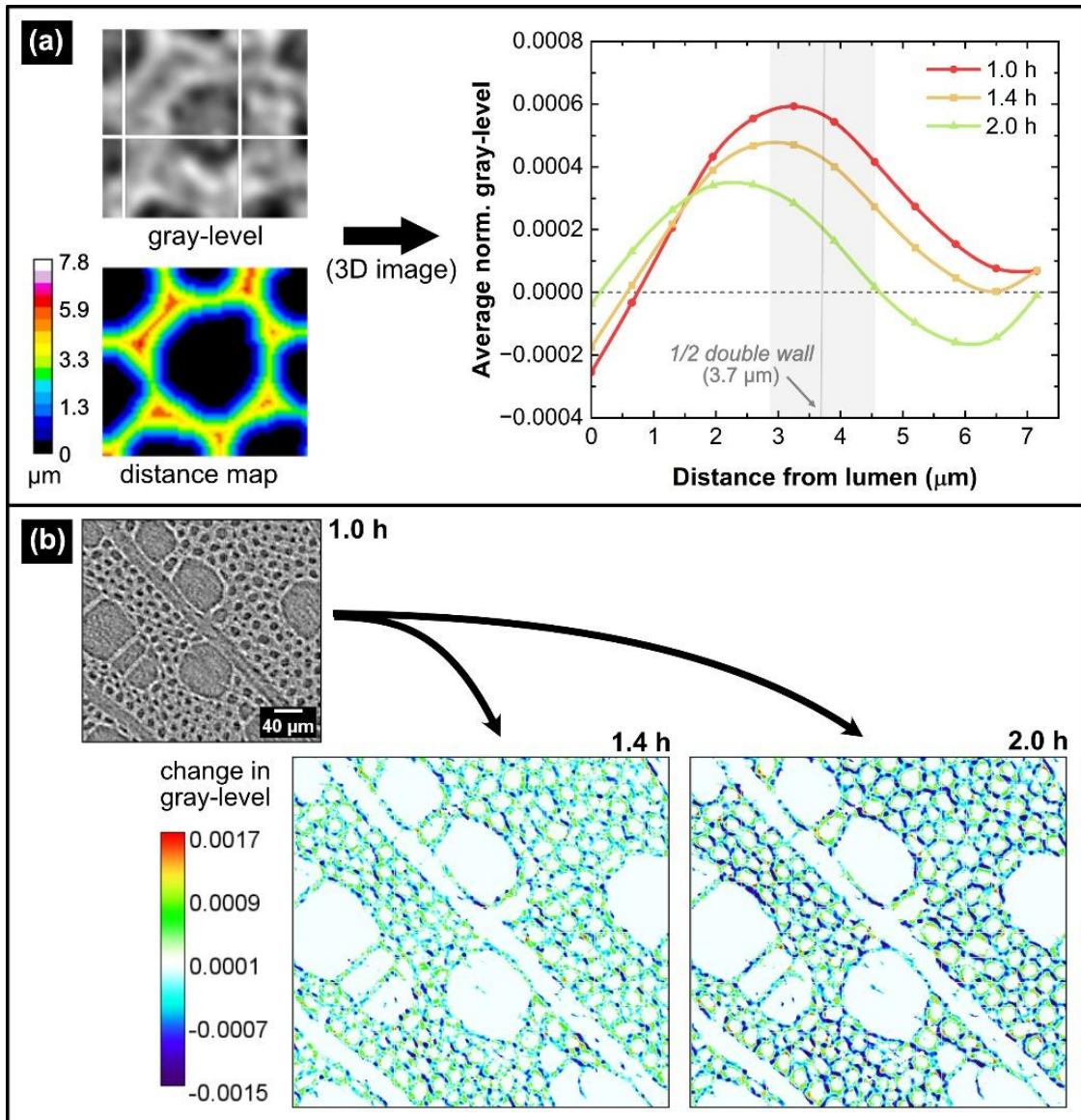


**Figure 4.6** Cell wall separation in birch (pulping: 141 °C). (a) Average evolution of cell wall separation over the 3D reconstructed CT images according to variations in grayscale levels across the cell walls and middle lamella. The line at 3.7  $\mu\text{m}$  denotes half of the average double wall thickness in untreated birch. Max. standard deviation of gray-level = 0.0006 (dimensionless). (b) Relative gray-level variation illustrated in 2D reconstructed images indicating the uniformity of delignification across the transverse section of birch. Reference: 1.0 h of pulping. On the left: 1.4 h of pulping, on the right: 2.0 h of pulping. Adapted from Paper IV.

The potential local influence of different hardwood cells on delignification is also investigated in Figure 4.6. This analysis was conducted by examining the uniformity of delignification across the wood tissue, which is presented in Figure 4.6 (b) in the form of a comparison between the gray-levels in transverse sections of reconstructed CT images acquired at different cooking times. Based on visual inspection of the changes in gray-level, it was not possible to identify any preference for early delignification close to specific cells. Thus, it appears that, on a microscale, the position of a fiber relative to

other cells (e.g., rays and vessels) has no substantial impact on its delignification rate.

Besides cell wall separation, other structural changes take place during kraft cooking. For example, the evolution of porosity and cell wall thickness in different hardwoods can be observed in Figure 4.7.

Porosity was shown to increase continuously during cooking (Figure 4.7 a), initially due to the separation of fibers and afterwards possibly due to cell wall shrinkage and marginal distancing/movement of the cells. Nevertheless, the increase in porosity appears to happen faster during cell wall separation. In terms of differences between the hardwoods, birch was the species with the largest increase in porosity (from 56.6% to 75.7%), despite remaining less porous than aspen and alder during the process. This large increase is probably related to the volumetric ratio between fibers and other cells – which seems to be higher in birch than in the other species (Figure 4.1).

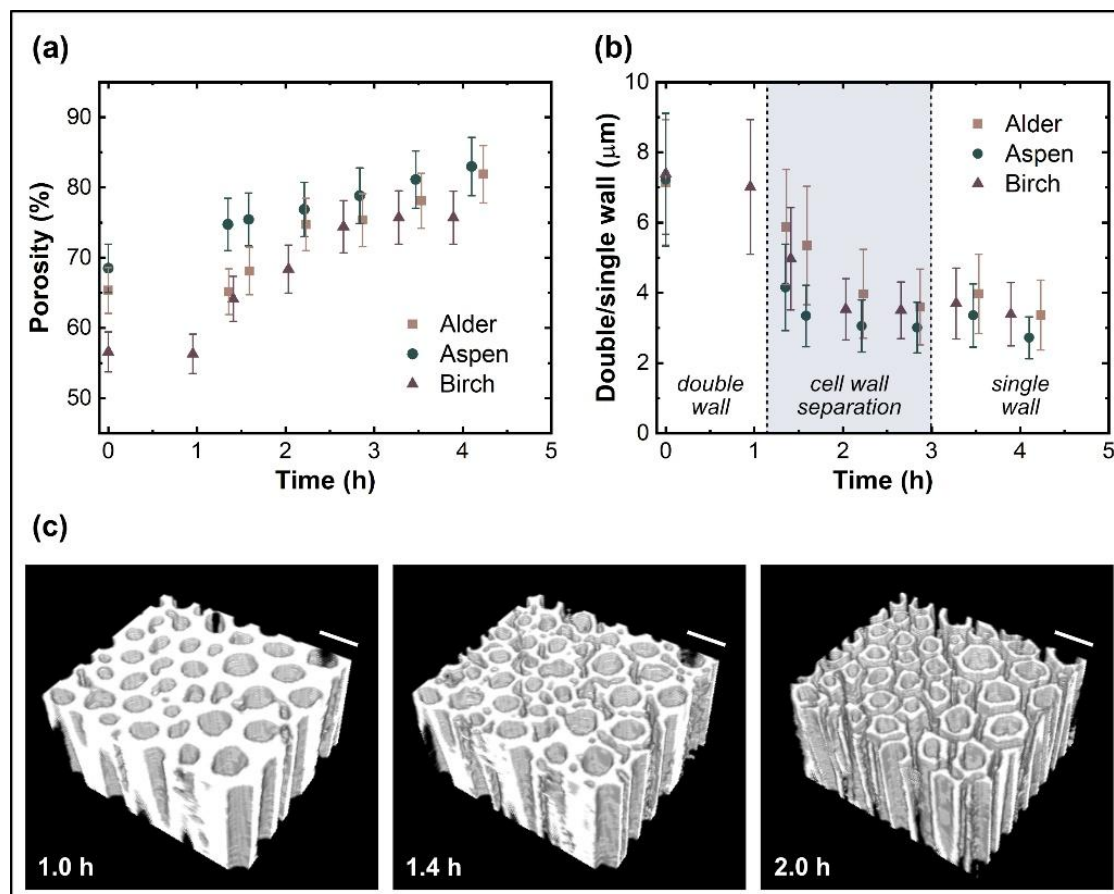


**Figure 4.7** Evolution of (a) porosity and (b) cell wall thickness in the center of aspen, alder and birch during kraft cooking (141 °C). Error bars represent the estimated segmentation error (5%) in the porosity measurements and the standard deviation in the cell wall measurements (calculated based on the histogram of the results). (c) Segmented images of birch showing fiber separation; from left to right: sample after liquor penetration (1.0 h of pulping), sample in the initial stage of fiber separation (after 1.4 h of pulping), and sample with mostly separated fibers (after 2.0 h of pulping). Scale bar = 20 μm. Adapted from Paper IV.

Regarding cell wall thickness (Figure 4.7 b), no significant increase was observed in any of the hardwoods, even when comparing results measured in untreated wood (time = 0 h) and in samples filled with liquor (time ~ 1 h). These results imply that the fiber swelling caused by the kraft liquor is solely related to an increase in liquor uptake (i.e., mass of liquor per mass of fibers), with no substantial changes in radial dimensions. This behavior confirms that the wood ultrastructure, particularly the sublayers of the secondary wall, is able to constrain the expansion of the fiber walls during swelling (Stone and Scallan, 1967; Hubbe *et al.*, 2024).

As delignification intensified, fiber separation began. This process took approx. 1-1.5 h, as illustrated in Figure 4.7 (c), and it is shown for each wood species in Figure 4.7 (b) by the transition from double wall measurements to single wall measurements. After separation (~ 2.5-3 h), cell wall thickness displayed only minor changes. Notably, the single wall values at the end of pulping were smaller than half the original double wall values in untreated wood, which aligns with the loss of the middle lamella and also reflects cell wall shrinkage. Moreover, while cell wall thickness in birch and alder was only 6-8% lower after pulping, in aspen it decreased by 25%, which suggests that the extent of cell wall shrinkage depends on the wood species.

## **4.3.2 Batch kraft cooking of model chips**

### **4.3.2.1 Lignin removal**

This section is devoted to assessing the rate and uniformity of delignification in different hardwoods during kraft cooking. However, before comparing wood species, the influence of cooking conditions on lignin removal is briefly analyzed, focusing on the effect of alkali concentration and cooking temperature. Figure 4.8 illustrates this analysis by presenting the overall lignin gradient (i.e., lignin concentrations at the most and least accessible areas of the samples) within birch chips over time for each cooking condition. The effect of hydroxide concentration has already been discussed to some extent in Section 4.2.2, particularly the importance of ensuring sufficient residual alkali within the chips after impregnation to enable more uniform lignin removal during cooking. In Figure 4.8 (a), the impact of the remaining alkali after impregnation can also be inferred. In this case, two liquors with relatively low hydroxide concentrations (0.25 and 0.55 mol HO<sup>-</sup>/kg liquor) were used during impregnation and cooking, likely resulting in almost complete depletion of alkali in the middle of the chips. Hence, while the extent of lignin removal in the surface layer of the samples was heavily influenced

by the content of alkali in the cooking liquor, the delignification in the middle layers was compromised due to the low availability of hydroxide ions, causing the samples to exhibit substantial lignin gradients regardless of the analyzed conditions.

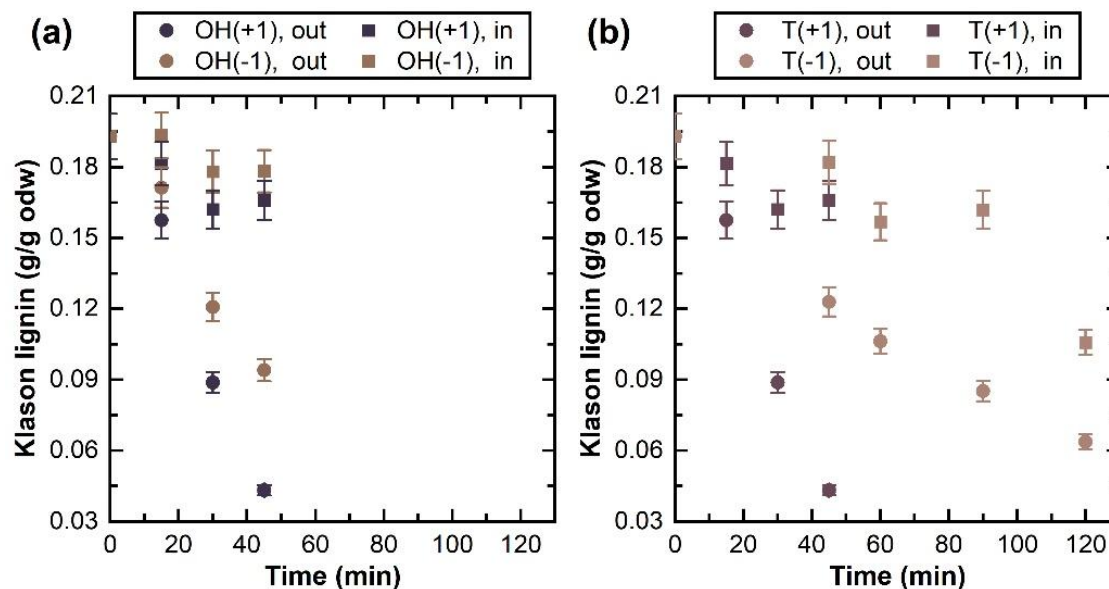


**Figure 4.8** Klason lignin content over time at the most exposed region of the chips (“out”, i.e., the corners of the surface layer) and at the least accessible region (“in”, i.e., the center of the middle layer). (a) Comparison between high and low alkali concentrations: OH(-1) = 0.25 mol OH<sup>-</sup>/ kg liquor, OH(+1) = 0.55 mol OH<sup>-</sup>/ kg liquor. All samples were cooked at 165 °C. (b) Comparison between utilizing high and low temperatures: T(-1) = 145 °C, T(+1) = 165 °C. All samples were cooked with 0.55 mol OH<sup>-</sup>/ kg liquor. Estimated error = 5%. Adapted from Paper II.

Figure 4.8 (b) demonstrates the major effect cooking temperature has on both the rate and the uniformity of delignification. The lignin contents in the surface layer of the chips indicate a significant decrease in the rate of lignin removal with lower temperatures, as delignification was approximately three times slower at 145 °C than at 165 °C. In terms of uniformity, the difference between the concentration of lignin in the surface and middle layers of the chips dropped considerably when the lower cooking temperature was used. Thus, the results imply higher availability of alkali in the middle of the samples when low cooking temperatures are applied, most likely caused by a significant decrease in the rate of alkali consumption compared to the rate of alkali diffusion in the chips. This behavior aligns with the decrease in rejects that is often reported when performing kraft cooking at low temperatures (Colodette *et al.*, 2002; Favaro *et al.*, 2021).

Based on the previous results, a relatively high cooking temperature (165 °C) was selected for the experiments comparing the impact of wood structure on delignification of different hardwoods. This temperature should minimize limiting effects associated with reaction kinetics and, consequently, highlight differences between mass transport in the samples. The comparison between wood species is presented in Figure 4.9.

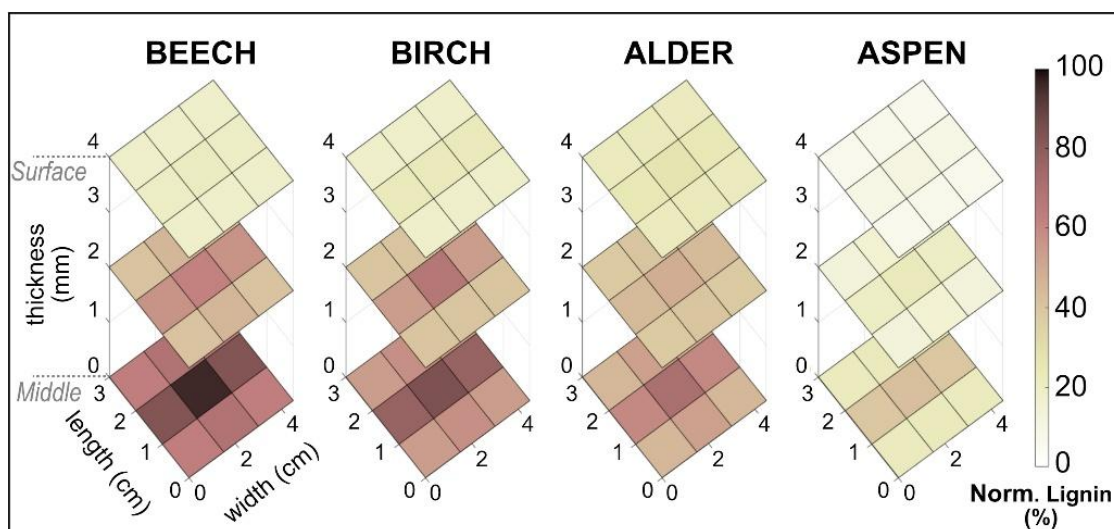


**Figure 4.9** Distribution of Klason lignin (%) within wood chips of different hardwoods after 45 min of kraft cooking at 165 °C using 0.55 mol HO<sup>-</sup>/kg liquor. The results were normalized based on the original Klason lignin content present on each wood species (Table 4.1). Max. RSD = 13%. Adapted from Paper III.

In Figure 4.9, the lignin concentrations measured in the surface layer of the chips were the least affected by the transport of cooking chemicals, thus reflecting differences among the hardwoods regarding the rates of lignin depolymerization and the transport of lignin fragments across the fiber walls. Based on these results, aspen was the easiest species to delignify, with more than 90% of the original lignin content removed after 45 minutes of cooking. This rapid removal of lignin has also been reported in studies using aspen wood meal (Kron *et al.*, 2024), however the reasons for such behavior remain unclear. Among the other hardwoods, no major differences in the extent of delignification were observed at the surface of the samples.

Nevertheless, in the intermediate and middle layers of the chips, lignin removal varied substantially according to the wood species, as the process became more influenced by wood structure. In particular, porosity appeared to dictate the uniformity of delignification: the most homogeneous lignin distribution was detected in aspen chips, which exhibited the highest porosity among the species examined, whereas the most uneven distribution was observed in beech chips (the least porous material). This behavior is

consistent with the alkali distribution inside the hardwoods. As discussed in Section 4.2.2, under identical impregnation conditions, chips with high porosity tend to display a higher and more evenly distributed alkali content than chips with low porosity. This, in turn, favors lignin removal in the middle of the more porous chips by increasing depolymerization rates and lignin solubility in the inner layers of the samples.

Figure 4.9 also illustrates the effect of wood anisotropy in the progression of delignification, as the extent of lignin removal varied substantially between the sides of the chips. In the sides with a transverse border, delignification was often similar to that observed in the corners, whereas lignin removal in the sides with a tangential border was always significantly lower. Although the comparison between these sections (i.e., transverse and tangential) is not straightforward, their delignification levels likely reflect differences in the transport rates of cooking chemicals along the longitudinal and tangential directions of wood. The effective capillary cross sectional area (ECCSA), for example, is known to be higher in the longitudinal direction (preferred direction of diffusion in transverse sides) than in the other directions of wood (Stone, 1957).

A more thorough analysis of the delignification in the transverse and tangential sides of different hardwoods is given in Figure 4.10.

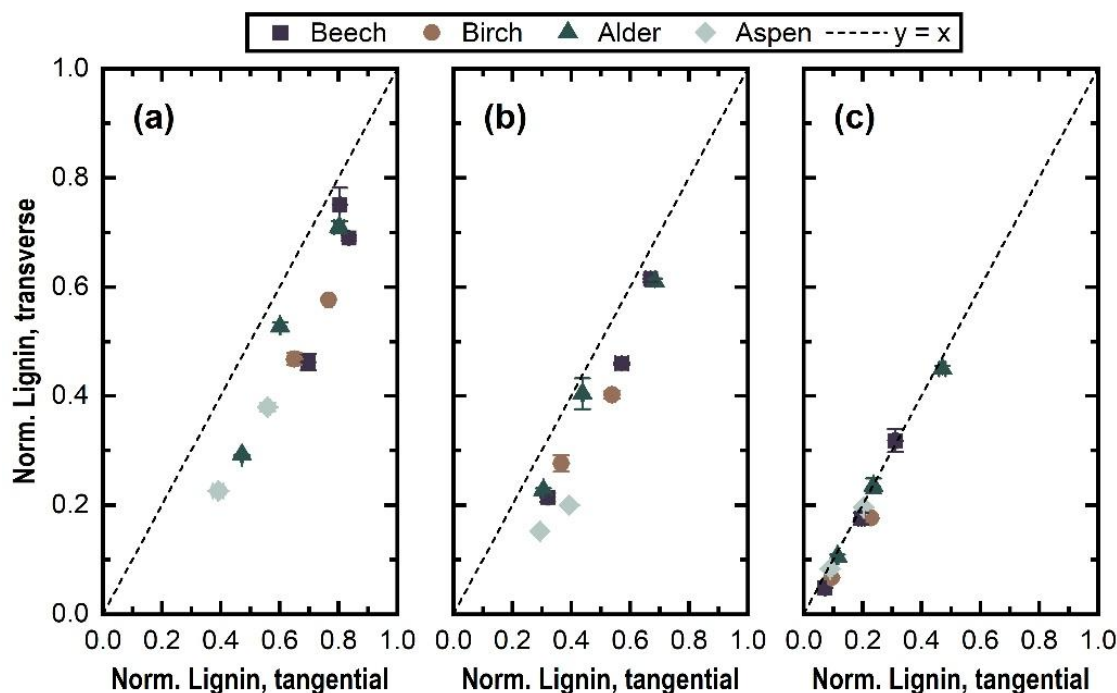


**Figure 4.10** Comparison between the normalized Klason lignin content in the tangential side (x axis) and in the transverse side (y axis) of wood chips of different species throughout pulping. (a) Middle layer. (b) Intermediate layer. (c) Surface layer. Cooking conditions: 165 °C, 0.55 mol HO<sup>-</sup>/ kg liquor. Error bars denote the standard deviation. Adapted from paper III.

Two main conclusions can be drawn from the profiles in Figure 4.10. First, the results in the outer layer (Figure 4.10 c) confirm that lignin removal at the surface of the chip was not significantly limited by the transport of cooking chemicals, as no differences in the extent of delignification were observed between the transverse and tangential sides. Second, in the inner layers (Figure 4.10 a,b), the gaps between the lignin content in different sides of the chips were similar for all hardwoods. Hence, the rates of alkali diffusion along different directions of wood appear to vary by similar extents in all species investigated, which suggests that specific microstructural features, such as aggregate rays and wide ray cells, did not affect the tangential diffusion of ions substantially.

#### **4.3.2.2 Xylan removal**

As shown in Table 4.1, xylan is one of the main components of hardwoods and, as such, it has a large impact on the final yield of pulping. Moreover, as established in Section 2.1.3, xylan is associated with both cellulose and lignin through interactions that may be significantly affected during pulping. Therefore, the behavior of xylan during kraft cooking was investigated.

In general, the extent of xylan removal was strongly affected by the local availability of hydroxide ions inside the wood chips. For instance, lower concentrations of xylan were measured in chips treated with 0.55 mol HO<sup>-</sup>/kg liquor than in those treated with 0.25 mol HO<sup>-</sup>/kg liquor. In addition, similar to what was observed with lignin, xylan removal was more uniform in hardwood chips with higher porosity.

Nevertheless, regardless of wood species or cooking conditions, most of the xylan lost during pulping was dissolved from the chips during the first minutes of cooking, even before the target temperature was reached, which is in line with other studies (Pinto *et al.*, 2005a; Danielsson, 2007). After that, an almost constant difference in xylan content was measured over time between the most and least exposed regions of the chips. These trends are illustrated in Figure 4.11 (a), which presents the xylan content within birch chips over time during two cooking experiments: one at high temperature (165 °C) and the other at low temperature (145 °C).

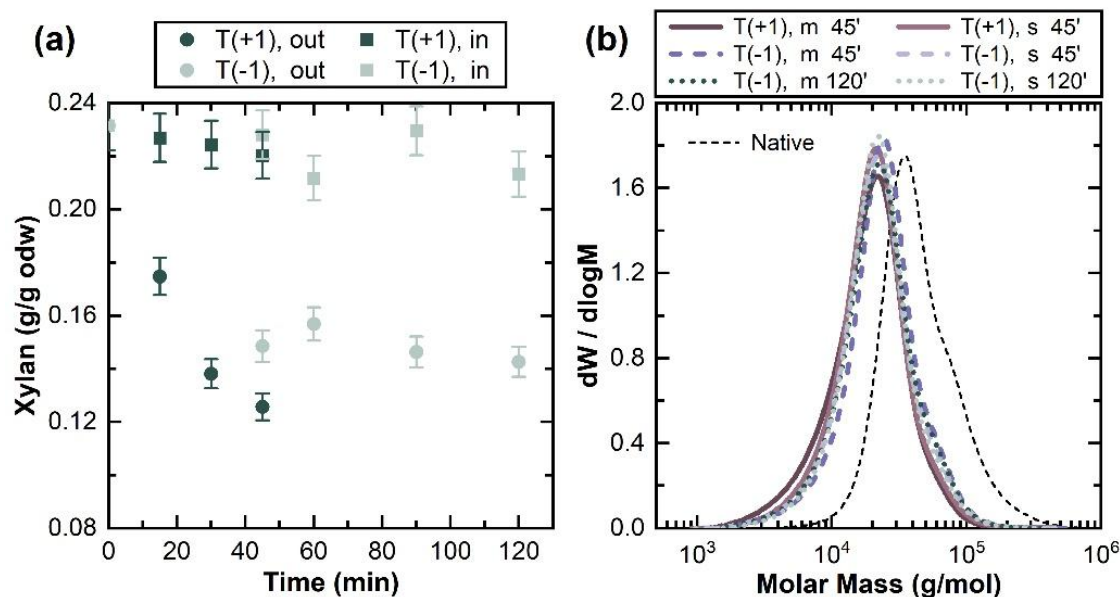


**Figure 4.11** The behavior of xylan during kraft cooking. (a) Xylan content over time at the most exposed region of the chips (“out”, i.e., the corners of the surface layer) and at the least accessible region (“in”, i.e., the center of the middle layer). All samples were cooked with 0.55 mol OH<sup>-</sup>/ kg liquor. Cooking temperature was either T(-1) = 145 °C or T(+1) = 165 °C. Error bars represent the estimated error (4%). (b) Corresponding molar mass distribution according to RI detection of xylan isolated from the middle layer of the chips (“m”) and from the surface layer (“s”) after 45 and 120 minutes of cooking. Molar mass of xylan isolated from untreated birch wood (“native”) is provided for comparison. Adapted from Paper II.

The rapid decline in the rate of xylan removal can be traced back to a combination of factors. The first one is related to xylan’s relative high resistance to peeling. In hardwood xylan, the presence of xylose units substituted with 4-O-methylglucuronic acid (later converted into hexenuronic acid) prevents extensive peeling of the xylan backbone (Sjöström, 1993d; Potthast, 2006). Hence, the rate of xylan loss due to peeling is expected to slow down significantly with time. This behavior is confirmed by the molar mass distributions presented in Figure 4.11 (b), which shows no significant differences between xylan samples isolated from pulps collected at different time points, from different layers, or using different cooking conditions. Therefore, following the initial decrease in molar mass caused by deacetylation and peeling, the xylan remaining in the pulp appears to be quite stable under the studied conditions.

The second factor that may contribute to the decrease in xylan removal during cooking is the presence of distinct xylan fractions in wood. For instance, Dammström *et al.* (2009) suggests the existence of two xylan fractions: one associated with lignin and the other associated with cellulose. In this sense, it is possible that the fraction interacting with lignin is more easily dissolved in the alkaline liquor, contributing to the initial high rates of xylan removal. Then,

as the amount of this xylan fraction decreases in the pulp, so does the xylan removal rate.

In addition, increased interactions between xylan and cellulose, including the adsorption of dissolved xylan, may also influence xylan removal. During cooking, structural changes in xylan – such as the removal of substituents – have been shown to favor its adsorption onto cellulose (Kabel *et al.*, 2007; Lan *et al.*, 2024). Moreover, as delignification progresses, cellulose becomes increasingly exposed, facilitating interactions with xylan.

### 4.3.3 Batch kraft cooking of chips prepared in industrial chipper

As explained in Section 4.2.3, the model samples used to analyze local changes inside hardwoods during delignification differ significantly from the wood chips produced in industrial chippers. Therefore, to better understand how industrial samples behave during kraft cooking and to investigate the extent of mass transport limitations in this process, the current section presents data acquired in pulping experiments involving industrial chips (*Betula pubescens* / *Betula pendula*).

Figure 4.12 shows the concentration of Klason lignin during cooking measured in two black liquor fractions: bulk liquor (BL, separated from the pulp via filtration) and centrifuged liquor (CL, representing the black liquor in the wood chip pores). In addition, lignin was precipitated from these two liquor fractions to determine the variation of molar mass distribution (MMD) throughout pulping. The results acquired with samples collected after 30 and 90 min of cooking are shown in Figure 4.12 (b).

Despite mass transport occurring more rapidly in industrial chips than in model samples, the concentration of dissolved lignin differed substantially between the bulk and centrifuged liquors (Figure 4.12 a), indicating the existence of fairly different chemical environments inside and outside the chips. Moreover, the lignin profile in the CL fraction reveals that, up to approx. 60 min of cooking, the outward diffusion of dissolved lignin was slower than the rate of lignin leaving the cell walls, causing the accumulation seen in Figure 4.12 (a). However, after 60 min, this balance changed and more lignin was transported out of the chip than out of the cells, decreasing the concentration of lignin in the CL fraction. This behavior was also found in other studies (Egas *et al.*, 2002; Simão *et al.*, 2011; Brännvall and Rönnols, 2021) and can be traced back to different phenomena taking place during cooking. For instance, the resistance to mass transport inside the chips decreases with time, as the structural changes mentioned in Section 4.3.1 (e.g., the increase in porosity) progress.

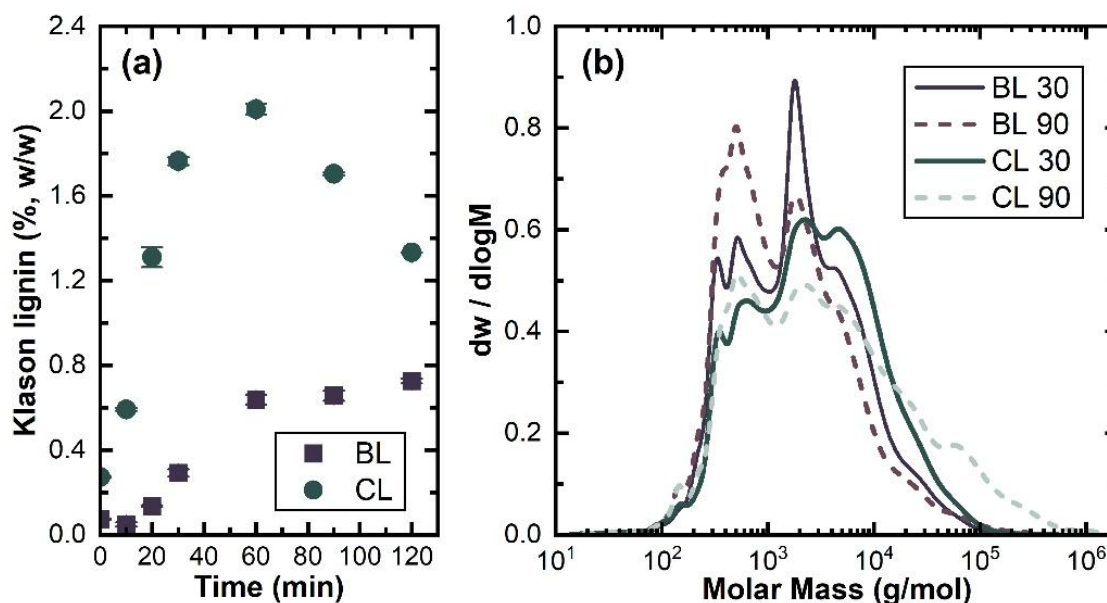


**Figure 4.12** Impact of mass transport resistance on kraft cooking (160 °C) of samples prepared in an industrial chipper. (a) Content of Klason lignin over time in the bulk black liquor (BL) and in the centrifuged black liquor isolated from the pulp (“pore liquor”, CL). Values at 0 min represent the composition of the respective spent fractions of impregnation liquor (white liquor). Error bars indicate the standard deviation of the measurements. (b) Differential molar mass distribution based on UV detection of precipitated lignin from bulk (BL) and centrifuged (CL) liquors collected after 30 and 90 min of pulping. Adapted from Paper I.

Variations in the molar mass of lignin leaving the fibers could also explain the change observed in the CL lignin profile, as large lignin fragments would demand more time to diffuse out of the cell walls. In fact, this increase in the size of dissolved lignin is hinted at in Figure 4.12 (b): when comparing the MMD of the material isolated from the CL fractions, there was a shift towards higher molar mass at later cooking times.

In addition, a thorough analysis of Figure 4.12 (b) also exposes further differences between the CL and BL fractions. The dissolved lignin isolated from the bulk liquor had consistently lower values of average molar mass. Furthermore, the MMD of the material in the bulk shifted to lower values with time. These observations imply that the lignin in the bulk is more degraded than in the pores of the wood chips, which was also confirmed via HSQC NMR. Hence, the material in the pores of the chips is likely freshly removed from the cell walls. Additionally, the lower concentrations of cooking chemicals in the center of the chips probably contribute to the less extensive degradation of the dissolved material in the CL.

## 4.4 Multiscale model

The results measured during the kraft cooking experiments with model chips of birch were used to develop a simplified multiscale model to describe lignin removal in the least accessible fibers inside wood chips. The model, which was restricted to 1D across the chip thickness (radial direction), was able to capture the delignification behavior with reasonable accuracy after adjusting some of the parameters mentioned in Section 3.11, namely:

- a) The estimated initial concentration of hydroxide inside the wood chip ( $OH_0$ ). This parameter should represent all alkali that was transported to the center of the chip during impregnation, without accounting for the decrease in concentration caused by the initial consumption of hydroxide (e.g., in neutralization). Hence, it could assume any value between 0.55 M, i.e., the approximate concentration of hydroxide in the cooking liquor, and 0.06 M, i.e., the value measured in the center of the chip after impregnation (Figure 4.3). After sensitivity analysis, this value was set to 0.31 M.
- b) The effective capillary cross sectional area (ECCSA). To calculate the effective diffusivity of hydroxide in the chip, local values of ECCSA were initially estimated based on experimental data reported for aspen samples. Given the microstructural differences between birch and aspen, these values were likely overestimated. In addition, the initial approach to calculate the effective diffusivity assumed the ECCSA varied instantaneously according to the local pH, which has been disputed (Inalbon and Zanuttini, 2008). Moreover, when applying the original data, the model predicted consistently higher extents of lignin removal in the outer layer of the chip than those determined experimentally. Therefore, based on sensitivity analysis, the ECCSA value was decreased to 0.20 and its pH dependence was removed.
- c) The intrinsic reaction rate. Originally, the model relied on the kinetic parameters reported by Kron *et al.* (2025). However, this data described the total conversion of bound lignin ( $L_S$ ) to reacted lignin ( $L_D$ ) in about 5 min (at 150 °C), which is faster than the 10-20 min previously found for lignin depolymerization reactions (Mattsson *et al.*, 2017). Thus, the kinetic parameters were re-estimated, but without changing the apparent delignification rate, i.e., re-estimation occurred by decreasing the intrinsic rate and increasing the rate of diffusion of  $L_D$  in the fiber walls. The new intrinsic reaction rate was about four times lower than the original (i.e., conversion of  $L_D$  in ~20 min instead of 5 min). This adjustment reduced the rate of alkali

consumption, allowing the model to capture the delignification behavior in the inner layers of the samples (where it had previously predicted the complete depletion of alkali).

The fit of the model after the aforementioned adjustments can be seen in Figure 4.13, which presents the radial lignin gradients in the center of the chips at different pulping times according to experimental data and model predictions.

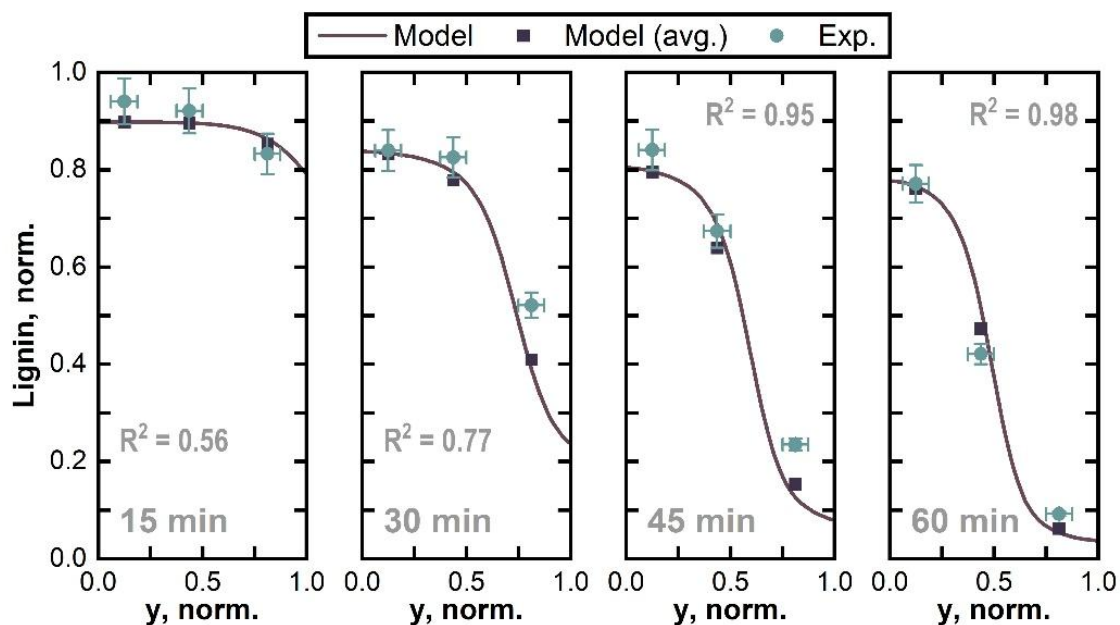


**Figure 4.13** Normalized Klason lignin content over the radial direction in the middle of the wood chip for different cooking times. Model parameters: low intrinsic reaction rate (~20 min), ECCSA = 0.20. Initial alkali concentration = 0.31 M. Pulping conditions: 165 °C, 0.55 mol HO<sup>-</sup>/kg liquor. Adapted from Paper V.

Figure 4.13 indicates that the adjusted model fits the experimental data satisfactorily, especially those acquired after the target cooking temperature was reached. Still, some assumptions used to develop the model may warrant further scrutiny. For example, instead of considering fixed hydroxide consumption factors (0.21 g NaOH/g of lignin and 0.49 g NaOH/g of carbohydrates), more accurate expressions could be introduced. This change could potentially improve the predictive power of the model at the beginning of the cooking process, as most of the alkali consumption related to carbohydrate reactions occurs early on (Zanuttini *et al.*, 1998; Santos *et al.*, 2012b). Also, altering the model to include the effect of sulfidity explicitly may be of interest to account for local variations in the concentrations of HS<sup>-</sup> and to describe systems running with different sulfidity levels.

In addition to the profiles shown in Figure 4.13, an overview of the predicted distributions of Klason lignin and hydroxide ions across the thickness of the chip over time is presented in Figure 4.14. As expected, when the temperature was still significantly lower than the target (i.e., up to 500 s of cooking) only minor changes in lignin concentration were predicted, and the diffusion of  $\text{HO}^-$  increased the concentration of alkali close to the surface of the chip. Then, as the temperature rose above 140 °C, alkali was rapidly consumed, causing the hydroxide concentration to drop to less than 0.05 M across more than 60% of the chip after 900 s of cooking. From this point onward, the alkali concentration exhibited an almost linear gradient along the chip thickness, extending from the surface gradually toward the middle of the chip. This distinct availability of hydroxide ions along the chip shaped the progression of delignification: substantial lignin removal happened first close to the surface of the chip and then spread inward with time. Moreover, Figure 4.14 (a) shows that, under the evaluated cooking conditions, somewhat uniform delignification could only occur in the 30% of the chip closest to the chip surface. In other words, limitations imposed by alkali transport could be considered negligible only in thin chips (thickness  $\leq 2\text{-}3$  mm), which is consistent with earlier findings from kraft cooking of softwood chips (Gullichsen *et al.*, 1992).

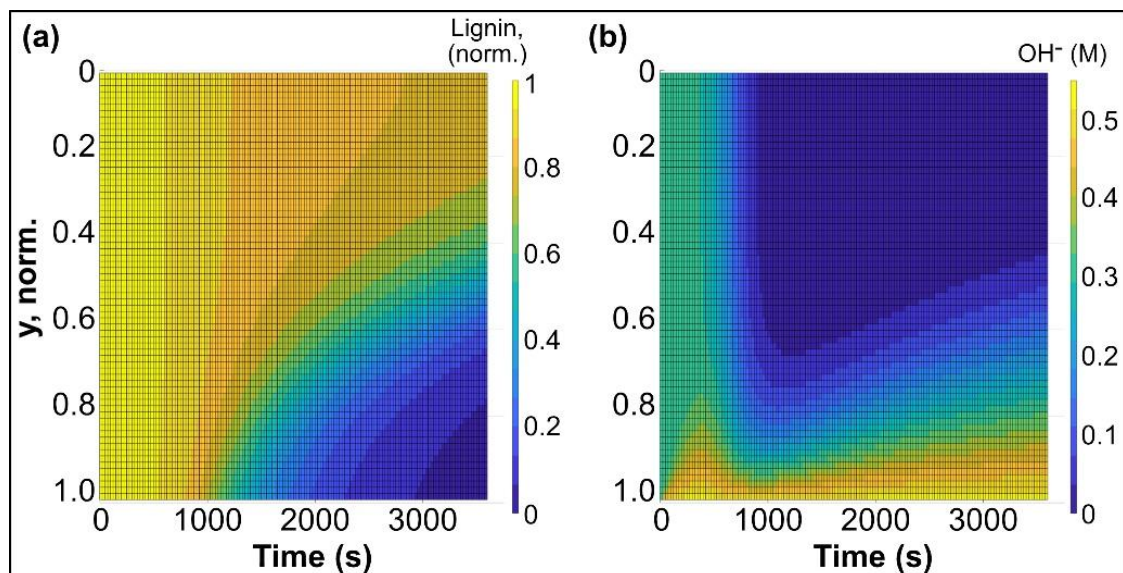


**Figure 4.14** Distribution of (a) normalized Klason lignin and (b) hydroxide ions across the radial direction of the wood chip over time. Model parameters: low intrinsic reaction rate ( $\sim 20$  min), ECCSA = 0.20. Initial alkali concentration = 0.31 M. Cooking conditions: 165 °C, 0.55 mol  $\text{HO}^-/\text{kg}$  liquor. Adapted from Paper V.



# 5 Conclusion

## 5.1 Concluding remarks

This doctoral project studied the progression of delignification in hardwoods during kraft pulping, evaluating how species with distinct morphological features respond to different impregnation liquors and cooking conditions. By combining compositional analyses, imaging techniques and modeling efforts, the following conclusions were drawn:

- a) Impregnation conditions: The composition of the liquor used during impregnation has lasting effects on the evolution of lignin removal. In particular, the concentration of hydroxide ions inside the chips after impregnation is of great importance, as low alkali content can result in highly heterogeneous delignification. In this sense, the impregnation step should be designed not only to ensure the penetration of liquor inside the chips, but also to allow enough hydroxide ions to diffuse inward to balance the initial consumption of alkali due to reactions with carbohydrates and other wood components. This is especially relevant for hardwoods with low porosity (e.g.: birch and beech), since the mass ratio between liquor and wood inside the chips is low and, therefore,

more alkali must be transported inwards to avoid depletion in the middle of the chips.

- b) Cooking conditions: The cooking temperature and the composition of the cooking liquor affect the rate and uniformity of lignin removal, with high alkali concentrations and low temperatures ( $\sim 145\text{ }^{\circ}\text{C}$ ) favoring homogeneous delignification. Nevertheless, extremely high hydroxide concentrations should be avoided, as they increase the amount of xylan that is dissolved before structural and compositional changes in the cell walls facilitate xylan-cellulose interactions, hindering further xylan removal. Interestingly, pulping conditions strongly influence xylan dissolution but appear to have little effect on the extent of structural changes of the xylan remaining in the pulp after cooking.
- c) Impact of wood structure on kraft pulping:
- c.1) Macroscale: porosity is one of the main factors influencing the uniformity of delignification in hardwoods, with highly porous species (e.g., aspen) experiencing a more homogeneous removal of lignin than hardwoods with low porosity. In addition, lignin removal is influenced by wood anisotropy, occurring faster along the longitudinal direction of the chips (i.e., along their length) than along their width, which can be explained by faster rates of mass transport through the lumen of fibers and vessels. Moreover, differences in radial features (e.g., presence of aggregate rays) do not seem to affect the extent of delignification along the radial and tangential directions of the chips.
  - c.2) Microscale: in terms of individual morphological features, vessels play the most significant role during impregnation, providing the preferred path for penetration and for spreading the liquor toward the lumen of adjacent fibers. Ray cells, on the other hand, contribute to the radial penetration of liquor, but do not seem to provide an efficient path to spread the liquor to other cells. During cooking, however, the proximity between fibers and vessels or between fibers and other cells does not affect the rate of fiber separation substantially.
  - c.3) Structural changes during pulping: while wood structure influences the progression of pulping, it is also changed by the pulping process. Delignification causes the dissolution of the middle lamella and potential shrinkage of the secondary wall. Additionally, the porosity of the wood chip increases, first due to

cell wall separation, and later due to small changes in cell wall thickness and minor movements of the cells. Nevertheless, no substantial changes in porosity or cell wall thickness are observed during liquor penetration.

- d) Modeling insights: Delignification of hardwood chips can be described as a multiscale process combining mass transport and different reaction rates. Moreover, it is possible to simplify the system and model the behavior of the least accessible fibers by solving a one-dimensional problem across the chip thickness, which can be of interest, for instance, when investigating the defibration point. According to the proposed model, reaction kinetics and diffusion of lignin fragments limit the rate of lignin removal inside the fiber walls. Across the chip, the uniformity of delignification is influenced by the availability of alkali, which depends on the interplay between the diffusion of cooking chemicals in the radial direction of the chip and the rate of alkali consumption. Furthermore, model simulations suggest that, under the evaluated pulping conditions, hardwood chips require thickness below 2-3 mm to achieve a virtually homogeneous delignification.

## 5.2 Future work

The findings presented in this thesis give general insight into the behavior of different hardwoods during kraft pulping through a systematic analysis of industrial and model chips under controlled impregnation and cooking conditions. However, many research questions can still be explored to complement and expand upon the results observed in this work.

For instance, the *ex-situ* experiments described in the thesis provide data on the rates of delignification and xylan removal in the sapwood of alder, aspen, beech, and birch, as well as data regarding the spatial distribution of lignin and xylan within their respective wood chips during cooking – information that is otherwise hard to come by in the literature. Naturally, the next steps on this front involve expanding the scope of analyzed materials. The inclusion of tropical species, such as *Acacia* spp. and *Eucalyptus* spp., is of great interest, given their economic relevance and distinct microstructural features. Also, evaluating heartwood delignification is extremely relevant due to its distinct composition, which comprises higher contents of extractives (potentially affecting the pit system), and it is of particular importance for species prone to the formation of tyloses.

Expanding the scope of materials is also a possible strategy to continue the *in-situ* tomography experiments. However, in this case, a more promising

route may involve further development of the reaction cell. The results achieved with *in-situ* tomography are part of pioneering efforts toward temporal and spatial resolved analysis of pulping processes, yet the experimental setup could benefit from changes. For example, the current system is quite limited regarding the maximum temperature of operation, which could be fixed by changing the recirculation pump. More ambitious changes could include adding sampling points to the system (to collect black liquor) and altering the sample cover and external cover to allow performing complementary measurements (e.g., X-ray scattering). The cell could also be tested for *in-situ* nanotomography, as the higher spatial resolution would allow analyzing pits and changes in the ultrastructure of wood – although changes in the sample holder would probably be needed to minimize sample movement.

In terms of modeling, the proposed approach provides a promising framework for the development of multiscale delignification models. Future efforts could focus on incorporating the effect of hydrosulfide ions in the delignification rate, as well as introducing specific equations for the rates of carbohydrates degradation and alkali consumption. The increase in wood chip porosity during delignification could also be included.

# Acknowledgements

Financial support of the Resource-smart Processes Graduate School, financed by Vinnova via BioInnovation and industrial partners (Billerud, Holmen, SCA, Stora Enso, Södra Skogsägarna, and Valmet), is gratefully acknowledged.

Likewise, the MAX IV Laboratory is acknowledged for the beamtime on the ForMAX beamline under proposal 20240397. Research conducted at MAX IV, a Swedish national user facility, is supported by Vetenskapsrådet under contract 2018-07152, Vinnova under contract 2018-04969, and Formas under contract 2019-02496.

I would also like to thank everyone who made this thesis possible:

**Merima Hasani**, for supervising this work and managing our research group with attention and care. Thank you for giving me the opportunity to be your PhD student; these 4.5 years have been some of the best experiences in my life.

**Hans Theliander**, for sharing your vast knowledge and experience, and for showing continuous dedication to and enthusiasm for this work.

**Linus Kron**, for sharing this PhD journey. Thank you for making every day at work a bit brighter!

**Ebba Sundquist** and **Moa Andersson**, for your scientific contributions to this work. It was a pleasure supervising you!

All the people involved in the beamtime at ForMAX: **Mira Viljanen** (MAX IV); **Endri Laçaj** and **Stephen Hall** (Lund University); **Klara Hackenstrass**, **Haiyang Yu**, **Sara Florisson**, and **Malin Wohlert** (Uppsala University); and **Luigi Galluccio** (Chalmers). Thank you for your time and dedication. The experiment would not have been possible without you. Also, special thanks to Endri and Stephen for all the support during image processing.

**Michael Andersson-Sarning** and **Patrik Skansen**, for taking care of our labs and for always being willing to help.

**Torbjörn Jönsson**, for the great job preparing the wood samples and the spare parts of the small delignification reactor.

**Malin Larsson** and **Johanna Spång**, for the administrative support and for making our working environment so enjoyable.

Everyone involved in the **Resource-smart Processes** network, for the nice discussions during meetings, courses, and conferences.

All my **colleagues** at Chalmers, past and present, for creating a positive, collaborative, and welcoming work environment. Thank you also for all the fun outside work! Our karaoke nights, board game sessions, day trips, and happy hours will not be forgotten.

Last, but not least, I would like to thank my **family** for all the love and support.

***Muito obrigada!***

# References

- Aguayo, M.G., Ferraz, A., Elissetche, J.P., Masarin, F., Mendonça, R.T. (2014). Lignin chemistry and topochemistry during kraft delignification of *Eucalyptus globulus* genotypes with contrasting pulpwood characteristics. *Holzforschung* 68: 623-629.
- Ahmed, S.A., Chun, S.K. (2011). Permeability of *Tectona grandis* L. as affected by wood structure. *Wood Sci. Technol.* 45: 487-500.
- Ahmed, S.A., Chun, S.K., Miller, R.B., Chong, S.H., Kim, A.J. (2011). Liquid penetration in different cells of two hardwood species. *J. Wood Sci.* 57: 179-188.
- Andersson, N., Wilson, D.I., Germgård, U. (2003). An improved kinetic model structure for softwood kraft cooking. *Nordic Pulp Pap. Res. J.* 18: 200-209.
- Arganda-Carreras, I., Kaynig, V., Rueden, C., Eliceiri, K.W., Schindelin, J., Cardona, A., Seung, H.S. (2017). Trainable Weka segmentation: a machine learning tool for microscopy pixel classification. *Bioinformatics* 33: 2424-2426.
- Bacarin, G.B., Cabrera, F.C., da Silva, M.R., Job, A.E. (2017). The distribution of lignin and xylan in the inner and surface layers of the fiber from eucalyptus kraft pulp and its effects on oxygen delignification. *Mat. Res.* 20: 945-950.
- Bajpai, P. (2015). State-of-the-art pulp mills. In: *Green chemistry and sustainability in pulp and paper industry*. Springer, Cham. pp. 217-246.
- Bardage, S., Donaldson, L., Tokoh, C., Daniel, G. (2004). Ultrastructure of the cell wall of unbeaten Norway spruce pulp fibre surfaces. *Nord. Pulp Pap. Res. J.* 19: 448-452.
- Biermann, C.J. (1996a). Wood and fiber fundamentals. In: Biermann, C.J. (Ed.). *Handbook of Pulping and Papermaking*. 2<sup>nd</sup> ed. Academic Press. pp. 13-54.
- Biermann, C.J. (1996b). Kraft spent liquor recovery. In: Biermann, C.J. (Ed.). *Handbook of Pulping and Papermaking*. 2<sup>nd</sup> ed. Academic Press. pp. 101-122.
- Bijok, N., Fiskari, J., Gustafson, R.R., Alopaeus, V. (2022). Modelling the kraft pulping process on a fibre scale by considering the intrinsic heterogeneous nature of the lignocellulosic feedstock. *Chem. Eng. J.* 438: 135548.
- Bijok, N., Fiskari, J., Gustafson, R.R., Alopaeus, V. (2023). Chip scale modelling of the kraft pulping process by considering the heterogeneous nature of the lignocellulosic feedstock. *Chem. Eng. Res. Des.* 193: 13-27.
- Bogren, J., Brelid, H., Theliander, H. (2007). Reaction kinetics of softwood kraft delignification - General considerations and experimental data. *Nordic Pulp Pap. Res. J.* 22: 177-183.
- Bogren, J., Brelid, H., Theliander, H. (2008). Assessment of reaction kinetic models describing delignification fitted to well-defined kraft cooking data. *Nord. Pulp Paper Res. J.* 23: 210-217.
- Bogren, J., Brelid, H., Bialik, M., Theliander, H. (2009a). Towards a general kraft delignification model. *Nord. Pulp Paper Res. J.* 24: 33-37.

- Bogren, J., Brelid, H., Bialik, M., Theliander, H. (2009b). Impact of dissolved sodium salts on kraft cooking reactions. *Holzforschung* 63: 226-231.
- Brännvall, E. (2009). Pulping technology. In: Ek, M., Gellerstedt, G., Henriksson, G. (Eds.). *Pulp and paper chemistry and technology*. Volume 2. 1<sup>st</sup> ed. De Gruyter. pp. 121-147.
- Brännvall, E., Annergren, G. (2009). Pulp characterisation. In: Ek, M., Gellerstedt, G., Henriksson, G. (Eds.). *Pulp and paper chemistry and technology*. Volume 2. 1<sup>st</sup> ed. De Gruyter. pp. 430-459.
- Brännvall, E., Bäckström, M. (2016). Improved impregnation efficiency and pulp yield of softwood kraft pulp by high effective alkali charge in the impregnation stage. *Holzforschung* 70: 1031-1037.
- Brännvall, E. (2017). The limits of delignification in kraft cooking. *BioResources*. 12: 2081-2107.
- Brännvall, E. (2018). Increasing pulp yield in kraft cooking of softwoods by high initial effective alkali concentration (HIEAC) during impregnation leading to decreasing secondary peeling of cellulose. *Holzforschung* 72: 819-827.
- Brännvall, E., Rönnols, J. (2021). Analysis of entrapped and free liquor to gain new insights into kraft pulping. *Cellulose* 28: 2403-2418.
- Busse-Wicher, M., Gomes, T.C.F., Tryfona, T., Nikolovski, N., Stott, K., Grantham, N.J., Bolam, D.N., Skaf, M.S., Dupree, P. (2014). The pattern of xylan acetylation suggests xylan may interact with cellulose microfibrils as a twofold helical screw in the secondary plant cell wall of *Arabidopsis thaliana*. *Plant J.* 79: 492-506.
- Bygrave, G., Englezos, P. (2000). A thermodynamics-based model and data for Ca, Mg, and Na ion partitioning in kraft pulp fibre suspensions. *Nordic Pulp Pap. Res. J.* 15: 155-159.
- Carlquist, S. (2007). Bordered pits in ray cells and axial parenchyma: The histology of conduction, storage, and strength in living wood cells. *Bot. J. Linn. Soc.* 153: 157-168.
- Chang, V.S., Holtzaple, M.T. (2000). Fundamental factors affecting biomass enzymatic reactivity. *Appl. Biochem. Biotechnol.* 84: 5-37.
- Colodette, J.L., Gomide, J.L., Girard, R., Jääskeläinen, A.S., Argyropoulos, D.S. (2002). Influence of pulping conditions on eucalyptus kraft pulp yield, quality, and bleachability. *Tappi J.* 1: 14-20.
- Corradini, F.A.S., Baldez, T.O., Milessi, T.S.S., Tardioli, P.W., Ferreira, A.G., Giordano, R.C., Giordano, R.L.C. (2018). Eucalyptus xylan: An in-house-produced substrate for xylanase evaluation to substitute birchwood xylan. *Carbohydr. Polym.* 197: 167-173.
- Correa, I.B., de Souza Jr., M.B., Secchi, A.R. (2023). On the modeling of continuous kraft pulp digesters: Inclusion of wood characteristics. *Chem. Eng. Res. Des.* 196: 711-724.

- Dammström, S., Salmén, L., Gatenholm, P. (2009). On the interactions between cellulose and xylan, a biomimetic simulation of the hardwood cell wall. *BioResources* 4: 3-14.
- Dang, V.Q., Nguyen, K.L. (2008). A universal kinetic model for characterisation of the effect of chip thickness on kraft pulping. *Bioresour. Technol.* 99: 1486-1490.
- Dang, B.T.T., Brelid, H., Köhnke, T., Theliander, H. (2013). Impact of ionic strength on delignification and hemicellulose removal during kraft cooking in a small-scale flow-through reactor. *Nordic Pulp Pap. Res. J.* 28: 358-365.
- Dang, B.T.T., Brelid, H., Theliander, H. (2016). The impact of ionic strength on the molecular weight distribution (MWD) of lignin dissolved during softwood kraft cooking in a flow-through reactor. *Holzforschung* 70: 495–501.
- Daniel, G. (2009). Wood and fibre morphology. In: Ek, M., Gellerstedt, G., Henriksson, G. (Eds.). *Pulp and paper chemistry and technology*. Volume 1. 1<sup>st</sup> ed. De Gruyter. pp. 46-70.
- Danielsson, S., Lindström, M.E. (2005). Influence of birch xylan adsorption during kraft cooking on softwood pulp strength. *Nordic Pulp Pap. Res. J.* 20: 436-441.
- Danielsson, S. (2007). *Xylan reactions in kraft cooking – Process and product considerations*. PhD thesis. Stockholm, Royal Institute of Technology.
- Dence, C.W. (1992). The determination of lignin. In: Lin, S.Y., Dence, C.W. (Eds.). *Methods in lignin chemistry*. Springer Series in Wood Science. Springer, Berlin, pp. 33-61.
- Dougherty, R., Kunzelmann, K. (2007). Computing local thickness of 3D structures with ImageJ. *Microsc. Microanal.* 13: 1678-1679.
- Dowd, B.A., Campbell, G.H., Marr, R.B., Nagarkar, V.V., Tipnis, S.V., Axe, L., Siddons, D.P. (1999). Developments in synchrotron X-ray computed microtomography at the national synchrotron light source. *Proc. SPIE* 3772: 224-236.
- Egas, A.P.V., Simão, J.P.F., Costa, I.M.M., Francisco, S.C.P., Castro, J.A.A.M. (2002). Experimental methodology for heterogeneous studies in pulping of wood. *Ind. Eng. Chem. Res.* 41: 2529-2534.
- Esteban, L.G., Palacios, P., Gasson, P., García-Iruela, A., García-Fernández, F., García-Esteban, L. (2024). Hardwoods: Anatomy and functionality of their elements – A short review. *Forests* 15: 1162.
- Evtuguin, D.V., Tomás, J.L., Silva, A.M.S., Pascoal Neto, C. (2003) Characterization of an acetylated heteroxyylan from *Eucalyptus globulus* Labill. *Carbohydr. Res.* 338: 597-604.
- FAO (2023). *Forestry Production and Trade*. Available at: <<https://www.fao.org/faostat/en/#data/FO>>
- Favaro, J., Ventrone, G., De Oliveira, I., De Oliveira, C. (2021). Temperature and effective alkali effect on brown pulp kraft cooking. *Nord. Pulp Pap. Res. J.* 36: 227-233.

- Foelkel, C. (2009). O processo de impregnação dos cavacos de madeira de eucalipto pelo licor kraft de cozimento. In: Foelkel, C. (Ed.). *Eucalyptus Online Book & Newsletter*. Available at: <<https://www.eucalyptus.com.br/disponiveis.html>>
- Forest Europe (2020). *Adaptation to climate change in sustainable forest management in Europe*. Zvolen. Available at: <<https://efi.int/publications/adaptation-climate-change-sustainable-forest-management-europe-2020-09-01>>
- Gabriellii, I., Gatenholm, P., Glasser, W.G., Jain, R.K., Kenne, L. (2000). Separation, characterization and hydrogel-formation of hemicellulose from aspen wood. *Carbohydr. Polym.* 43: 367-374.
- Gao, C., Cui, X., Matsumura, J. (2024). Multidimensional exploration of wood extractives: A review of compositional analysis, decay resistance, light stability, and staining applications. *Forests* 15: 1782.
- Gellerstedt, G. (2009). Chemistry of chemical pulping. In: Ek, M., Gellerstedt, G., Henriksson, G. (Eds.). *Pulp and paper chemistry and technology*. Volume 2. 1<sup>st</sup> ed. De Gruyter. pp. 91-120.
- Ghaffari, R. (2023). *Mass transport in wood disintegration: Implications for the pulp and paper industry*. PhD thesis. Gothenburg, Chalmers University of Technology.
- Gierer, J. (1980). Chemical aspects of kraft pulping. *Wood Sci. Technol.* 14: 241-266.
- Gilbert, W., Allison, B., Radiotis, T., Dort, A. (2021). A simplified kinetic model for modern cooking of aspen chips. *Nordic Pulp Pap. Res. J.* 36: 399-413.
- Giummarella, N., Lawoko, M. (2016). Structural basis for the formation and regulation of lignin-xylan bonds in birch. *ACS Sustainable Chem. Eng.* 4: 5319-5326.
- Grantham, N.J., Wurman-Rodrich, J., Terrett, O.M., Lyczakowski, J.J., Stott, K., Iuga, D., Simmons, T.J., Durand-Tardif, M., Brown, S.P., Dupree, R., Busse-Wicher, M., Dupree, P. (2017). An even pattern of xylan substitution is critical for interaction with cellulose in plant cell walls. *Nat. Plants* 3: 859-865.
- Grénman, H., Wärnå, J., Mikkola, J.P., Sifontes, V., Fardim, P., Murzin, D.Y., Salmi, T. (2010). Modeling the influence of wood anisotropy and internal diffusion on delignification kinetics. *Ind. Eng. Chem. Res.* 49: 9703-9711.
- Gullichsen, J., Kolehmainen, H., Sundqvist, H. (1992). On the nonuniformity of the kraft cook. *Paperi ja Puu* 74: 486-490.
- Gustafson, R.R., Snelcher, C.A., McKean, W.T., Finlayson, B.A. (1983). Theoretical model of the kraft pulping process. *Ind. Eng. Chem. Process Des. Dev.* 22: 87-96.
- Gustafson, R.R., Jiménez, G., McKean, W.T., Chian, D. (1989). The role of penetration and diffusion in nonuniform pulping of softwood chips. *Tappi J.* 72: 163-167.
- Gürsoy, D., De Carlo, F., Xiao, X., Jacobsen, C. (2014). Tomopy: a framework for the analysis of synchrotron tomographic data. *J. Synchrotron Radiat.* 21: 1188-1193.
- Hart, P.W., Nutter, D.E. (2012). Use of cold tolerant eucalyptus species as a partial replacement for southern mixed hardwoods. *Tappi J.* 11: 29-35.

- Heinonen, E., Sivan, P., Jiménez-Quero, A., Lindström, M.E., Wohler, J., Henriksson, G., Vilaplana, F. (2025). Pattern of substitution affects the extractability and enzymatic deconstruction of xylan from Eucalyptus wood. *Carbohydr. Polym.* 353: 123246.
- Henriksson, G. (2009). Lignin. In: Ek, M., Gellerstedt, G., Henriksson, G. (Eds.). *Pulp and paper chemistry and technology*. Volume 1. 1<sup>st</sup> ed. De Gruyter. pp. 121-145.
- Henriksson, G., Lennholm, H. (2009). Cellulose and carbohydrate chemistry. In: Ek, M., Gellerstedt, G., Henriksson, G. (Eds.). *Pulp and Paper Chemistry and Technology*. Volume 1. 1<sup>st</sup> ed. De Gruyter. pp. 71-99.
- Hubbe, M.A., Sjöstrand, B., Lestelius, M., Håkansson, H., Swerin, A., Henriksson, G. (2024). Swelling of cellulosic fibers in aqueous systems: A review of chemical and mechanistic factors. *BioResources* 19: 6859-6945.
- Hujala, M., Arminen, H., Hill, R.C., Puumalainen, K. (2013). Explaining the shifts of international trade in pulp and paper industry. *For. Sci.* 59: 211-222.
- Hult, E.L., Larsson, P.T., Iversen, T. (2001) Cellulose fibril aggregation – An inherent property of kraft pulps. *Polymer*. 42: 3309-3314.
- Inalbon, M.C., Zanuttini, M. (2008). Dynamics of the effective capillary cross-sectional area during the alkaline impregnation of eucalyptus wood. *Holzforschung*, 62: 397-401.
- Inalbon, M.C., Montagna, P.N., Galván, M.V., Demonte, L., Zanuttini, M.A. (2013). Wood capillarity and deacetylation during eucalyptus alkaline impregnation. Sulphidity effects and comparison between transverse directions. *Holzforschung* 67: 41-46.
- Jedvert, K., Saltberg, A., Lindström, M.E., Theliander, H. (2012). Mild steam explosion and chemical pre-treatment of Norway spruce. *BioRes.* 7: 2051-2074.
- Jiang, Z.H., Lierop, B.V., Berry, R. (2000). Hexenuronic acid groups in pulping and bleaching chemistry. *Tappi J.* 83: 167-175.
- Kabel, M.A., van den Borne, H., Vincken, J.P., Voragen, A.G.J., Schols, H.A. (2007). Structural differences of xylans affect their interaction with cellulose. *Carbohydr. Polym.* 69: 94-105.
- Kiaei, M., Moya, R. (2015). Physical properties and fiber dimension in stem, branch and root of alder wood. *Fresenius Environ. Bull.* 24: 335-342.
- Kishani, S., Vilaplana, F., Ruda, M., Hansson, P., Wågberg, L. (2020). Influence of solubility on the adsorption of different xyloglucan fractions at cellulose–water interfaces. *Biomacromolecules* 21: 772-782.
- Klemm, D., Heublein, B., Fink, H.P., Bohn, A. (2005). Cellulose: Fascinating biopolymer and sustainable raw material. *Angew. Chem. Int. Ed.* 44: 3358-3393.
- Koch, G., Rose, B., Patt, R., Kordsachia, O. (2003). Topochemical investigations on delignification of *Picea abies* [L.] Karst. during alkaline sulfite (ASA) and bisulfite pulping by scanning UV microspectrophotometry. *Holzforschung* 57: 611-618.
- Koch, G. (2006). Raw material for pulp. In: Sixta, H. (Ed.). *Handbook of pulp*. John Wiley & Sons, Ltd. pp. 21-68.

- Koddenberg, T. (2025). A new dimension in wood anatomy education: Exploring softwood and hardwood structures in 3D. *Eur. J. Wood Wood Prod.* 83: 201.
- Kron, L., Hasani, M., Theliander, H. (2024). A comparative study of the cell wall level delignification behaviour of four Nordic hardwoods during kraft pulping. *Holzforschung* 78: 434-445.
- Kron, L., Hasani, M., Theliander, H. (2025). Heterogenous diffusion and reaction model of kraft delignification at the cell wall level. *Ind. Eng. Chem. Res.* 64: 1497-1507.
- Kumar, R., Hu, F., Hubbell, C.A., Ragauskas, A.J., Wyman, C.E. (2013). Comparison of laboratory delignification methods, their selectivity, and impacts on physiochemical characteristics of cellulosic biomass. *Bioresour. Technol.* 130: 372-381.
- Lan, X., Fu, S., Song, J., Leu, S., Shen, J., Kong, Y., Kang, S., Yuan, X., Liu, H. (2024). Structural changes of hemicellulose during pulping process and its interaction with nanocellulose. *Int. J. Biol. Macromol.* 255: 127772.
- Lawoko, M., Henriksson, G., Gellerstedt, G. (2005). Structural differences between the lignin-carbohydrate complexes present in wood and in chemical pulps. *Biomacromolecules* 6: 3467- 3473.
- Legland, D., Arganda-Carreras, I., Andrey, P. (2016). MorphoLibJ: integrated library and plugins for mathematical morphology with ImageJ. *Bioinformatics* 32: 3532-3534.
- Liu, Z., Suntio, V., Kuitunen, S., Roininen, J., Alopaeus, V. (2014). Modeling of mass transfer and reactions in anisotropic biomass particles with reduced computational load. *Ind. Eng. Chem. Res.* 53: 4096-4103.
- Malkov, S., Tikka, P., Gullichsen, J. (2001a). Towards complete impregnation of wood chips with aqueous solutions, Part 2: Studies on water penetration into softwood chips. *Paperi ja Puu* 38: 468-473.
- Malkov, S., Tikka, P., Gullichsen, J. (2001b). Towards complete impregnation of wood chips with aqueous solutions, Pat 3: Black liquor penetration into pine chips. *Paperi ja Puu* 83: 605-609.
- Malkov, S., Tikka, P., Gullichsen, J. (2002). Towards complete impregnation of wood chips with aqueous solutions, Pat 4: Effects of front-end modifications in displacement batch kraft pulping. *Paperi ja Puu* 84: 526-530.
- Malkov, S., Tikka, P., Gustafson, R., Nuopponen, M., Vuorinen, T. (2003). Towards complete impregnation of wood chips with aqueous solutions, Pat 5: Improving uniformity of kraft displacement batch pulping. *Paperi ja Puu* 85: 215-220.
- Marion de Godoy, C. (2024). *Kraft pulping of birch: Insights into delignification and xylan removal*. Licentiate thesis. Gothenburg, Chalmers University of Technology.
- Matsumura, J., Booker, R.E., Ridoutt, B.G., Donaldson, L.A., Mikajiri, N., Matsunaga, H., Oda, K. (1999). Impregnation of radiata pine wood by vacuum treatment II: Effect of pre-steaming on wood structure and resin content. *J. Wood Sci.* 45: 456-462.

- Mattsson, C., Hasani, M., Dang, B., Mayzel, M., Theliander, H. (2017). About structural changes of lignin during kraft cooking and the kinetics of delignification. *Holzforschung* 71: 545-553.
- Mboowa, D. (2024). A review of the traditional pulping methods and the recent improvements in the pulping processes. *Biomass Conv. Bioref.* 14: 1-12.
- McKibbins, S. (1960). Application of diffusion theory to the washing of kraft cooked wood chips. *Tappi* 43: 801-805.
- Montagna, P.N., Inalbon, M.C., Paananen, M., Sixta, H., Zanuttini, M.A. (2013). Diffusion dynamics in *Pinus sylvestris* kraft impregnation: Effect of deacetylation and galactoglucomannan degradation. *Ind. Eng. Chem. Res.* 52: 3658-3662.
- Neiva, D., Fernandes, L., Araújo, S., Lourenço, A., Gominho, J., Simões, R., Pereira, H. (2015). Chemical composition and kraft pulping potential of 12 eucalypt species. *Ind. Crops Prod.* 66: 89-95.
- Nieminen, K., Sixta, H. (2012). Comparative evaluation of different kinetic models for batch cooking: A review. *Holzforschung* 66: 791-799.
- Nieminen, K., Kuitunen, S., Paananen, M., Sixta, H. (2014). Novel insight into lignin degradation during kraft cooking. *Ind. Eng. Chem. Res.* 53: 2614-2624.
- Pakkanen, H., Alén, R. (2012). Molecular mass distribution of lignin from the alkaline pulping of hardwood, softwood, and wheat straw. *J. Wood Chem. Technol.* 32: 279-293.
- Patt, R., Kordsachia, O., Fehr, J. (2006). European hardwoods versus *Eucalyptus globulus* as a raw material for pulping. *Wood Sci. Technol.* 40: 39-48.
- Pettersen, R.C. (1984). The chemical composition of wood. In: Rowell, R. (Ed). *The chemistry of solid wood*. Advances in chemistry series. American Chemical Society. pp. 57-126.
- Pinto, P.C., Evtuguin, D.V., Pascoal Neto, C. (2005a). Structure of hardwood glucuronoxylans: modifications and impact on pulp retention during wood kraft pulping. *Carbohydr. Polym.* 60: 489-497.
- Pinto, P.C., Evtuguin, D.V., Pascoal Neto, C. (2005b). Effect of structural features of wood biopolymers on hardwood pulping and bleaching performance. *Ind. Eng. Chem. Res.* 44: 9777-9784.
- Poling, B.E., Prausnitz, J.M., O'Connell, J.P. (2001). *Properties of gases and liquids*. 5<sup>th</sup> ed. McGraw-Hill: New York. 768 p.
- Potthast, A. (2006). Chemistry of kraft cooking. In: Sixta, H. (Ed.). *Handbook of pulp*. John Wiley & Sons, Ltd. pp. 164-185.
- Qaseem, M.F., Zhang, W., Dupree, P., Wu, A.M. (2025). Xylan structural diversity, biosynthesis, and functional regulation in plants. *Int. J. Biol. Macromol.* 291: 138866.
- Rajan, K., Berton, P., Rogers, R.D., Shamshina, J.L. (2024). Is kraft pulping the future of biorefineries? A perspective on the sustainability of lignocellulosic product development. *Polymers* 16: 3438.

- Ralph, J., Lapierre, C., Boerjan, W. (2019). Lignin structure and its engineering. *Curr. Opin. Biotechnol.* 56: 240-249.
- Rehbein, M., Pereira, M., Koch, G., Kordsachia, O. (2010). Topochemical investigation into the delignification of *Eucalyptus globulus* chips during semi-chemical sulfite pulping. *Wood Sci. Technol.* 44: 435-449.
- Rivers, M.L. (2012). tomoRecon: high-speed tomography reconstruction on workstations using multi-threading. *Proc. SPIE* 8506: 169-181.
- Rowell, R.M., Pettersen, R., Tshabalala, M.A. (2005). Cell wall chemistry. In: Rowell, R.M. (Ed.). *Handbook of wood chemistry and wood composites*. 1<sup>st</sup> ed. CRC Press. pp. 33-72.
- Ruffinatto, F., Crivellaro, A. (2019). *Atlas of macroscopic wood identification: with a special focus on timbers used in Europe and CITES-listed species*. 1<sup>st</sup> ed. Springer Cham. 439 p.
- Santiago, A.S., Pascoal Neto, C., Vilela, C. (2008). Impact of effective alkali and sulfide profiling on *Eucalyptus globulus* kraft pulping. Selectivity of the impregnation phase and its effect on final pulping results. *J. Chem. Technol. Biotechnol.* 83: 242-251.
- Santos, R.B., Capanema, E.A., Balakshin, M.Y., Chang, H.M., Jameel, H. (2011). Effect of hardwoods characteristics on kraft pulping process: Emphasis on lignin structure. *BioResources* 6: 3623-3637.
- Santos, R.B., Capanema, E.A., Balakshin, M.Y., Chang, H.M., Jameel, H. (2012a). Lignin structural variation in hardwood species. *J. Agric. Food Chem.* 60: 4923-4930.
- Santos, R.B., Jameel, H., Chang, H.M., Hart, P.W. (2012b). Kinetics of hardwood carbohydrate degradation during kraft pulp cooking. *Ind. Eng. Chem. Res.* 51: 12192-12198.
- Schindelin, J., Arganda-Carreras, I., Frise, E., *et al.* (2012). Fiji: an open-source platform for biological-image analysis. *Nat Methods* 9: 676-682.
- Shunn, K.C., Gee, C.T. (2023). Cross-sectioning to the core of conifers: pith anatomy of living Araucariaceae and Podocarpaceae, with comparisons to fossil pith. *IAWA J.* 45: 1-26.
- Simão, J.P.F., Egas, A.P.V., Carvalho, M.G., Baptista, C.M.S.G., Castro, J.A.A.M. (2008). Heterogeneous studies in pulping of wood: Modelling mass transfer of alkali. *Chem. Eng. J.* 139: 615-621.
- Simão, J.P.F., Carvalho, M.G.V.S., Baptista, C.M.S.G. (2011). Heterogeneous studies in pulping of wood: Modelling mass transfer of dissolved lignin. *Chem. Eng. J.* 170: 264-269.
- Singh, A., Dawson, B., Franich, R., Cowan, F., Warnes, J. (1999). The relationship between pit membrane ultrastructure and chemical impregnability of wood. *Holzforschung* 53: 341-346.

- Sivan, P., Heinonen, E., Escudero, L., Gandla, M.L., Jiménez-Quero, A., Jönsson, L.J., Mellerowicz, E.J., Vilaplana, F. (2024). Unraveling the unique structural motifs of glucuronoxylan from hybrid aspen wood. *Carbohydr. Polym.* 343: 122434.
- Sixta, H., Potthast, A., Krottschek, A.W. (2006). Chemical pulping processes. In: Sixta, H. (Ed.). *Handbook of pulp*. John Wiley & Sons, Ltd. pp. 109-164.
- Sjöström, E. (1993a). The structure of wood. In: Sjöström, E. (Ed.). *Wood chemistry: Fundamentals and applications*. 2<sup>nd</sup> ed. Academic Press. pp. 1-20.
- Sjöström, E. (1993b). Wood polysaccharides. In: Sjöström, E. (Ed.). *Wood chemistry: Fundamentals and applications*. 2<sup>nd</sup> ed. Academic Press. pp. 51-70.
- Sjöström, E. (1993c). Lignin. In: Sjöström, E. (Ed.). *Wood chemistry: Fundamentals and applications*. 2<sup>nd</sup> ed. Academic Press. pp. 71-89.
- Sjöström, E. (1993d). Wood pulping. In: Sjöström, E. (Ed.). *Wood chemistry: Fundamentals and applications*. 2<sup>nd</sup> ed. Academic Press. pp. 114-164.
- Skogsstyrelsen (2026). Price on roundwood. *Statistical database*. Available at: <<https://skogsstyrelsen.se/en/statistics/statistical-database/>>
- Sluiter, A., Hames, B., Ruiz, R., Scarlata, C., Sluiter, J., Templeton, D., Crocker, D. (2012). *Determination of structural carbohydrates and lignin in Biomass - NREL/TP-510-42618*. Laboratory Analytical Procedure (LAP), 17.
- Smith, C.C. (1974). *Studies of the mathematical modelling, simulation, and control of the operation of a Kamyr continuous digester for the kraft process*. PhD thesis. West Lafayette, Purdue University.
- Stone, J.E. (1957). The effective capillary cross-sectional area of wood as a function of pH. *Tappi J.* 40: 539-541.
- Stone, J.E., Green, H.V. (1959). Penetration and diffusion into hardwoods. *Tappi* 42: 700-709.
- Stone, J.E., Scallan, A.M. (1967). The effect of component removal upon the porous structure of the cell wall of wood. II. Swelling in water and the fiber saturation point. *Tappi* 50: 496.
- Takada, M., Tanaka, Y., Minami, E., Saka, S. (2016). Comparative study of the topochemistry on delignification of Japanese beech (*Fagus crenata*) in subcritical phenol and subcritical water. *Holzforschung* 70: 1047-1053.
- Takada, M., Minami, E., Kawamoto, H. (2021). Topochemistry of the delignification of Japanese beech (*Fagus crenata*) wood by supercritical methanol treatment. *ACS Omega* 6: 20924-20930.
- Tavast, D., Brännvall, E. (2017). Increased pulp yield by prolonged impregnation in softwood kraft pulping. *Nordic Pulp Pap. Res. J.* 32: 14-20.
- Teleman, A. (2009). Hemicelluloses and pectins. In: Ek, M., Gellerstedt, G., Henriksson, G. (Eds.). *Pulp and paper chemistry and technology*. Volume 1. 1<sup>st</sup> ed. De Gruyter. pp. 102-120.
- Tripathi, S.K., Mishra, O.P., Bhardwaj, N.K. (2018). Effect of mixed hardwood chips thickness on unbleached and bleached pulp quality. *J. Sci. Ind. Res.* 77: 516-519.

- Vegunta, V., Senthilkumar, E.R., Lindén, P., Sevastyanova, O., Vilaplana, F., Garcia, A., Björk, M., Jansson, U., Henriksson, G., Lindström, M.E. (2022). High calcium content of *Eucalyptus dunnii* wood affects delignification and polysaccharide degradation in kraft pulping. *Nordic Pulp Pap. Res. J.* 37: 338-348.
- Vroom, K.E. (1957). The 'H' factor: A means of expressing cooking times and temperatures as a single variable. *Pulp Paper Mag. Can.* 58C: 228-231.
- Wagih, A., Hasani, M., Hall, S.A., Novak, V., Theliander, H. (2022). *In situ* microstructural evolution of spruce wood during soda pulping using synchrotron X-ray tomography. *Holzforschung* 76: 611-621.
- Wardrop, A., Davies, G. (1961). Morphological factors relating to the penetration of liquids into wood. *Holzforschung* 15: 129-141.
- Whiting, P., Goring, D.A.I. (1981). The topochemistry of delignification shown by pulping middle lamella and secondary wall tissue from black spruce wood. *J. Wood Chem. Technol.* 1: 111-122.
- Whiting, P., Goring, D.A.I. (1982). Relative reactivities of middle lamella and secondary wall lignin of black spruce wood. *Holzforschung* 36: 303-306.
- Wiedenhoef, A.C. (2005) Structure and function of wood. In: Rowell, R.M. (Ed.). *Handbook of wood chemistry and wood composites*. 1<sup>st</sup> ed. CRC Press. pp. 9-32.
- Wisnewski, P.A., Doyle III, F.J., Kayihan, F. (1997). Fundamental continuous-pulp-digester model for simulation and control. *AIChE J.* 43: 3175-3192.
- Wojtasz-Mucha, J., Hasani, M., Theliander, H. (2017). Hydrothermal pretreatment of wood by mild steam explosion and hot water extraction. *Bioresour. Technol.* 241: 120-126.
- Yamashita, D., Kimura, S., Wada, M., Takabe, K. (2016). Improved Mäule color reaction provides more detailed information on syringyl lignin distribution in hardwood. *J. Wood Sci.* 62: 131-137.
- You, T., Zhang, L., Zhou, S., Xu, F. (2015). Structural elucidation of lignin-carbohydrate complex (LCC) preparations and lignin from *Arundo donax* Linn. *Ind. Crops Prod.* 71: 65-74.
- Zanuttini, M., Citroni, M., Martínez, M.J., Marzocchi, V. (1998). Chemimechanical pulping of poplar wood. Alkaline wood pretreatment at low temperature. *Holzforschung* 52: 405-409.
- Zanuttini, M., Citroni, M., Marzocchi, V. (2000). Pattern of alkali impregnation of poplar wood at moderate conditions. *Holzforschung* 54: 631-636.
- Zhao, Y., Shakeel, U., Rehman, M.S.U., Li, H., Xu, X., Xu, J. (2020). Lignin-carbohydrate complexes (LCCs) and its role in biorefinery. *J. Clean. Prod.* 253: 120076.

# List of symbols

The symbols used for each variable in the developed multiscale model are as follows:

$D_{L_D,i}$	Effective diffusivity of dissolved lignin fraction $i$ along the cell wall, [m <sup>2</sup> /s]
$D_{OH,free}$	Adjusted diffusivity of sodium hydroxide in water at infinite dilution, [m <sup>2</sup> /s]
$D_{OH_C}$	Effective hydroxide diffusivity in the wood chip, [m <sup>2</sup> /s]
$D_{OH_w}$	Effective hydroxide diffusivity in the cell wall, [m <sup>2</sup> /s]
$ECCSA$	Effective capillary cross sectional area, [-]
$L_0$	Mass fraction of Klason lignin in the wood before pulping, [-]
$L_C$	Norm. lignin content at a given position in the wood chip, [-]
$L_D$	Norm. content of all dissolved lignin fractions at a given position in the cell wall, [-]
$\overline{L_D}$	Norm. average content of dissolved lignin in the cell wall, [-]
$L_{D,i}$	Norm. content of dissolved lignin fraction $i$ at a given position in the cell wall, [-]
$L_S$	Norm. bound lignin content at a given position in the cell wall, [-]
$\overline{L_S}$	Norm. average content of “bound” lignin in the cell wall, [-]
$M_{NaOH}$	Molar mass of sodium hydroxide, [g/mol]
$OH_0$	Initial hydroxide concentration at the wood chip and cell wall levels, [M]
$OH_C$	Hydroxide concentration at a given position in the wood chip, [M]
$OH_w$	Hydroxide concentration at a given position in the cell wall, [M]
$\overline{OH_w}$	Average hydroxide concentration in the cell wall, [M]
$r_L$	Intrinsic reaction rate of lignin dissolution, [s <sup>-1</sup> ]
$t$	Time, [s]
$w_i$	Mass fraction of dissolved lignin fraction $i$ , [-]
$y$	Position along the thickness of the wood chip, [m]
$z$	Position along the cell wall, [m]
$\alpha$	Ratio between carbohydrates and lignin in the pulp, [-]
$\beta$	Alkali consumption factor, [M]
$\varepsilon$	Wood chip porosity, [-]
$\rho_w$	Density of the wood substance, [g/L]



# Appendix

## Determination of extractives

A preliminary test was conducted to assess the impact of extractives on the Klason lignin content measured in model chips after kraft cooking. The experiment began by pulping model heartwood chips with 16 mm of thickness at 155°C, using a liquor:wood ratio of 22. The liquor composition was 0.4 mol HO<sup>-</sup>/kg liquor and 0.1 mol HS<sup>-</sup>/kg liquor. Then, after washing, leaching, and sectioning, part of the samples was extracted, as described below.

Extraction: Pulp samples from different sections of the model chips were ground (particle size < 1 mm) and dried in an oven (105°C) overnight. Then, Soxhlet extraction was performed with acetone (0.5-1.0 g of dry sample / 160 mL acetone) at a rate of 24 extraction cycles / 4.5 h. The solid residue was dried at 40°C for 24 h and the mass was determined.

Afterwards both the extracted and non-extracted samples were subjected to Klason lignin and carbohydrates analyses.

### Results:

Table A.1 displays the content of extractives in two different sections of the model cooked chips. Tables A.2 and A.3 show the measured composition of the samples in comparison to the results attained without performing extraction.

**Table A.1** Content of extractives in different sections of cooked model chips.

Section	Extractives (% w/w)
Surface-corner	1.02
Middle-center	1.88

**Table A.2** Klason lignin content in cooked samples with and without prior extraction.

Section	$\mu$ (% w/w)	RSD (%)
Surface-corner, Extracted	16.14	2.13
Surface-corner	16.89	0.38
Middle-center, Extracted	19.13	0.60
Middle-center	20.36	1.56

**Table A.3** Content of carbohydrates (% w) in cooked samples with and without prior extraction. Measurement error: 0.05% < RSD (%) < 1.50%.

<b>Section<sup>a</sup></b>	<b>Arabinan (%)</b>	<b>Galactan (%)</b>	<b>Glucan (%)</b>	<b>Xylan (%)</b>	<b>Mannan (%)</b>
S-Cor, Extracted	0.28	0.43	49.27	23.15	-
S-Cor	0.29	0.45	49.69	23.52	-
M-C, Extracted	0.34	0.66	39.64	25.02	1.40
M-C	0.34	0.66	39.32	24.79	1.35

<sup>a</sup> Sections: S-Cor = Surface-corner, M-C = Middle-center.

The concentration of extractives varied within the kraft cooked samples. In the surface layer, their content was about 46% lower than in the middle layer. In terms of the impact extractives had on Klason lignin measurements, the results attained after extraction were 4.5% lower for the sample taken from the surface layer and 6.0% lower for the sample from the middle layer (compared to the lignin concentrations in samples not subjected to prior extraction).

Regarding the carbohydrates analysis (Table A.3), the results showed the extractives had no clear influence on the measured values.

#### Conclusion:

It appears that not performing the extraction step prior to acidic hydrolysis leads to deceptively higher Klason lignin values. Nevertheless, the extent of this effect seems to be fairly similar for different sections of the wood chip. In addition, extractives had no substantial impact on the quantification of sugars. Hence, for the purposes of the present study, the gain in accuracy provided by the extraction step is eclipsed by the time it demands.